1-1-2016

Engineering Phonon, Photon, Electron and Plasmon interactions in Silicon - Metal Nanocavitiies for Silicon Photonics and Thermoplasmonics

Daksh Agarwal
University of Pennsylvania, agarwaldaksh@gmail.com

Engineering Phonon, Photon, Electron and Plasmon interactions in Silicon - Metal Nanocavitiies for Silicon Photonics and Thermoplasmonics

Abstract
ENGINEERING PHONON, PHOTON, ELECTRON AND PLASMON INTERACTIONS IN SILICON - METAL NANOCAVITIIES FOR SILICON PHOTONICS AND THERMOPLASMONICS

Daksh Agarwal

Ritesh Agarwal, PhD

Silicon photonics offers a cost effective solution to achieve ultrafast data processing speeds. But due to its indirect bandgap structure, making lasers from silicon is extremely difficult. Thus research has focused on nonlinear Raman processes in silicon as a method to achieve optical gain. Silicon nanowires provide an interesting platform for enhancing these nonlinearities because of their small size, geometry and relevant length scales. In the current work Raman measurements done on silicon nanowires reveal that up to twelvefold enhancement in Stokes scattering intensity and fourfold enhancement in anti Stokes scattering intensity can be attained depending on cavity structure and size, and excitation wavelength. In some cavities Stokes intensity depends on the sixth power of pump intensity, indicating extreme nonlinearity. Numerical calculations, done to understand the mechanism of these results indicate that silicon nanowires confine light to highly intense electric field modes inside the cavity which lead to stimulated Stokes and anti Stokes Raman scattering. Cavity modes can also be tuned to enhance the relative emission of either one of anti Stokes or Stokes photons which could enhance cavity cooling. These results would enable the development of smallest monolithically integratable silicon laser with extremely low lasing threshold and could lead to the development of next generation of high speed and energy efficient processors. The intense electric field inside the nanowire could also be used to enhance the degree of plasmon excitation in metallic nanoparticles. Silicon nanowires coated with a 10 nm thick gold film lead to strong plasmon excitation in gold and high cavity absorption which enable the cavity to heat up to temperatures of 1000K at relatively low pump powers. The cavities also give the ability to measure temperature attained during plasmon excitation and control the plasmon resonance wavelength. Because of the strong heating and plasmonic effects, these cavities show enhanced evolution rates of hydrogen, a crucial industrial building block and a promising fuel, in photoreforming reactions of alcohols.

Degree Type
Dissertation

Degree Name
Doctor of Philosophy (PhD)

Graduate Group
Materials Science & Engineering

ENGINEERING PHONON, PHOTON, ELECTRON AND PLASMON INTERACTIONS IN SILICON - METAL NANOCAVITIIES FOR SILICON PHOTONICS AND THERMOPLASMONICS

Daksh Agarwal

A DISSERTATION

in

Materials Science and Engineering

Presented to the Faculties of the University of Pennsylvania

in

Partial Fulfillment of the Requirements for the

Degree of Doctor of Philosophy

2016

Supervisor of Dissertation

_____

Ritesh Agarwal, PhD

Professor of Materials Science and Engineering

Graduate Group Chairperson

_____

Shu Yang, PhD, Professor of Materials Science and Engineering

Dissertation Committee

Nader Engheta, PhD, H. Nedwill Ramsey Professor of Electrical and Systems Engineering, Physics and Astronomy and Materials Science and Engineering and Bioengineering

Christopher B. Murray, PhD, Richard Perry University Professor of Chemistry, and Materials Science and Engineering

Cherie R. Kagan, PhD, Stephen J. Angello Professor of Electrical and Systems Engineering, Materials Science and Engineering, and Chemistry

ENGINEERING PHONON, PHOTON, ELECTRON AND PLASMON INTERACTIONS IN SILICON - METAL NANOCAVITIIES FOR SILICON PHOTONICS AND THERMOPLASMONICS

To my dad, for his unconditional love and for his smiles no matter what.

ACKNOWLEDGMENT

I would like to take this opportunity to first thank my supervisor Dr. Ritesh Agarwal, whose esteemed guidance and support has helped me tremendously in these past five years. I would also like to thank my thesis committee members (past and present) Dr. Nader Engheta, Dr. Cherie Kagan, Dr. Chris Murray and Dr. Ertugrul Cubukcu for providing valuable counsel and insights. I would like to thank Dr. Carlos Aspetti, former member of the Agarwal group for his guidance early on in my PhD; and Jacob Berger and Rob Middleton for helping me navigate difficult times. The current and former members of the Agarwal group have made these years truly transformative and memorable; I would like to thank Dr. Joohee Park, Dr. Mingliang Ren, Dr. Pavan Nukala, Wenjing Liu, Dr. Liaoxin Sun, Dr. Bumsu Lee, Dr. Sajal Dhara, Dr. Rahul Agarwal, Stephanie Malek and Gerui Liu, for all their insightful scientific discussions.

I must not forget to mention other members of my PhD cohort- Dan, Frank and Nick, and friends from Penn Taekwondo- Becky, Jessie, Tom, Robin and Kevin for enriching my life these past five years.

Lastly, and most importantly, I want to thank my family especially my father who always strived to bring happiness in my life, my mother for always standing beside me, my sisters for make me believe in me, my brother in laws for supporting me in the most difficult times of my life, and my wife for being there for me no matter what.

ABSTRACT

ENGINEERING PHONON, PHOTON, ELECTRON AND PLASMON INTERACTIONS IN SILICON - METAL NANOCAVITIIES FOR SILICON PHOTONICS AND THERMOPLASMONICS

Daksh Agarwal

Ritesh Agarwal, PhD

Silicon photonics offers a cost effective solution to achieve ultrafast data processing speeds. But due to its indirect bandgap structure, making lasers from silicon is extremely difficult. Thus research has focused on nonlinear Raman processes in silicon as a method to achieve optical gain. Silicon nanowires provide an interesting platform for enhancing these nonlinearities because of their small size, geometry and relevant length scales. In the current work Raman measurements done on silicon nanowires reveal that up to twelvefold enhancement in Stokes scattering intensity and fourfold enhancement in anti Stokes scattering intensity can be attained depending on cavity structure and size, and excitation wavelength. In some cavities Stokes intensity depends on the sixth power of pump intensity, indicating extreme nonlinearity. Numerical calculations, done to understand the mechanism of these results indicate that silicon nanowires confine light to highly intense electric field modes inside the cavity which lead to stimulated Stokes and anti Stokes Raman scattering. Cavity modes can also be tuned to enhance the relative emission of either one of anti Stokes or Stokes photons which could enhance cavity cooling. These results would enable the development of smallest monolithically integratable silicon laser with extremely low lasing threshold and could lead to the

development of next generation of high speed and energy efficient processors. The intense electric field inside the nanowire could also be used to enhance the degree of plasmon excitation in metallic nanoparticles. Silicon nanowires coated with a 10 nm thick gold film lead to strong plasmon excitation in gold and high cavity absorption which enable the cavity to heat up to temperatures of 1000K at relatively low pump powers. The cavities also give the ability to measure temperature attained during plasmon excitation and control the plasmon resonance wavelength. Because of the strong heating and plasmonic effects, these cavities show enhanced evolution rates of hydrogen, a crucial industrial building block and a promising fuel, in photoreforming reactions of alcohols.

TABLE OF CONTENTS

LIST OF TABLES

LIST OF FIGURES/ILLUSTRATIONS

CHAPTER 1. Introduction

1.1 Case for nanoscale silicon photonics

The advances in the CMOS technology have greatly enhanced processor speed of devices. However, device size is expected to reach saturation soon[1] with Intel already working on a 14 nm transistor[2]. Moreover, with the ever increasing demand for faster speeds and larger bandwidths from interconnects, copper interconnects are expected to soon lag behind the requirements[3]. Both of these would greatly affect the potential speeds at which chips could operate. Optical interconnects provide an alternative, allowing much faster speeds and larger bandwidths and are already being used to connect racks of equipment that span 1-100 meters. Over the next decade they are expected to slowly make way into backplane communication- connecting separate printed circuit boards over a distance of 20-100 cm, and eventually to chip to chip applications, spanning less than 20 cm [3]. These would allow for much faster device speeds and faster communication between different components of a chip. They would also directly greatly increase the rate at which data can be transferred across a network.

Silicon because of its low cost and compatibility with the CMOS industry offers itself as the obvious choice for optical interconnect material. Using silicon would allow for easy assembly and integration of optical components within the existing devices leading to much lower cost given that packaging and assembly account for ~ 60-70% of the total costs[3]. But silicon does not emit light at because of its indirect bandgap[4] and

therefore alternate mechanisms such as Raman scattering for light emission need to be explored. Decade long research has opened up exciting possibilities; with silicon laser[5] and optical modulation being realized[6], which could dramatically revolutionize the industry. To give some perspective, copper interconnects typically allow for a speed of ~100Mbits/sec and the best ones available can potentially go as fast as 10-20Gbits/second[3]. Today silicon devices can modulate signals electro-optically and process data at speeds higher than that[7]. It can be used to process optical signals at speeds of 100Gbit/s and beyond[7 8]. Tbits/s speed is the next goal[9] and while the developments so far have been promising, there are still a variety of issues that need to be addressed. Silicon based photonic devices typically have large footprints (>10 μm). Hence they require higher operating powers; which along with their size-mismatch with electronic components limits their potential for ultra dense device integration. High manufacturing cost for high volume production, high heat generation originating from high power requirements further limit the applications. Moreover some silicon-germanium (or III-V) hybrid components are still required especially for applications as a lasing source, which further complicates the integration steps. Therefore, new advances in materials design, fundamental understanding of nanoscale optical physics and innovative optical engineering are required to solve this problem.

Nanoscale silicon photonics could go a long way in addressing these issues. Efficient silicon photonics at the nanoscale would bring down the size of optical components making integration much easier. Nanowire geometry as well as all (only) silicon optical components would further simplify the integration process. Smaller size

would enable smaller chip sizes and bring down the cost of manufacturing. These nanoscale components would also work at much lower operating power and voltages (possibly a few orders of magnitude lower). Given that interconnects today consume about 80% of the microprocessors power; this would bring about a dramatic decrease in the power consumption[10]. Lower powers consumption would decrease the amount of heat that needs to be removed from the system bringing the load on the cooling infrastructure[10]. Given the amount of heat that can be removed from a chip in cost effective manner is expected to be constant in the foreseeable future[10], minimizing power losses is extremely important for larger scale integration of devices. An all silicon laser at the nanoscale which could be easily integrated would be another big step which would greatly reduce the power requirements both in terms in operating power and cooling infrastructure, making the system more energy efficient and economical, as well as make device integration feasible allowing for much faster speeds especially required in data centers and super computers.

Other potential applications areas for silicon photonics include telecommunications, optical sensing, biomedical applications, imaging, quantum cryptography and atmospheric sensing and monitoring[11 12].

1.2 Recent advances in silicon photonics

Silicon is an indirect band gap material with a bandgap of 1.12 eV[4]. Conventional lasers employ direct band gap semiconductors in which the maxima of the valence band and minima of the conduction band are momentum matched (at k = 0). Thus an electron-

hole recombination event almost always results in a photon emission (figure 1.1[13]) leading to high quantum efficiency. However for silicon, the minima of conduction band and the maxima of valence band do not lie at the same point in k-space (Figure 1.1[13]). As a result non radiative processes such as Auger recombination and free Carrier absorption (FCA) dominate carrier relaxation processes. The rate of radiative recombination is about 6 orders of magnitude lower than the rate of non-radiative recombination[13]. Thus it is extremely difficult to make silicon lasers via the conventional electron-hole recombination processes.

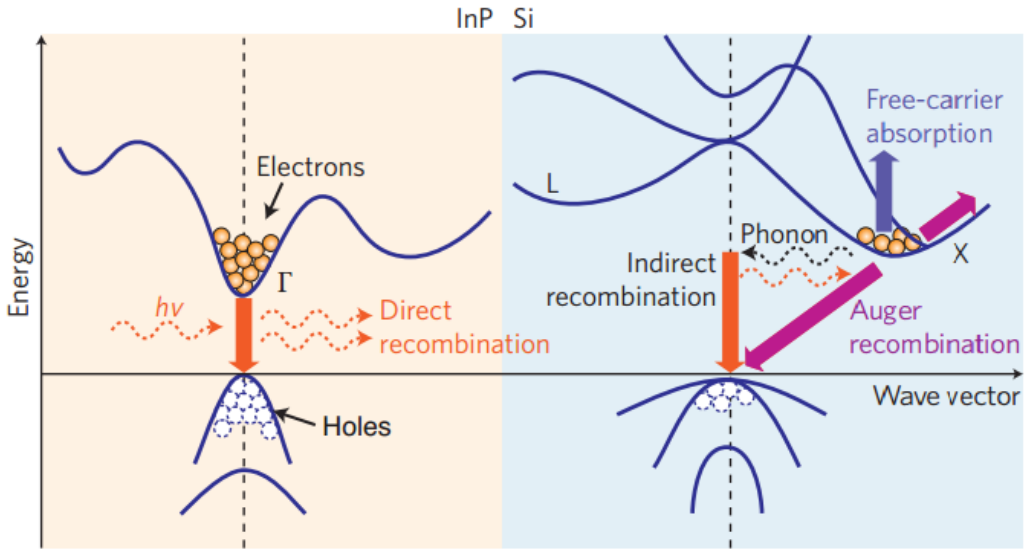

Figure 1.1[13]: Energy – momentum band diagram of a direct (InP) and an indirect (Si) bandgap semi conductor showing major charge carrier transition processes

One of the alternate ways that has been exploited to make a silicon laser is by using Stimulated Raman scattering (SRS, discussed in next section). But high losses from

mechanisms such as free carrier absorption (FCA) and low gain make it extremely difficult to achieve net cavity gain[14 15]. Liu et.al showed via simulations that the free carrier density via two photon absorption (TPA) in a silicon waveguide can be significantly reduced if the pump width is small compared to the carrier lifetime; which led to the observation of SRS, a precursor for Raman lasing, being observed in bulk silicon for the first time using pulsed laser pumping[16]. The first silicon Raman laser was also built using pulsed lasing[17] with a lasing threshold of 9 watts.

The mechanisms used with pulsed lasing could not be used with a continuous wave pumping and the free carrier density with continuous pumping is always high. But losses could still be reduced by reducing the effective carrier lifetime[18]. To decrease the carrier transit time Jones et.al[19] used a p-i-n junction which was formed by depositing a p^+ layer and an n^- layer on either side of the waveguide. The carrier transit time (free carrier lifetime) could be varied by applying different reverse bias voltage across this junction. Higher the reverse bias voltage lowered the carrier transit time leading to lower losses. Lowest carrier life time of ~ 1 ns, with a reverse bias voltage of 25V, was reported. Using this they were able to show, net optical gain with continuous wave pumping. This was followed by lasing using continuous wave pumping with the application of a reverse bias in a 'S' shaped cavity of size 4.8 cm (figure 1.2a)[20]. In this cavity, lasing threshold and conversion efficiency (of pump to Stokes wavelength) was a direct function of losses in the cavity. Lower losses decreased the lasing threshold and increased conversion efficiency while higher losses increased the lasing threshold and decreased the conversion efficiency. At a reverse bias voltage of 25 V a lasing threshold

of 180 mW was observed. With a 5 V bias, the lasing threshold was 280 mW (laser output characteristics in figure 1.2b). Note that this threshold power values correspond to the amount of power coupled into the cavity and not the total pump power. Figure 1.2 [20] shows the schematic of this cavity and the output of laser for two reverse bias voltages.

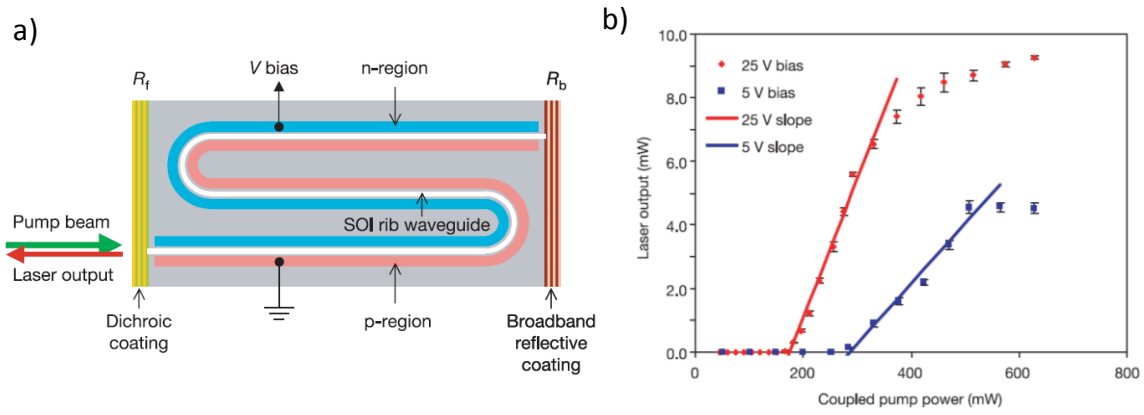

Figure 1.2[20]: Continuous wave Raman silicon laser: a) Schematic layout of silicon waveguide used in the Raman laser experiment; b) Silicon Raman laser output power as a function of the input pump power at a reverse bias of 25 and 5 V. Pump wavelength: 1,550 nm; laser wavelength: 1,686 nm. Error bars represent standard deviations

The first monolithically integrated laser (schematic in figure 1.3[21]) was made by forming a racetrack resonator cavity with a length of 3 cm and the bent radius was 400 µm. The quality factor of the cavity was calculated to be ~ 6E5, and depending on the device architecture and applied reverse bias voltage, lasing threshold powers in between ~150 and 250 mW were reported[21]. This laser could be integrated on the chip and paved way for a plethora of applications. More recently, a cascaded laser[22] and a 0-reverse bias voltage laser[23] have also been made, primarily by decreasing cavity losses and increasing the cavity quality factor.

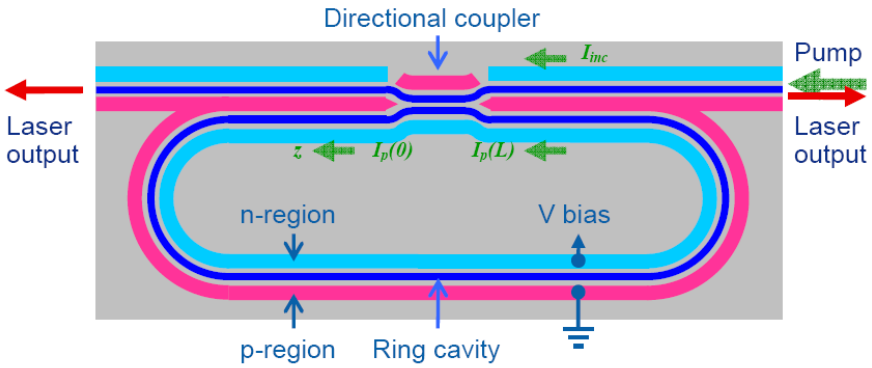

Figure 1.3[21]: Layout of the silicon ring laser cavity with a p-i-n structure along the waveguide

While the developments in achieving optical amplification have been phenomenal, these devices have the footprint of a few centimeters which increases the power consumption and also makes it difficult to integrate these lasers with other nanoscale components of the chip. Such larger cavities are required because although the Raman gain for silicon is higher than Raman gain for a lot of other materials, the gain value is still very small due to low Raman scattering cross section. These lasers also require cavities with very high quality factors as well as application of a reverse bias voltage to further decrease cavity losses.

Hybrid silicon lasers have also been fabricated which have a III-V semiconductor gain medium integrated with a SOI waveguide[24 25 26 27]. These hybrid lasers have a device footprint of a few microns and require a few 100 of μA of current for lasing but are harder to fabricate on-chip, involving multiple complicated fabrication steps which would make the chip structure more complex and increase the production costs.

1.3 Raman scattering and Raman lasing

Raman Scattering is the process by which photons get inelastically scattered from phonons (lattice vibration modes) in a lattice, leading to new photons, shifted (Raman shift) in energy from the incident photons by an amount equal to the vibrational energy of the phonons. The up-converted photons are anti-Stokes scattered while the down shifted photons are Stokes scattered. The relations in between photon frequencies for Stokes and anti Stokes scattering can be summarized by the following two expressions:

$$\omega_{stokes} = \omega_{pump} - \omega_{RamanShift} \quad (1.1)$$

$$\omega_{anti-stokes} = \omega_{pump} + \omega_{RamanShift} \quad (1.2)$$

At room temperature Stokes scattering and hence Stokes photons are more common than anti-Stokes scattering and anti-Stokes photons. This is because at room temperature, a larger fraction of phonons are in the ground state. Figure 1.4[28] shows the schematic of Stokes and anti-Stokes scattering in a Raman process.

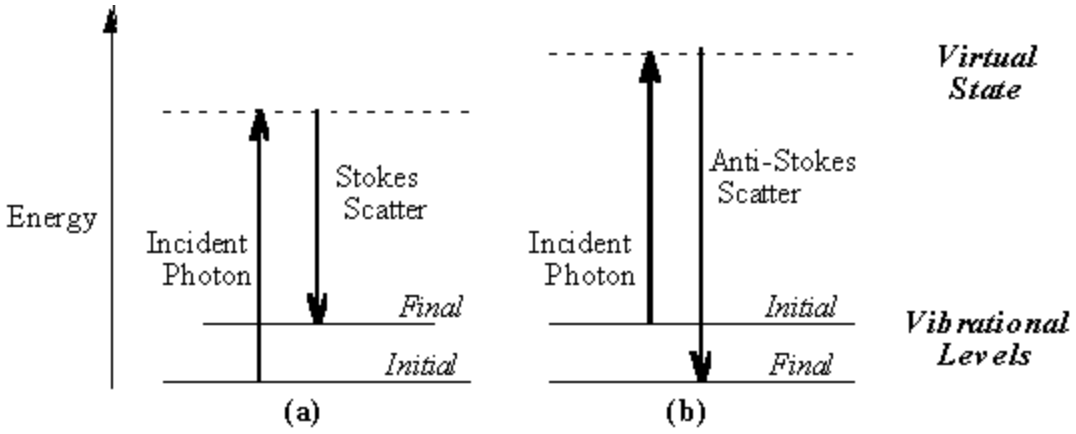

Figure 1.4[28]: Schematic diagram of (a) Stokes and (b) Anti Stokes, Raman scattering

First order and higher order Raman scattering processes:

Spontaneous Raman scattering is a first order optical process in which Stokes intensity is proportional to the first power of incident laser (pump) intensity. This is typically observed at low pump powers.

Stimulated Raman scattering (SRS) is a third order optical process in which Stokes intensity is proportional to the second power of the pump intensity and first power of probe (at Stokes wavelength) intensity. Accordingly a probe wavelength (λ_{St}), in a Raman active (gain) medium, is amplified in the presence of a pump wavelength (λ_P) if the energy difference in between the two wavelengths is equal to the Raman shift of the material of the medium. This is explained in the schematic in figure 1.5. The probe beam while propagating in the medium, experiences attenuation and as a result the intensity of beam coming out of the medium is less than the intensity of light going into the medium. In the presence of a pump beam, the intensity of the probe beam coming out of the

medium could be greater than the intensity of the probe beam coming out without the pump beam if the difference in the energy of pump and probe photons is equal to the Raman shift of the medium. This apparent increase in intensity is because of SRS. If the losses in the system are minimized enough and the length of the medium is long enough, then the intensity of the probe beam coming out of the cavity could be greater than the intensity going in, leading to a net gain. This happens when the gain from SRS is greater than the cavity losses. To convert this gain from SRS into a laser, mirrors can be placed on either side of the cavity to keep the probe beam into the medium leading so that it can experience gain leading to build up of intensity of the probe beam resulting in lasing (assuming net roundtrip gain is positive).

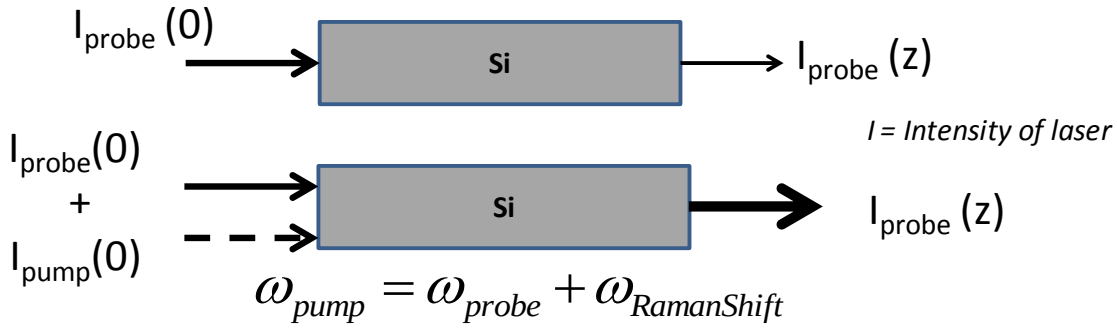

Figure 1.5: Schematic showing Stimulated Raman Scattering

Typically in operation of a Raman laser, only a pump beam is used. Stokes scattered wave acts as the probe beam and is amplified as a result of Raman gain. Thus during SRS, Stokes intensity is super linearly dependent on the pump power experiencing gain as it propagates in the medium. The proportion of increase in Stokes emissions is greater than the proportion of increase in the pump power. From a practical point of view,

as long as the gain medium can be placed inside a cavity such that the net roundtrip gain is positive, a laser can be built. Raman scattering cross section for materials are extremely small and typically only one photon in a few million is Raman scattered. As a result the gain coefficient associated with Raman scattering is also very small. For silicon it is of the order of 10 GW/cm[19] which although is much larger than the corresponding value for silica fibers but is inherently much smaller. Just increasing the propagation distance in the gain medium is not enough to achieve Raman gain/lasing. Minimization of cavity losses is also very critical as was discussed in the last section. As a result Raman lasers typically require long propagation lengths for the gain to build up in the cavity. It is for this reason that SRS reports in nanostructures have been few.

Stimulated anti Stokes Raman Scattering (SARS) refers to the process in which the anti Stokes scattering intensity experiences a gain in the Raman medium. The anti-Stokes intensity is proportional to the second power of pump intensity and the first power of anti Stokes intensity. Conceptually it is exactly similar to SRS[29] except is observed less commonly due to much lower anti Stokes scattering cross section. One of the reasons for that is the fact that at room temperature only a small fraction of phonons are present in the higher energy levels from where they could transition to ground state to emit an anti Stokes scattered phonon. Nevertheless anti Stokes lasing has been demonstrated in $BaWO_4$ crystal by placing the crystal at an angle to the incident beam so that there is non-collinear phase matching for the generation of first anti Stokes wave from four wave mixing used pulsed pumping[30].

1.4 Relation between Raman scattering, phonon occupation number and temperature of the system

Temperature Determination from Bose Einstein distribution

Since phonons are bosons they follow the Bose Einstein distribution. Accordingly, the probability that a particle will have energy E is given by the expression:

$$f(E) = \frac{1}{Ae^{E/K_BT} - 1} \tag{1.3a}$$

where A is a constant (1 for phonons), T is the temperature and K_B is the Boltzmann constant. Since the anti Stokes and Stokes line correspond to the absorption and emission of an optical phonon, the ratio of their intensities I_{AS} and I_{St} is given by[31]:

$$\frac{I_{AS}}{I_{St}} = \frac{N_o}{N_o + 1} \tag{1.3b}$$

where No is the equilibrium occupation number of the q = 0 optical phonon of frequency ω_o is given by[34]

$$N_o = (\exp(\frac{\hbar\omega_o}{K_BT}) - 1)^{-1} \tag{1.3c}$$

where ħ is the Planck's constant. This simplifies equation 1.3b to[34]:

$$\frac{I_{AS}}{I_{St}} = \exp(\frac{-\hbar\omega_o}{K_BT}) \tag{1.3d}$$

Using this relation, the temperature of the system can be calculated by the determining by the ratio of anti Stokes scattering to Stokes scattering. Various relations similar to equation 1.3d have been suggested. And while there is agreement on the general form of this expression various proportionality constants have been proposed to replace the '1' before the exponential term[32 33 34 35 36]. Most of these expressions have been widely used by various researchers for temperature determination applications. The general form of this expression is presented in equation 1.4.

$$\frac{I_{AS}}{I_{St}} \propto \exp\left(\frac{-\hbar\omega_o}{K_B T}\right) \tag{1.4}$$

Temperature determination from change in Raman shift

Temperature of the system can also be determined by the temperature dependent phonon energy (Raman shift) or uncertainty in phonon energy which is determined by the full width half maximum (FWHM) of the Raman peak. Lattice anharmonicity typically leads to a decrease in the phonon energy and an increase in the uncertainty of the phonon energy which leads to a red shift and a broadening of the Raman peak[37 38]. For silicon, the temperature dependence of this red shift and change in FWHM is well understood and various theoretical models have been developed and verified experimentally for the same. The model developed by Balkanski et.al[39] (equations 1.5 and 1.6), has been widely used for temperature calculations from change in Raman shift for bulk silicon as well as various silicon nanostructures such as nanowires and nanocrystals[40 41 42 43].

The following relation for red shift in Raman spectra vs. temperature from this model has been used to determine temperature in the current work presented in chapters 2, 3 and 4.

$$\Delta(T) = C*(1+\frac{2}{e^{x}-1}) + D(1+\frac{3}{e^{y}-1}+\frac{3}{(e^{y}-1)^{2}}) \quad (1.5)$$

where Δ is the change in Raman shift, T is the temperature, C and D are constants and were determined to be -2.96 -0.174 by Balkanski et.al.

$$x = \frac{\hbar\omega_o}{2k_BT} \quad \text{and} \quad y = \frac{\hbar\omega_o}{3k_BT} \quad (1.6)$$

Other models relating phonon energy to temperature (for silicon) have also been proposed. One of them predicts the change in Raman shift to be .022 cm-1 for every 1K rise in temperature[44 45].

Phonons and Temperature

Temperature of a system is a measure of energy of the system. In crystalline solids, most of that energy is stored in the form of lattice vibrations. A system at a higher temperature will have more vibrational energy and the occupation number for phonons will be higher. A system at a lower temperature would have lower vibrational energy and most of the phonons will be in ground state (lower occupancy number). It follows that in order to decrease the temperature of a system, one only needs to bring phonons from higher energy state to ground state, or in other words to annihilate the phonons.

Since anti Stokes scattering involves transition of a photon from an excited state to the ground state (phonon annihilation), it leads to cooling of the system. Stokes scattering, on the other hand leads to generation of a phonon which would lead to heating. Cavity heating is a major concern for operation of Raman lasers[46] and much work has focused on decreasing the heating by increasing the anti Stokes scattering in the cavity[47 48]. If somehow the anti Stokes scattering could be enhanced in the system, the material would lose heat more quickly. But since Stokes scattering is always greater than anti Stokes scattering (because of low occupancy number) more phonons are always being generated than are being annihilated. If somehow the relative intensity of anti Stokes scattering were to be increased, it could bring about optical cooling in materials, even in indirect bandgap semi-conductors.

1.5 Localized surface plasmons and thermoplasmonics

Metal nanoparticles possess interesting optical properties because of presence of collective oscillations of electrons called plasmons. These plasmons lead to generation of high electric fields close to the metal surface, the extent of enhancement of field depending on the material, its structure and the surrounding medium. The hot electrons generated via plasmon excitation can either be used to aid electron transfer in chemical reactions[*49*] or to generate local heat for various applications such as photothermal therapy for cancer treatment, nano-surgery, photothermal drug delivery, photothermal imaging and nanochemistry[50]. There has been a growing interest in exploring various metallic nanostructures for heat generation applications.

Key developments in plasmonic structures

Gold is the most commonly used plasmonic metal because of its inert nature and its plasmonic resonance lying in the visible to infrared range[51 52]. The success of a metallic nanostructure for plasmonic applications depends on the ease with which the structure can be synthesized, the lifetime of the structure and the control it offers over tuning its properties. A variety of plasmonic structures such as nanospheres and nanorods[53], dielectric core-metallic shells[54], nanomatryushkas (metal-dielectric-metal core-shell-shell structure)[55] and metallic ring/disc cavities[56] have been engineered for various applications.

Of all of these structures, nanospheres are the easiest to synthesize. Irradiation of the light on the nanosphere at the plasmon resonance leads to high absorption and scattering efficiencies because of which they find uses as localized heat generators. The plasmon resonance depends on the diameter of the nanosphere and a larger diameter typically leads to red shifting of the plasmon resonance due to retardation effects[53]. But because of this nanospheres only allow a narrow spectrum in which the plasmon resonance wavelength could be tuned. This makes them unsuitable for a variety of nanoscale applications. It is difficult to tune the resonance wavelength to infrared regions for therapeutic applications. This problem is overcome by use of geometrically asymmetric shapes such as rods. The asymmetric shape leads to red shifting of the plasmon resonance due to retardation effects and provides a broader resonance spectrum. Resonance wavelength is typically found to change with the aspect ratio of the rods[53]. Gold nanoshells with a dielectric core allow for a wider spectrum of plasmon resonance

because of hybridized energy states of the structure. But it is hard to get plasmon resonance in the infrared regions for particles of small size[54]. Nanomatryushkas which are core-shell-shell structures of metal-dielectric-metal provide better resonance wavelength control at much smaller sizes compared to nanoshells because of additional hybridized energy states arising out of interactions in between the inner and outer metal structure. They also give the flexibility to control relative scattering and absorption cross sections by changing the diameter of inner and outer metallic structures. Having a large absorption cross section leads to generation of localized heat and applications in therapeutics[55].

Applications

Plasmonic structures have found use in a variety of biological in-vivo applications. Cognet et.al used 10 nm gold particles for protein detection in cells based on photothermal interference contrast[57]. Orozco used the heat generated from gold nanomatryushkas and gold nanoshells for treating triple negative breast cancer tumors in mice[58]. In plasmonic photothermal delivery, a therapeutic agent attached to a gold nanoparticle, which acts as the carrier, is released at the target upon laser induced heating of the nanoparticle[59]. Plasmonic nanostructures also have been used for various high temperature applications. High temperatures have been attained in plasmonic structures using laser irradiation and have been shown to promote nanowire growth[60 61]. A variety of chemical reactions have shown enhanced reaction rates either due to high temperatures attained by localized heat generation or due to generation of energetic hot electrons

which increase the speed of redox reactions[62, 63 64]. Generation of super heated water vapor/steam using focused sunlight and gold nanoparticles was also shown [65 66 67].

The ability to measure the change in temperature of the system as a result of heating induced by the plasmonic system is critical since many applications require a precise temperature control. Techniques to measure heat released or temperature change exploit change in phase[68], photoluminescence intensity[69], fluorescence polarization anisotropy[70], Raman scattering[71] or extended x-ray absorption fine structure[72]. In high temperature systems temperatures measurements have been limited to estimates being made using various chemical reactions[62, 63, 64] or Stokes/anti-Stokes ratio[66] or thermal models[60, 73] and only a few methods exits which work for temperatures beyond 100°C[74] [75]. In one the works Raman peak width of ZnO was used to measure temperature[76] but it has been shown that non-uniform heating which is likely to happen with localized heating in nanostructures, causes additional peak broadening[77] and hence may lead to an overestimation of the temperature. Fano interactions as a result of scattering of photogenerated charge carriers with phonons which is commonly observed in semi conductors may also lead to broadening of Raman peak leading[78] to additional errors in temperature determination from peak width of Raman spectrum.

Limitations in existing plasmonic structures

Majority of the work on engineering plasmonic structures has focused on tuning the plasmon resonance wavelength and little work has been done on increasing the strength of plasmonic interactions themselves which could be done by using techniques

such as increasing the effective electric field experienced by the gold particles or promoting interparticle interactions[79]. Thus the structures engineered thus far have either been completely made out of a metal or have an inactive core such as silica. While such core-shell structures lead to new hybridized energy states and have various advantages, such systems limit the interactions between the metal and electric field of the light because of the low refractive index of the core. Use of complex structures at high temperatures is undesirable since gold is known to anneal at high temperatures[80] which could not only change the plasmon resonance drastically but also destroy the complete structure itself. Thus a new strategy for plasmonic enhancement and wavelength control could be great significance. Using a high refractive material such silicon for the core in a core shell structure could have multiple advantages. The high refractive index core could confine light to extremely small energy densities which could increase the degree of plasmonic excitations. An active core could also provide temperature measuring capability which could be extremely important in the field of catalysis.

Chapter 4 discusses the work done on silicon-gold cavities that have been fabricated to enhance the plasmonic interactions in gold and the temperature measuring capabilities of these cavities.

1.6 Current work

In the current work, interactions in between phonons, photons, electrons and plasmons have been engineered by changing the structure and size of silicon nanowire cavities. Chapter 2 discusses the effects of cavity modes on nonlinear optical properties

of silicon such as stimulated Stokes Raman scattering and stimulated anti Stokes Raman scattering. Alignment of the cavity mode with either of Stokes or anti Stokes wavelength and the pump wavelength leads to strong confinement of electric field intensity inside the nanowire which decreases the threshold for Raman non linear effects. A metallic layer on of silicon helps the cavity dissipate heat faster. Fano interactions can also be tuned by choosing an adequate metallic layer. Chapter 3 discuss the effects of selectively tuning the cavity mode with either one of Stokes or anti Stokes wavelength on the anti Stokes to Stokes scattering ratio.

In chapter 4 the discussion moves away from non linear optics onto plasmonics. The chapter investigates how the intense electric field inside the silicon nanowire at cavity mode resonance can be used to excite strong localized surface plasmons in thin plasmonic metallic films covering the nanowire and its effect on the cavity temperature.

---

[1] Nawrocki, W. Physical limits for scaling of integrated circuits. *J. Phys. Conf. Ser.* **248,** 012059 (2010).

[2] http://www.intel.com/content/www/us/en/silicon-innovations/standards-14nm-explained-video.html.

[3] Alduino, A. & Paniccia, M. Interconnects: Wiring electronics with light. *Nat. Photonics* **1,** 153–155 (2007).

[4] Sze, S.M. & Kwok K.N. Physics of semi conductor devices, third edition. (2006).

[5] Fang, Z., Chen, Q. Y. & Zhao, C. Z. A review of recent progress in lasers on silicon. *Opt. Laser Technol.* **46,** 103–110 (2013).

[6] Reed, G., Mashanovich, G., Gardes, F. & Thomson, D. Silicon optical modulators. *Nat. Publ. Gr.* **4,** 518–526 (2010).

[7] Leuthold J., Koos C., Freude W. Nonlinear silicon photonics. Nature Photonics **4**, 535-544 (2010).

[8] www.intel.com.

[9] Paniccoa, M. Integrating Silicon photonics. *Nat. Photonics* **4,** 498–499 (2010).

[10] Miller, D. A. B. Device requirements for optical interconnects to silicon chips. *Proc. IEEE* **97,** 1166–1185 (2009).

[11] Rong, H. *et al.* Monolithic integrated Raman silicon laser. *Opt. Express* **14,** 6705–6712 (2006).

[12] Paniccia, M. Integrating Silicon photonics. Nature Photonics **4**, 498-499 (2010).

[13] Liang D. & Bowers J.E. Recent progress in lasers on silicon. Nature Photonics **4**; 511-517 (2010).

[14] Rong, H., Liu, A., Nicolaescu, R. & Paniccia, M. J. Raman gain and nonlinear optical absorption measurements in a low-loss silicon waveguide. *Appl. Phys. Lett.* **85,** 2196–2198 (2004).

[15] Liang, T. K. & Tsang, H. K. Role of free carriers from two-photon absorption in Raman amplification in silicon-on-insulator waveguides. *Appl. Phys. Lett.* **84,** 2745–2747 (2004).

[16] Liu, A., Rong, H., Paniccia M. et.al Net optical gain in a low loss silicon-on-insulator waveguide by stimulated Raman scattering. Optics Express **12** (18), 4261-4268 (2004).

[17] Boyraz, O. & Jalali, B. Demonstration of a silicon Raman laser. Optics Express **12** (21), 5269-5273 (2004).

[18] Liang, T. K. & Tsang, H. K. Efficient Raman amplification in silicon-on-insulator waveguides. *Appl. Phys. Lett.* **85,** 3343–3345 (2004).

[19] Jones, R., Rong, H., Liu, A. et.al. Net continuous wave optical gain in a low loss silicon-on-insulator waveguide by stimulated Raman scattering. Optics Express **13** (2), 519-525 (2005).

[20] Rong, H., Jones, R., Liu, A. et.al. A continuous-wave Raman silicon laser. Nature **433**, 725-728 (2005).

[21] Rong, H., Kuo, Y., Xu, S. et.al. Monolithic integrated Raman silicon laser. Optics express **14** (15), 6705-6712 (2006).

[22] Rong, h., Xu, S., Cohen, O. et.al. A cascaded silicon Raman laser. Nature photonics **2**, 170-174 (2008).

[23] Rong, H., Xu, S., Kuo, Y. et.al. Low-threshold continuous-wave Raman silicon laser. Nature Photonics **1**, 232-237 (2007).

[24] Spuesens, T. *et al.* Improved design of an InP-based microdisk laser heterogeneously integrated with SOI. *IEEE Int. Conf. Gr. IV Photonics GFP* 202–204 (2009).

[25] Fang, A. W. *et al.* Electrically pumped hybrid AlGaInAs-silicon evanescent laser. *Opt. Express* **14,** 9203–9210 (2006).

[26] Liang, D. *et al.* Electrically-pumped compact hybrid silicon microring lasers for optical interconnects. *Opt. Express* **17,** 20355–20364 (2009).

[27] Van Campenhout, J. *et al.* A Compact SOI-Integrated Multiwavelength Laser Source Based on Cascaded InP Microdisks. *IEEE Photonics Technol. Lett.* **20,** 1345–1347 (2008).

[28] www.kosi.com.

[29] Boyd, R.W. Nonlinear optics. Third edition (2008).

[30] Wang, C. *et al.* Extracavity pumped $BaWO_4$ anti-Stokes Raman laser. *Opt. Express* **21,** 26014 (2013).

[31] Hart, T., Aggarwal, R. & Lax, B. Temperature Dependence of Raman Scattering in Silicon. *Phys. Rev. B* **1,** 638–642 (1970).

[32] Tsu, R. & Hernandez, J. G. Temperature dependence of silicon Raman lines. *Appl. Phys. Lett.* **41,** 1016–1018 (1982).

[33]Fujimori, H., Kakihana, M., Ioku, K., Goto, S. & Yoshimura, M. Advantage of anti-Stokes Raman scattering for high-temperature measurements. *Appl. Phys. Lett.* **79,** 937–939 (2001).

[34]Jellison, G. E., Lowndes, D. H. & Wood, R. F. Importance of temperature-dependent optical properties for Raman-temperature measurements for silicon. *Phys. Rev. B* **28,** 3272–3276 (1983).

[35] Gupta, R., Xiong, Q., Adu, C. K., Kim, U. J. & Eklund, P. C. Laser-induced fano resonance scattering in silicon nanowires. *Nano Lett.* **3,** 627–631 (2003).

[36]Doerk, G. S., Carraro, C. & Maboudian, R. Temperature dependence of Raman spectra for individual silicon nanowires. *Phys. Rev. B* **80,** 073306 (2009).

[37] Ipatova, I. P., Maradudin, A. A. & Wallis, R. F. Temperature dependence of the width of the fundamental lattice-vibration absorption peak in ionic crystals. II. Approximate numerical results. *Phys. Rev.* **155,** 882–895 (1967).

[38] Haro, E., Balkanski, M. Wallis, R.F. & Wanser K.H. Theory of the anharmonic damping and shift of the Raman mode in silicon. Physical Review B **34**(8), 5358-5367 (1986).

[39]M. Balkanski, R. F. Wallis, ' and E. Haro . Anharmonic effects in light scattering due to optical phonons in silicon. Physical Review B **28** (4), 1928- 1934 (1983).

[40] Konstantinović, M. *et al.* Raman scattering in cluster-deposited nanogranular silicon films. *Phys. Rev. B* **66,** 161311–1–4 (2002).

[41] Niu, J., Sha, J. & Yang, D. Temperature dependence of the first-order Raman scattering in silicon nanowires. *Scr. Mater.* **55,** 183–186 (2006).

[42]Piscanec, S. *et al.* Raman spectroscopy of silicon nanowires. *Phys. Rev. B* **68,** 2–5 (2003).

[43] Adu, K. W., Gutiérrez, H. R., Kim, U. J. & Eklund, P. C. Inhomogeneous laser heating and phonon confinement in silicon nanowires: A micro-Raman scattering study. *Phys. Rev. B - Condens. Matter Mater. Phys.* **73,** 1–9 (2006).

[44] Doerk, G. S., Carraro, C. & Maboudian, R. Temperature dependence of Raman spectra for individual silicon nanowires. *Phys. Rev. B* **80,** 073306 (2009).

[45] Khachadorian, S., Scheel, H., Colli, A., Vierck, A. & Thomsen, C. Temperature dependence of first- and second-order Raman scattering in silicon nanowires. *Phys. Status Solidi* **247,** 3084–3088 (2010).

[46] Koechner, W. Solid-state laser engineering. Fourth Edition (1996).

[47] Vermeulen, N., Debaes, C., Muys, P. & Thienpont, H. Mitigating Heat Dissipation in Raman Lasers Using Coherent Anti-Stokes Raman Scattering. *Phys. Rev. Lett.* **99,** 093903 (2007).

[48] Vermeulen, N., Debaes, C. & Thienpont, H. Coherent anti-stokes Raman scattering in Raman lasers and Raman wavelength converters. *Laser Photonics Rev.* **4,** 656–670 (2010).

[49]Christopher, P., Xin, H. & Linic, S. Visible-light-enhanced catalytic oxidation reactions on plasmonic silver nanostructures. Nature Chemistry **3**, 467–472 (2011).

[50]Baffou, G. & Quidant, R. Thermo-plasmonics: using metallic nanostructures as nano-sources of heat. Laser & Photonics Reviews **7**(2), 171–187 (2013).

[51]Wang, H., Levin, C.S. & Halas N.J. Nanosphere Arrays with Controlled Sub-10-nm Gaps as Surface-Enhanced Raman Spectroscopy Substrates. Journal of the American Chemical Society **127**(43), 14992-14993 (2005).

[52]Cao, L., Barsic, D.N., Guichard, A.R. & Brongersma M.L. Plasmon-Assisted Local Temperature Control to Pattern Individual Semiconductor Nanowires and Carbon Nanotubes. Nano Letters **7**(11), 3523–3527 (2007).

[53] Link S., El-Sayed M.A.; Shape and size dependence of radiative, non-radiative and photothermal properties of gold nanocrystals ; International Reviews in Physical Chemistry **19** (3), 409-453 (2000).

[54] Oldenburg S.J., Averitt R.D., Westcott S.L., Halas N.J.; Nanoengineering of Optical Resonances; Chemical Physics Letters **288**, 243-247 (1998).

[55] Bardhan R., Mukherjee S., Halas N.J.; Nanosphere-in-a-nanoshell: A simple nanomatryushka; Journal of Physical Chemistry C **114**, 7378-7383 (2010).

[56] Hao F., Nordlander P., Maier S.A. et.al; Tunability of Subradiant Dipolar and Fano-Type Plasmon Resonances in Metallic Ring/Disk Cavities: Implications for Nanoscale Optical Sensing; ACS Nano **3** (3), 643-652 (2009).

[57] Cognet L., Tardin C., Boyer D., Choquet D., Tamarat P., Lounis B.; Single metallic nanoparticle imaging for protein detection in cells; PNAS **100** (20); 11350-11355 (2003).

[58] Ayala-Ozorco C., Urban C., Joshi A. et.al; Au Nanomatryoshkas as Efficient Near-Infrared Photothermal Transducers for Cancer Treatment: Benchmarking against Nanoshells; ACS Nano **8** (6), 6372-6381 (2014).

[59] Baffou G., Quidant R.; Thermo-plasmonics: using metallic nanostructures as nano-sources of heat; Laser and Photonics Reviews **7**(2), 171-187 (2013).

[60] Cao L., Barsic D.N., Guichard A.R., Mark L. Brongersma M.L.; Plasmon-Assisted Local Temperature Control to Pattern Individual Semiconductor Nanowires and Carbon Nanotubes; Nano Letters **7** (11), 3523–3527 (2007).

[61] Boyd D.A., Greengard L.,Brongersma M., El-Naggar M.Y., Goodwin D.G.; Plasmon-Assisted Chemical Vapor Deposition; Nanoletters **6** (11), 2592-2597 (2006).

[62] Adleman J.R., Boyd D.A., Goodwin D.G., Psaltis D.; Heterogeneous catalysis mediated by plasmon heating; Nano Letters **9** (12), 4417–4423 (2009).

[63] Fasciani C., BuenoAlejo C.J., Scaiano J.C. et.al; High-Temperature Organic Reactions at Room Temperature Using Plasmon Excitation: Decomposition of Dicumyl Peroxide; Organic Letters **13** (2), 204-207 (2011).

[64]Haas K.M., Lear B.J. ; Degradation of polypropylene carbonate through plasmonic heating; Nanoscale **5**, 5247-5251 (2013).

[65]Carlson M.T., Green A.J., Richardson H.H.; Superheating Water by CW Excitation of Gold Nanodots; Nanoletters **12** (3), 1534-1537 (2012).

[66]Fang Z., Zhen Y., Halas N.J. et.al; Evolution of Light-Induced Vapor Generation at a Liquid-Immersed Metallic Nanoparticle; Nanoletters **13** (4), 1736-1742 (2013)

[67]Baral S., Green A.J., Richardson H.H. et.al; Comparison of Vapor Formation of Water at the Solid/Water Interface to Colloidal Solutions Using Optically Excited Gold Nanostructures; ACS Nano **8**(2), 1439-1448 (2014).

[68] Govorov A.O., Zhang W., Kotov N.A. et.al ; Gold nanoparticle ensembles as heaters and actuators: melting and collective plasmon resonances; Nanoscale Research Letters **1**(1), 84-90 (2006).

[69] Lee J., Govorov A.O., Kotov N.A.; Nanoparticle Assemblies with Molecular Springs: A Nanoscale Thermometer; Angewandte Chemie **44** (45), 7439-7442 (2005).

[70] Baffou G., Kreuzer M.P., Kulzer F., Quidant R.; Temperature mapping near plasmonic nanostructures using fluorescence polarization anisotropy; Optics Express **17** (5), 3291-3298 (2009).

[71] Govorov A.O., Richardson H.H.; Generating heat with metal nanoparticles; Nanotoday **2** (1), 30-38 (2007).

[72] Broek B.V., Grandjean D., Van Bael M.J. et.al; Temperature determination of resonantly excited plasmonic branched gold nanoparticles by X-ray absorption spectroscopy; Small **7** (17), 2498-2506 (2011).

[73] Carlson M.T., Khan A., Richardson H.H.; Local Temperature Determination of Optically Excited Nanoparticles and Nanodots; Nanoletters **11** (3) , 1061-1069 (2011).

[74] Setoura K., Werner D., Hashimoto S.; Optical Scattering Spectral Thermometry and Refractometry of a Single Gold Nanoparticle under CW Laser Excitation; The Journal of Physical Chemistry C **116** (29), 15458-15466 (2012).

[75]Baffou G., Polleux J., Rigneault H., Monneret S.; Super-Heating and Micro-Bubble Generation around Plasmonic Nanoparticles under cw Illumination; The Journal of Physical Chemistry C **118** (9), 4890-4898 (2014).

[76]Wang C., Matranga C. et.al; Visible light plasmonic heating of Au–ZnO for the catalytic reduction of CO2; Nanoscale **5**, 6968-6974 (2013).

[77] Piscanec S., Robertson J. et.al; Raman spectroscopy of silicon nanowires; Physical Review B **68** (241312), (2003).

[78] Gupta, R., Xiong, Q., Adu, C. K., Kim, U. J. & Eklund, P. C. Laser-induced fano resonance scattering in silicon nanowires. *Nano Lett.* **3,** 627–631 (2003).

[79] Wang, H., Levin, C.S. & Halas N.J. Nanosphere Arrays with Controlled Sub-10-nm Gaps as Surface-Enhanced Raman Spectroscopy Substrates. Journal of the American Chemical Society **127**(43), 14992-14993 (2005).

[80] Karakouz, T., Maoz, B.M., Lando, G., Vaskevich, A. & Rubinstein I. Stabilization of Gold Nanoparticle Films on Glass by Thermal Embedding. Applied Materials and Interfaces **3**(4), 978-987, (2001).

CHAPTER 2: STIMULARED RAMAN SCATTERING IN SILICON NANOWIRES

2.1: SRS in nanostructures

Work on SRS in silicon nanostructures has been limited to gain in silicon rich silicon oxide films[1 2]. But in these studies, the actual enhancement in Raman scattering is extremely small and the mechanism of Raman gain was not explained. Moreover the hetero structures used are difficult for monolithic integration. Low threshold Raman lasing was observed in silicon photonic crystals which had an effective quality factor of 10^{11} [3]. In homogeneous microstructures, SRS has been observed in GaP nanowires[4], and carbon nanotubes (CNTs)[5]. The work on GaP wires used nanorods made from focused ion beam milling (FIB) of GaP nanowires which led to significant wire damage. Raman gain was reported to increase with a decrease in the nanorod length and was related to the theory developed for spherical microcavity lasers. Work done on SRS on CNTs reported the Raman gain to be a few orders higher than in bulk but the actual enhancement in Raman scattering intensity was extremely small and there was significant damage to the CNTs in the process because of heating. Significant heating of the gain medium was reported in each of the works, indicating that it could be an issue while performing SRS measurements on nanostructures.

2.2 Motivation

Till date there have been no reports of SRS in homogeneous silicon nanostructures. But as was discussed in chapter 1, SRS/Raman lasing in monolithically integratable silicon nanostructures would mark a significant development in the field of silicon photonics that could lead to the next generation of ultrafast low energy devices. Recently resonant silicon nanowire cavities were shown to emit bright white light[6]. While silicon is in indirect bandgap material, the optical properties were tuned by cavity engineering to enable white light emissions. Similarly other exciting properties in silicon nanowires such as voltage-tunable circular photogalvanic effect were also shown[7]. Silicon nanowires are easy to synthesize and given their one dimensional structure, they should be easy to integrate with the existing CMOS devices. Recently published work has indicated that reducing the waveguide dimensions could increase the Raman nonlinearities in silicon and also decrease carrier lifetime leading to a decrease in non-linear absorption[8].

In the current work Raman measurements on silicon nanowire cavities have been performed and possibility of achieving SRS and other non linear optical processes has been explored. Cavities of varying nanowire diameter and different structures have been fabricated and Raman measurements using two different wavelengths have been performed. The details are presented below.

2.3: Cavity fabrication and experimental details

Silicon nanowires were procured from Sandia National Laboratories where they were grown on a gold catalyst via vapor liquid solid mechanism. These nanowires were transferred onto a cover glass slip. Experiments were either conducted on these nanowires (bare) or a thick metal layer (either gold or silver) was deposited on these wires using electron beam deposition (PVD 75, Kurt J. Lesker Company) at a low deposition rate of 0.2 Å/s for the first 10 nm and 1.0 Å/s for the remaining film. The thickness of the metal was selected to be approximately 1.5 times the diameter of the silicon nanowire to form a thick conformal layer of metal on the nanowire without leaving any exposed nanowire areas. This ensured that light did not leak through the metal and that a thick uniform heat sink was available to the entire nanowire circumference allowing the nanowire to effectively dissipate heat. Experiments were performed on nanowires in the diameter range 50 nm to 400 nm to cover a broad range of spectrum. To measure the diameter of the wires, the gold layer was etched using a TFA gold etchant after all the optical measurements had been made. Following this a thin less than 10 nm thick gold/palladium layer was sputter coated onto the sample and high resolution scanning electron microscopy (JOEL 7500F) was performed. In some cases, diameter of the bare nanowire was measured using an Atomic Force Microscopy (Asylum AFM). It was also observed that the silicon nanowires had a 2 nm thick native oxide layer on the circumference[9].

Raman spectroscopy was performed at room temperature in backscattering geometry via a confocal set up (Ntegra, NTMDT) using either a 532 nm (Compass 315M,

Coherent) or a 659.4 nm (Flamenco, Cobolt) laser. For temperature dependent measurements, a thermoelectric heating stage was used. For measurements on bare nanowires, the nanowire cavity was excited from the nanowire side. Measurements on cavities with a thick metal layer around the nanowire were done by laser excitation through the cover glass slip. Raman scattered spectrum was detected using an Andor charge coupled detector maintained at a temperature of -50^{o} C. The spectral resolution of the grating used was ~ 0.5 cm^{-1}at 532 nm and 0.2 cm^{-1} at 660 nm when only one of either Stokes or anti Stokes spectrum was recorded. A coarser grating was required when both Stokes and anti-Stokes spectra was recorded. The resolution of this grating was 1.5 cm^{-1} at 532 nm and 0.6 cm^{-1} at 660 nm. Power dependent measurements were carried out with the power ranging from 5E3 W/cm^2 to 10^6 W/cm^2 with the 532 nm laser and from 5E3 W/cm^2 to 4E6 W/cm^2 with the 660 nm laser which was the maximum power possible for each of these lasers. Spot size was ~ 1μm in diameter. Laser power measurements were done on the sample stage after removing the objective lens. Transmission coefficient of the objective lens was calculated by measuring the power with and without the objective lens at low powers. Experiments were typically performed with the polarization of the incident electric field parallel to the nanowire long axis (TM polarization) to maximize the electric field intensity inside the nanowire. In some cases, experiments were also performed with the electric field polarization perpendicular to the nanowire long axis (TE polarization). Unless otherwise mentioned, the results discussed below would correspond to excitation in TM polarization. Device and cavity schematics for bare and metal coated nanowires have been presented in figure 2.1 and figure 2.2 respectively. A scanning

electron microscope image of the cavity (silicon nanowire coated with a 360 nm gold layer) cross section obtained after focused ion beam milling is shown in figure 2.3.

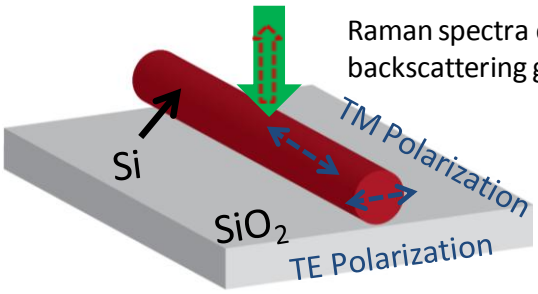

Figure 2.1: Schematic of Raman measurements on a bare nanowire

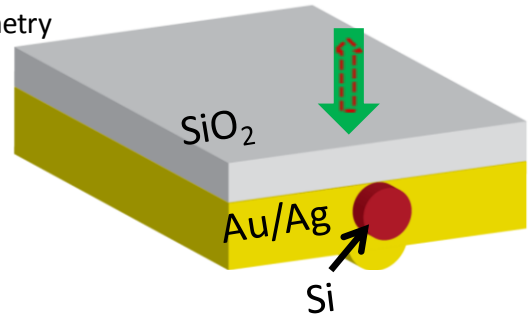

Figure 2.2: Schematic of Raman measurements on a metal coated nanowire

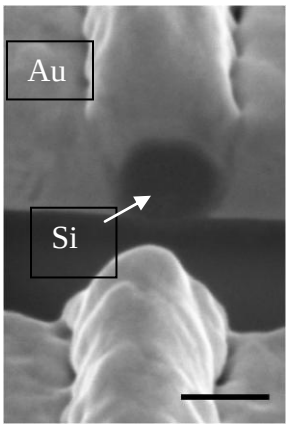

Figure 2.3: Scanning electron microscopy image of the cross section of a silicon nanowire coated with 360 nm gold. Scale bar is 200 nm.

The Raman spectrum of silicon is best described by a Lorentzian fit[10] (equation 2.1) but at high pump powers, scattering of photoexcited charge carriers from the lattice leads to an asymmetric fano broadening of the line shape[11]. Asymmetry in such cases is described by the asymmetry parameter q defined in equation 2.2[12].

$$I(\omega) = A * \frac{1}{1+x^2} \text{ ; where } x = \frac{(\omega - \omega_o)}{\Gamma/2} \quad (2.1)$$

$$I(\omega) = A * \frac{(q+\varepsilon)^2}{(1+\varepsilon^2)} \text{ ; where } \varepsilon = \frac{(\omega - \omega_o)}{\Gamma} \quad (2.2)$$

where I is the scattering intensity, A is a constant. In equation 2.1, ω_o is the phonon frequency, Γ is the line width. In equation 2.2, ω_o is the renormalized or dressed phonon frequency in the presence of the couple scattering, q is the asymmetry parameter (1/q is referred to as the coupling strength), Γ is the line width parameter and is related to the phonon lifetime.

In the current work, to best describe the experimental data, both fano and lorentzian profiles were tried to fit with the experimental data and the profile giving a better fit was selected. Details of fano interactions will be discussed a little later. Using the fano/lorentzian fits, the peak position, peak width and other parameters were calculated. Increase in the temperature of nanowire was calculated by the change in Raman shift of silicon at different laser powers. Heating typically leads to a decrease in the value of Raman shift due to phonon softening[13]. At higher temperatures, the atoms in the lattice move away from each other because of thermal expansion which decreases the attractive force in between them, leading to a decrease in the bond strength, which leads to a decrease in the phonon energy (Raman shift). This dependence of Raman shift on temperature has been characterized by Balkanski et.al[13] and has been used to determine the temperature of silicon in the current work.

$$\Delta(T) = C*(1+\frac{2}{e^{x}-1}) + D(1+\frac{3}{e^{y}-1}+\frac{3}{(e^{y}-1)^{2}}) \quad (2.3)$$

where Δ is the change in Raman shift, T is the temperature, C and D are constants and were determined to be -2.96 and -0.174 respectively by Balkanski et.al.

$$x = \frac{\hbar\omega_o}{2k_B T} \quad \text{and} \quad y = \frac{\hbar\omega_o}{3k_B T} \quad (2.4)$$

Similarly the change in full width at half maximum (FWHM or peak width) was found to be dependent on the temperature by the following relation:

$$\Gamma(T) = A(1+\frac{2}{e^{x}-1}) + B(1+\frac{3}{e^{y}-1}+\frac{3}{(e^{y}-1)^{2}}) \quad (2.5)$$

where Γ if the change in FWHM, A and B are constants and were determined to be 1.295 and 0.105 respectively, and other variables are the same as in equation 2.3. In the current work, this relation has been used to calculate the expected FWHM value calculated at the temperature determined from experimentally measured Raman shift and equation 2.3. The FWHM value obtained from equation 2.5 is then compared to the experimentally obtained FWHM value. This comparison lends credibility to the temperature calculations from equation 2.3 and provides insights about certain aspects such as fano broadening of the peak and non uniform heating in the nanowire.

Numerical calculations were performed using the finite-difference time-domain methodology using a commercially available software (Lumerical) for bare, gold and silver coated silicon nanowires using a Gaussian wave and were set up to best mimic the

experimental conditions. From the analytical calculations spatial distribution of electric field inside and outside the silicon nanowire was obtained. From the spatial distribution, average and maximum electric field intensity inside the silicon nanowire were calculated at the pump, Stokes and anti Stokes wavelength, for various nanowire sizes and cavity combinations. Native oxide layer thickness was set to 2 nm in designing cavity structure for simulations.

Experiments and computational simulations were also performed on a bulk silicon wafer to compare the results with those of a nanowire/cavity.

2.4: Optical Measurements on bulk silicon and bare silicon nanowires

Figure 2.4a shows the power dependent Raman spectra of a silicon wafer (bulk silicon) collected with a 660 nm laser excitation. The spectrum is centered at 521 cm^{-1} as expected and fits a Lorentzian peak very well (at low powers). Although it is difficult to notice on visual inspection but at high pump powers, the Raman peak experiences asymmetric broadening. This is because of (photoexcited) charge carriers scattering from lattice leading to fano resonance and has been previously reported as well[14 15]. Since the wavelength of laser that is used to excite silicon is above the bandgap of silicon (1.12 eV)[16]; the absorption is high which leads to high charge carrier concentration. Integrated peak intensity calculated from the fano fits (figure 2.4) shows a sub-linear dependence of Stokes scattering intensity on laser power. Ideally in the absence of non-linear losses or Stokes Raman scattering intensity is linearly dependent on pump power[17]. But because of high losses at higher powers, the dependence becomes sublinear. This intensity vs. pump

power represents the general trend of Raman scattering in bulk silicon and the net negative gain highlights the problem in making a Raman laser from bulk silicon. To achieve lasing, the net gain should be positive.

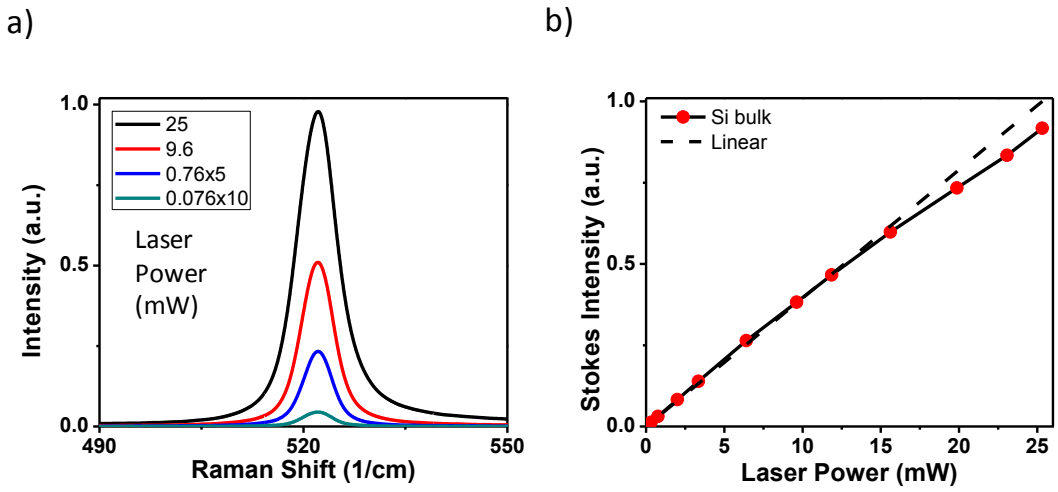

Figure 2.4: a) Power dependent Stokes Raman spectra of bulk Silicon using a 660 nm pump; b) Integrated Stokes intensity vs. pump power for bulk silicon. The dashed line represents the linear extrapolation of Stokes intensity from the lowest laser power.

The strength of the fano interactions is judged by the coupling strength, which is the inverse of the asymmetry parameter (q), and has been shown in figure 2.5a. A smaller 1/q value corresponds to weaker fano interactions or lower scattering of charge carriers from phonons leading to only a small amount of asymmetric broadening. Higher scattering leads to a higher asymmetric broadening and a higher 1/q value. In figure 2.5a, the asymmetry increases with increase in laser power because of higher concentration of photoexcited charge carriers at higher laser powers which would lead to more scattering and an increase in the fano interaction parameter. Fano interactions are observed at

Stokes side and at anti Stokes side with similar 1/q values (not shown here for the sake of redundancy). Moreover a positive value of 1/q and broadening at the higher Raman shift side point to electrons being the majority charge carriers. This observation agrees well with the previously reported studies on fano interactions in silicon[18]. It must be noted that there is hardly any shift in the Raman peak position at higher laser powers (figure 2.4a). Figure 2.5b shows the temperature and FWHM dependence of Raman on bulk silicon wafer. As expected because of the small change in the Raman peak position there is only a small change in temperature of silicon wafer even up to pump powers of 2.5E6 W/cm^2. The heat generated in the system because of absorption is dissipated quickly because of availability of a large heat sink (large and thick silicon wafer compared to ~ 1 µm spot size and 1 µm penetration depth of pump wavelength). The FWHM values increase with an increase in laser powers even because of increase in fano interactions which cause asymmetric broadening of the Raman peak.

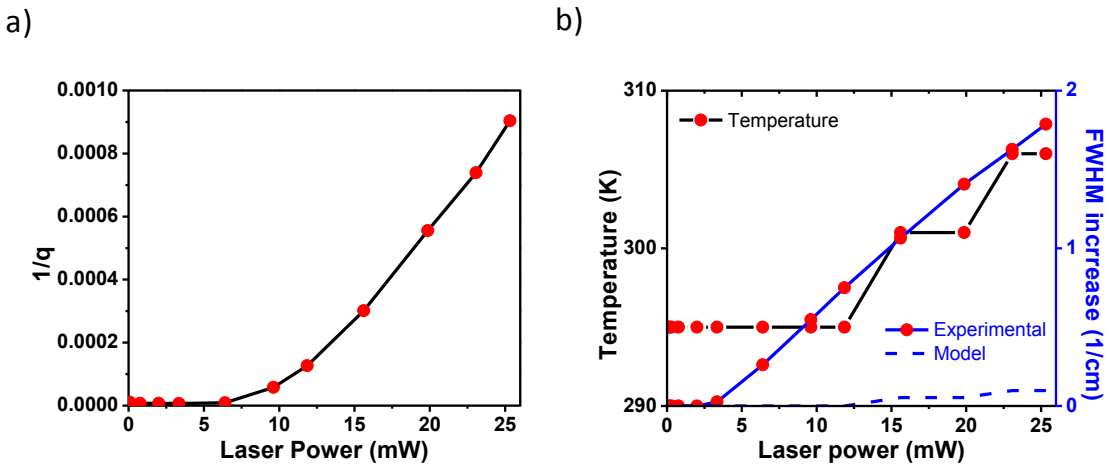

Figure 2.5: a) Fano coupling factor 1/q vs. laser power for bulk silicon with a 660 pump; b) Temperature (left vertical axis) and FWHM increase (right vertical axis) vs. pump power for bulk silicon.

FDTD calculations done to investigate the electric field intensity inside the silicon wafer revealed that the electric field intensity (at 660 nm) inside the sample, decreased with increasing depth in the sample (figure 2.6a). This is because as the wave penetrates into the sample, losses such as absorption decrease the electric field intensity. Moreover, the average intensity inside the silicon wafer was only ~8% of the applied electric field intensity at pump and at Stokes wavelength (figure 2.6b).

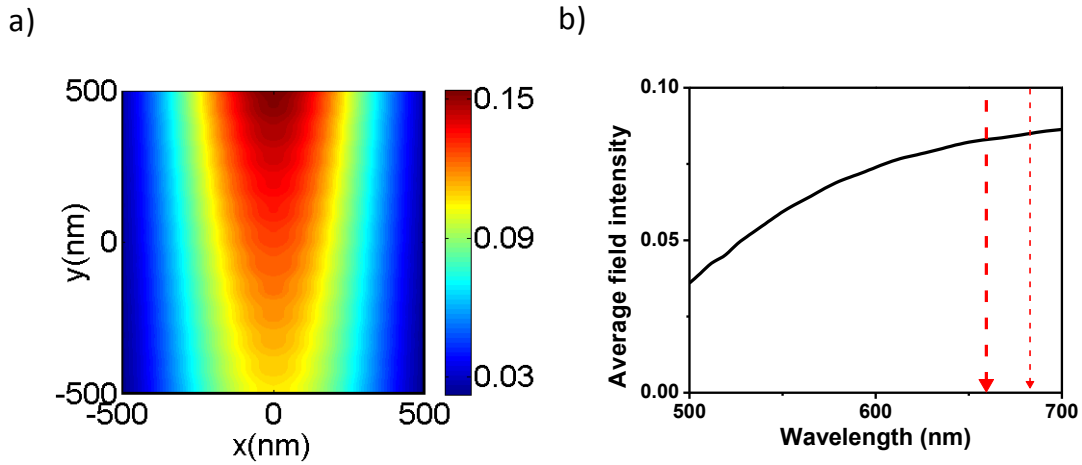

Figure 2.6: Electric field intensity distribution in bulk silicon. a) Spatial distribution of electric field intensity inside the cavity at 660 nm; b) Average electric field intensity inside silicon as a function of wavelength. The thick left vertical dashed line represents the position of pump wavelength and the thin right vertical dashed line represents the position of Stokes wavelength.

Raman spectroscopy performed on silicon nanowires gave very different results from those in bulk silicon depending on the diameter of the nanowire and the excitation wavelength. Figure 2.7a shows the Raman spectra of a bare silicon nanowire of diameter 100 nm excited at 532 nm in TM polarization. With an increase in laser power, a red shift and a broadening of the peak are seen, alluding to heating of the nanowire at higher laser

powers. Integrated intensity calculations (figure 2.7b) revealed that Stokes intensity was super linearly dependent on pump power in contrast with the trend observed in bulk silicon. A plot of pump power vs. Stokes intensity in the log-log space (figure 2.7c) revealed a slope greater than 1 at pump powers as low as 3E4 W/cm^2 which indicates the onset of SRS. A log-log plot of pump power vs. Stokes intensity slope should have a slope of 1 (or less than 1) for spontaneous Raman scattering since Stokes intensity is (at best) linearly dependent on pump power. At higher laser power slope as high as 1.76 is observed pointing to stronger SRS. This indicates that at higher pump power Stokes scattering intensity is proportional to ~ the second power of pump. This is the first time SRS has been observed in a silicon homogeneous nanostructure and is also the lowest reported threshold for SRS in any homogeneous silicon structure. A plot of the asymmetry parameter vs. laser power (figure 2.7d) revealed much higher asymmetry in nanowire compared to in bulk at much lower pump power (.003 at 5E5 W/cm^2 in nanowire compared to .0009 at 2.5E6 W/cm^2 in bulk). At higher pump power the asymmetry parameter starts to decrease again. This is most likely due to a large increase in the temperature of the nanowire.

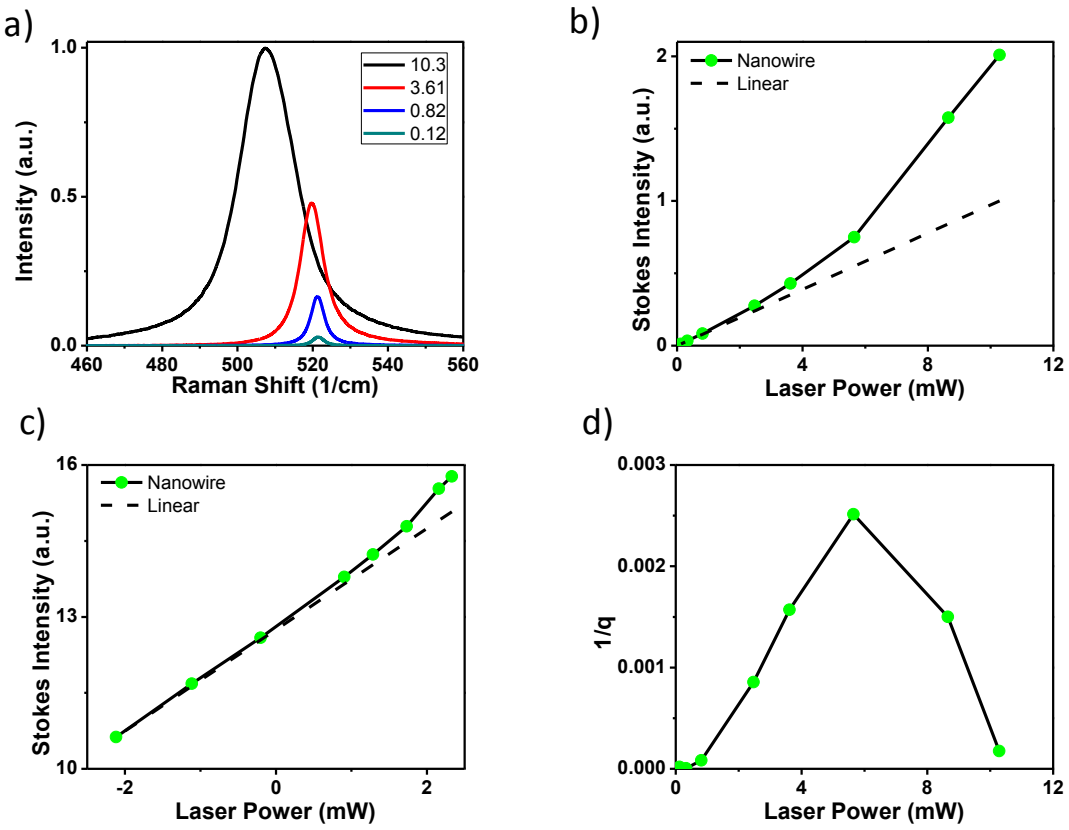

Figure 2.7: Raman spectroscopy of bare silicon nanowire of diameter 100 nm with a 532 nm pump. a) Power dependent Raman spectra; b) Integrated Stokes Raman intensity as a function of laser power; c) Integrated Stokes Raman intensity vs. laser power in log-log scale; d) Asymmetry parameter 1/q vs. laser power

To understand the nature of this SRS, FDTD calculations were done to understand the electric field confinement inside the silicon nanowire. Calculations revealed (figure 2.8a) that the electric field intensity is very tightly confined (high average electric field intensity) inside the nanowire compared to bulk. There is also a cavity mode at 547 nm (Stokes wavelength) leading to extremely high electric field intensity at Stokes wavelength. The average electric field inside the cavity is also very high at 532 nm. Compared to bulk silicon this represents almost a thirtyfold enhancement in average

electric field intensity inside the cavity at Stokes as well as pump wavelength (~1.5 in nanowire vs. ~0.05 in bulk-figure 2.6b). Since SRS intensity is proportional to the product of electric field intensity at Stokes and at pump wavelength, this enhancement should bring down the threshold for SRS by about three orders of magnitude. Calculations for spatial electric field distribution inside the cavity (fig. 2.8b) reveal the presence of TM_{21} mode at the Stokes wavelength with the electric field mode lying inside the nanowire cavity. Thus as a result of the high confinement brought about by the nanowire cavity, nanowire silicon experiences a much higher electric field compared to in bulk-silicon leading to SRS being observed at much lower powers.

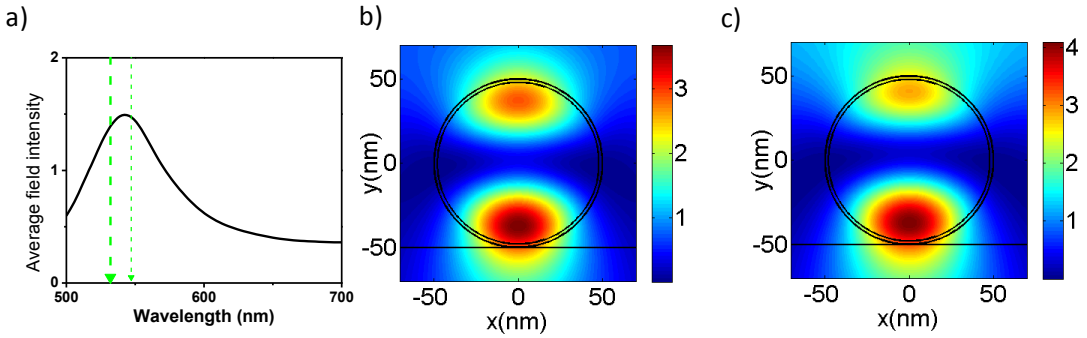

Figure 2.8: Electric field intensity distribution inside a bare silicon nanowire of diameter 100 nm. a) Average electric field intensity inside the silicon nanowire as a function of pump wavelength. Vertical dashed lines represent pump and Stokes wavelength from left to right; b, c) Spatial electric field intensity distribution inside the silicon nanowire at pump (532 nm) and at Stokes wavelength (547 nm) respectively. Circles represent silicon nanowire cross section. Inner core corresponds to the silicon nanowire and outer shell corresponds to the 2 nm thick silicon oxide layer. The horizontal straight line represents the substrate/air interface.

The high electric field intensity inside the medium also leads to high absorption in cavity. Since silicon is an indirect bandgap material most of this absorbed light is emitted

non-radiatively[19], generating heat which could cause cavity heating. Stokes scattering leads to generation of phonons which also lead to increase in the temperature of nanowire. This is evident in the red shift and peak broadening of the Raman peak at higher laser powers. Cavity temperature calculations done using the model proposed by Balkanski et.al[13] revealed an increase in cavity temperature with increasing pump power with peak temperature close to 850 K at a pump power of ~10^6 W/cm^2 (figure 2.9a). A comparison of increase in FWHM values measured experimentally and those predicted by the Balkanski model at corresponding temperature revealed that that experimental FWHM values were much larger. Such broader peaks have been observed previously during laser heating of nanowires and have been attributed to inhomogeneous heating in the nanowire[20 21]. A part of this increase in FWHM could also be brought about by the asymmetric fano broadening that was also observed in the nanowire although this contribution would be small since at the pump power of 10^6 W/cm^2 the asymmetry parameter is much lower than at lower powers but the mismatch in between the theoretical and experimental FWHM is much larger. It was previously discussed that the fano interaction parameter was much higher in the nanowire than in bulk. This increased asymmetry is also because of intense electric field intensity inside the nanowire.

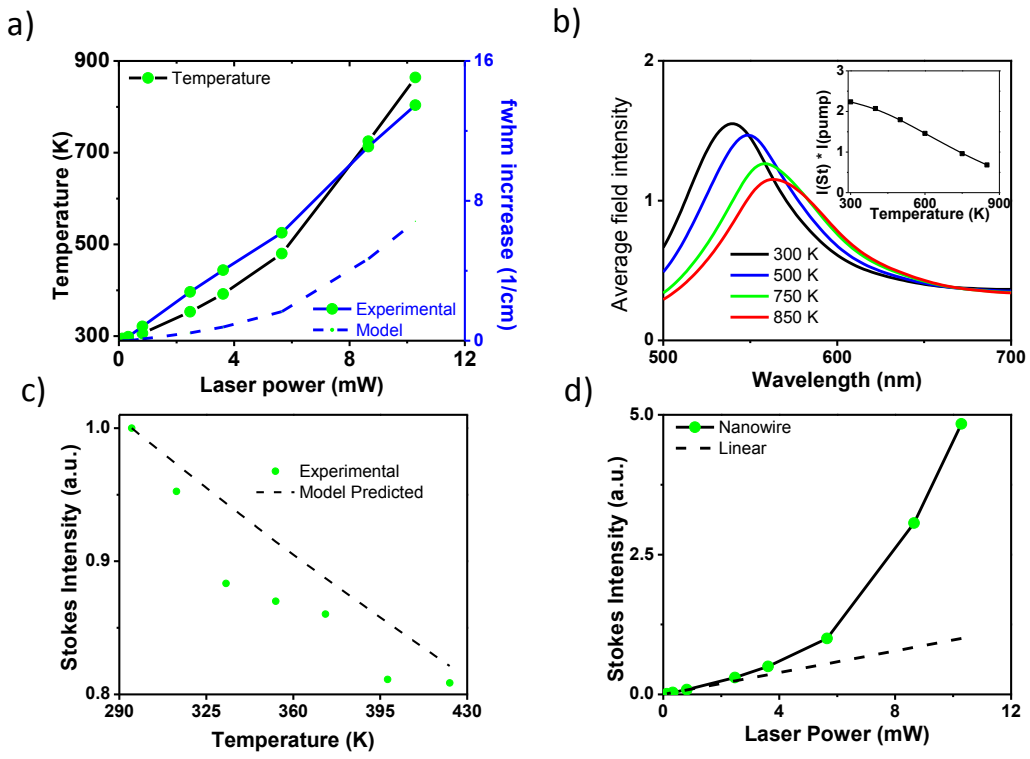

Figure 2.9: Effect of temperature on SRS in a bare silicon nanowire of diameter 100 nm at a 532 nm pump. a) Temperature (left vertical axis) and FWHM increase (right vertical axis) vs. pump power for the nanowire; b) Dependence of average electric field intensity inside the nanowire as a function of temperature. Inset shows the product of the electric field intensity at pump and at Stokes wavelength as a function of temperature; c) Experimentally measured temperature dependence of Stokes scattering intensity as a function of temperature for bulk silicon. The dotted line represents the scattering intensity predicted from the empirical model by Compaan et.al; d) Stokes scattering intensity for silicon nanowire shown in figure 2.7b corrected for temperature using the empirical relation by Compaan et.al

Higher temperatures are known to have a deleterious effect on Raman scattering[22] [23] [24] [25]and on SRS[26] because of multiple reasons such as higher absorption at higher temperatures[27] and decrease in first derivative of polarizability with respect to inter atomic distance[28]. Since absorption and Raman scattering are competing processes, a higher absorption would decrease Raman scattering. With an increase in temperature, the

absorption in semi conductors with an indirect bandgap increases[29] (because of availability of a larger number of phonons which aid in absorption) which should decrease Raman scattering. Raman scattering is directly proportional to the first derivative of polarizability with distance and thus decreases at higher temperatures. The dependence of electric field intensity inside the cavity as a function of wavelength at different temperatures is shown in figure 2.9b. With an increase in temperature a clear red shift and decrease in average electric field inside the cavity is observed. It is interesting to note that even though the refractive index of silicon increases at higher temperatures[30], the confinement (average electric field intensity inside the cavity) decreases contrary to what one would expect since higher refractive index should lead to higher confinement. The decrease is because of increase in losses (extinction coefficient) at higher temperature[31]. The higher refractive index causes the mode to red shift implying that a slightly larger wavelength can be fit inside the same cavity.

Inset figure 2.9b shows the product of the electric field intensity at pump wavelength and Stokes wavelength as a function of temperature. The fact that this product decreases is also a direct indication that at higher temperatures the intensity of Raman scattering and SRS would decrease. The temperature dependence of intensity of Raman scattering in bulk silicon was measured by Compaan et.al at different wavelengths and an empirical relation was deduced[24]. This relation was also verified experimentally by us at 532 nm pump (figure 2.9c). We found that up to a temperature of 423K (highest temperature possible with the existing thermoelectric stage) the experimentally observed scattering intensity was equal to or slightly less than the

intensity predicted by the empirical relation by Compaan et.al. Using this empirical relation we calculated temperature corrected Stokes intensity at each pump power. The resulting dependence shown in figure 2.9d is much more superlinear with a fivefold enhancement in scattering intensity at a pump power of 10^6 W/cm^2. Moreover at this pump power the slope of the log-log plot is 2.8 indicating that the scattering intensity is proportional to the ~ third power of pump intensity pointing to stronger SRS in the cavity.

To test the effect of field confinement on SRS, Raman measurements were performed on the same wire at a pump wavelength of 660 nm. With the 660 nm pump the field confinement is poor at the pump and at Stokes wavelength (figure. 2.10a) and the field intensity inside the nanowire is not enhanced as can be seen in spatial electric field intensity distribution profiles (figure 2.10 b and c). As a result no SRS is expected in this cavity with excitation from a 660 nm pump.

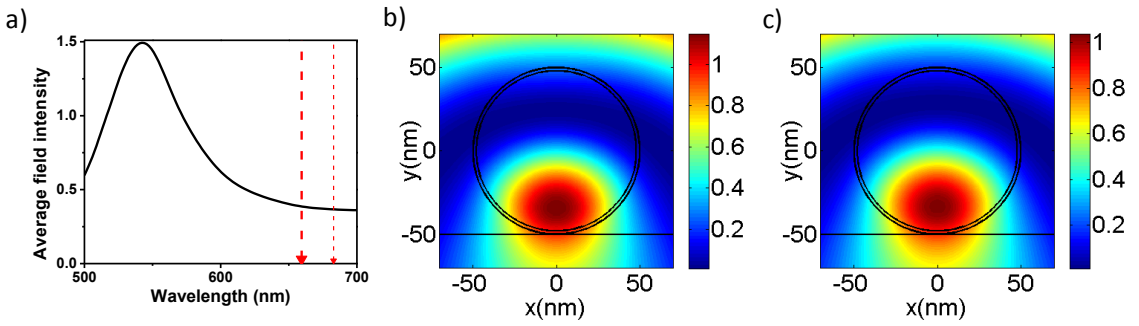

Figure 2.10: Electric field intensity inside a bare silicon nanowire of diameter 100 nm. a) Average electric field intensity inside the cavity as a function of pump wavelength. Vertical dash line represents the pump and the Stokes wavelength from left to right; b, c) Spatial electric field intensity distribution inside the cavity at pump (660 nm) and at Stokes wavelength (683 nm) respectively. The circles represent the silicon nanowire cross section. The inner core is the silicon nanowire and the outer shell is the oxide layer. The horizontal straight line is the substrate/air interface.

Pump power vs. Stokes scattering intensity plot shows a sub-linear dependence of Stokes intensity on pump power (figure 2.11a) similar to the dependence observed in bulk silicon. The change in the trend of dependence of Raman scattering on pump power is a direct result of poor confinement of pump and Stokes electric field in the nanowire leading to a smaller value of average electric field intensity inside the cavity. Temperature calculations from Raman peak shift revealed that temperature of the wire to be around 340K (figure 2.11b). Temperature corrected Stokes intensity using the empirical formula for 532 nm pump still revealed a sublinear dependence of Stokes scattering intensity on pump power (figure 2.11c). It must be noted that the empirical formula for 660 nm was not available in literature but it was empirically shown by Compaan et.al that the correction factor at 660 nm is slightly higher than that for 532 nm[25]. Therefore, at best the temperature corrected Stokes intensity at 660 nm could be linear or very slightly superlinear with the pump power which is much lower than the SRS observed in this wire at 532 nm when the field confinement was much more. The increase in experimentally observed FWHM values of the Raman peak (figure 2.11b) was more than what was predicted by the model because of asymmetric broadening caused by fano interactions. 1/q value was calculated to be ~ 2.5E-3 at a pump power of ~10^6 W/cm^2 (figure 2.11d). This value is higher than the value observed in bulk but slightly lower than the value observed for the wire at 532 nm and is also related to the average field intensity inside the field. Asymmetry parameter is directly proportional to amount of photoexcited carriers in the wire which increase with increase in absorption. Absorption is directly related to the electric field confinement in the wire. Thus more confinement leads to more absorption and more asymmetric broadening and higher 1/q parameter.

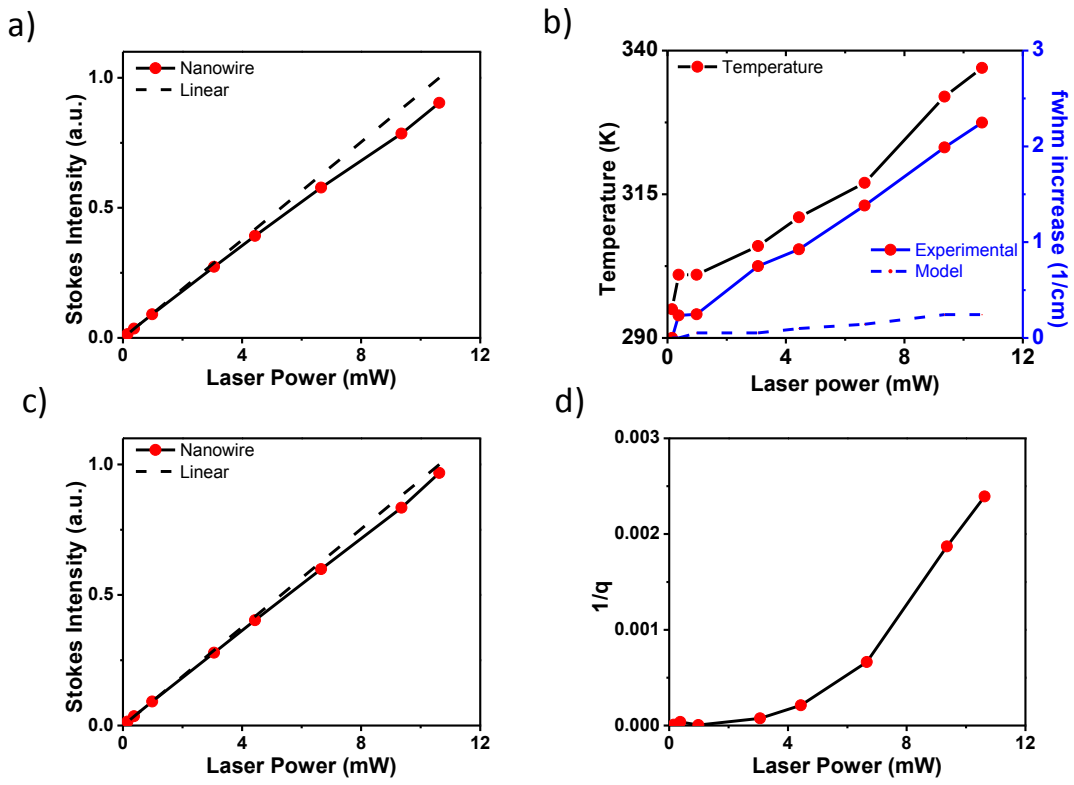

Figure 2.11: SRS in a nanowire without a cavity mode- bare silicon nanowire of diameter 100 nm excited with a 660 nm pump: a) Pump power dependence of integrated Stokes intensity; b) Temperature (left vertical axis) and FWHM increase (right vertical axis) vs. pump power for the nanowire; c) Temperature corrected Stokes scattering intensity for silicon nanowire shown in figure 2.11a; d) Fano asymmetry parameter as function of pump power

Similar sublinear dependence of SRS on pump power was also obtained using a 532 nm pump with a nanowire of diameter 125 nm in TE polarization confirming the importance of cavity mode in attained SRS in the nanowire. Figure 2.12a and b show the wavelength dependent average electric field intensity inside the nanowire and the pump power dependence of Stokes Raman scattering intensity. Misalignment of cavity mode

with the pump wavelength leads to linear/sub-linear dependence of Raman scattering intensity on pump power.

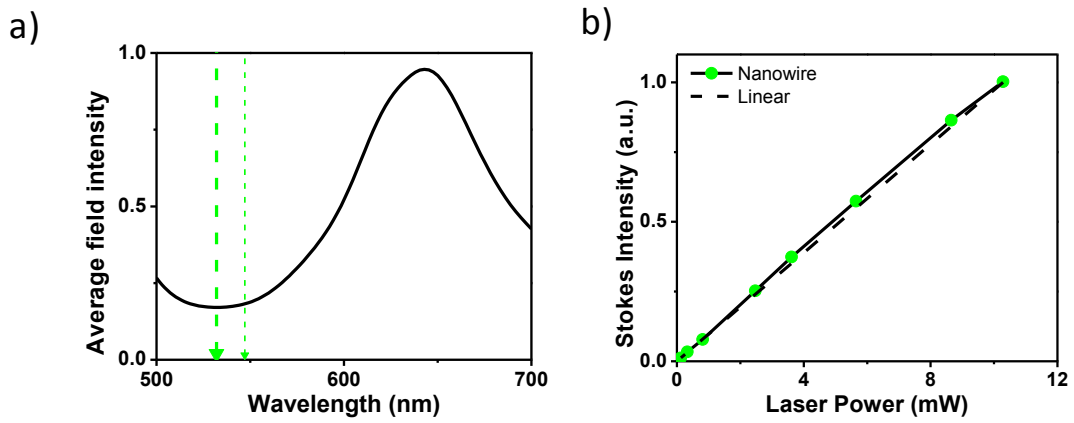

Figure 2.12: SRS without a cavity mode- bare silicon nanowire of diameter 125 nm excited with a 532 nm pump. a.) Electric field intensity distribution inside a bare silicon nanowire of diameter 125 nm in TE polarization. a) Average electric field intensity inside the cavity as a function of pump wavelength. The vertical arrows represent the pump and the Stokes wavelength from left to right; b) Pump (532 nm) power dependence of integrated Stokes intensity

Even though there was evidence of strong SRS in the nanowire with a 532 nm pump, lasing was not observed in any of the nanowires that were tested. The main reason for this was high losses in the nanowire which lead to an increase in the nanowire temperature which leads to a decrease in Raman scattering. Stokes Raman scattering also leads to generation of phonons which lead to heating. To negate the effect of absorption, measurements were performed at 660 nm with nanowires having a resonant mode at this wavelength. Absorption in silicon at 660 is 3 times less than at 532 nm[32] which should lead to lower losses, causing lower heating leading to higher SRS. Figure 2.16a shows the average electric field intensity inside the nanowire of diameter 225 nm (TM polarization) as a function of wavelength showing the presence of cavity mode and high electric field

intensity inside the nanowire at 660 nm. The spatial distribution of electric field intensity at the pump (figure 2.14b) and at the Stokes wavelength (figure 2.14b) reveals that the mode lies inside the nanowire with more than 2.5 times enhancement in intensity compared to incident field intensity which should cause high SRS.

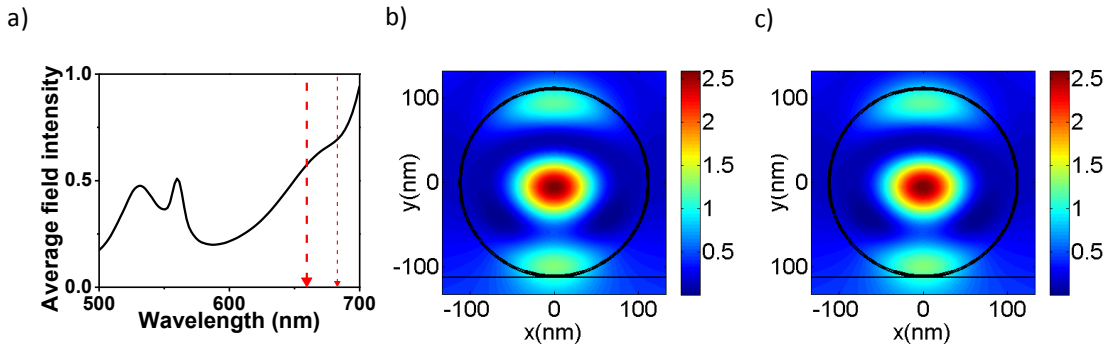

Figure 2.13: Electric field intensity distribution inside a bare silicon nanowire of diameter 225 nm. a) Average electric field intensity inside the cavity as a function of pump wavelength. Vertical dash line represents the pump and the Stokes wavelength from left to right; b, c) Spatial electric field intensity distribution inside the cavity at pump (660 nm) and at the Stokes wavelength (683 nm) respectively. The circles represent the silicon nanowire cross section. The inner core is the silicon nanowire and the outer shell is the oxide layer. The horizontal straight line is the substrate/air interface.

Figure 2.14a shows Stokes scattering intensity of the nanowire as a function of pump power. At a pump power as low as 6E5 W/cm^2, more than a fourfold enhancement in Stokes intensity is observed. The slope of the log-log plot (figure 2.14b) is three, implying that Stokes scattering is proportional to the third power of the pump intensity. Temperature calculations done using the change in Stokes shift revealed significant cavity heating with a peak temperature of ~1050K. Even though the absorption is lower at 660 nm, the increase in temperature is coming from the much stronger Raman scattering which generates extra phonons, leading to heating. Temperature corrected

Stokes scattering intensity using the empirical relation for 532 nm pump wavelength, reveals a more than twelvefold enhancement in Stokes scattering. This is still an underestimate of temperature corrected intensity since as discussed earlier the temperature correction factor for 660 nm is more than for 532 nm. Nevertheless, significant enhancement in SRS is seen using a 660 nm pump with resonant cavities because of lower absorption losses even though lasing is still not seen.

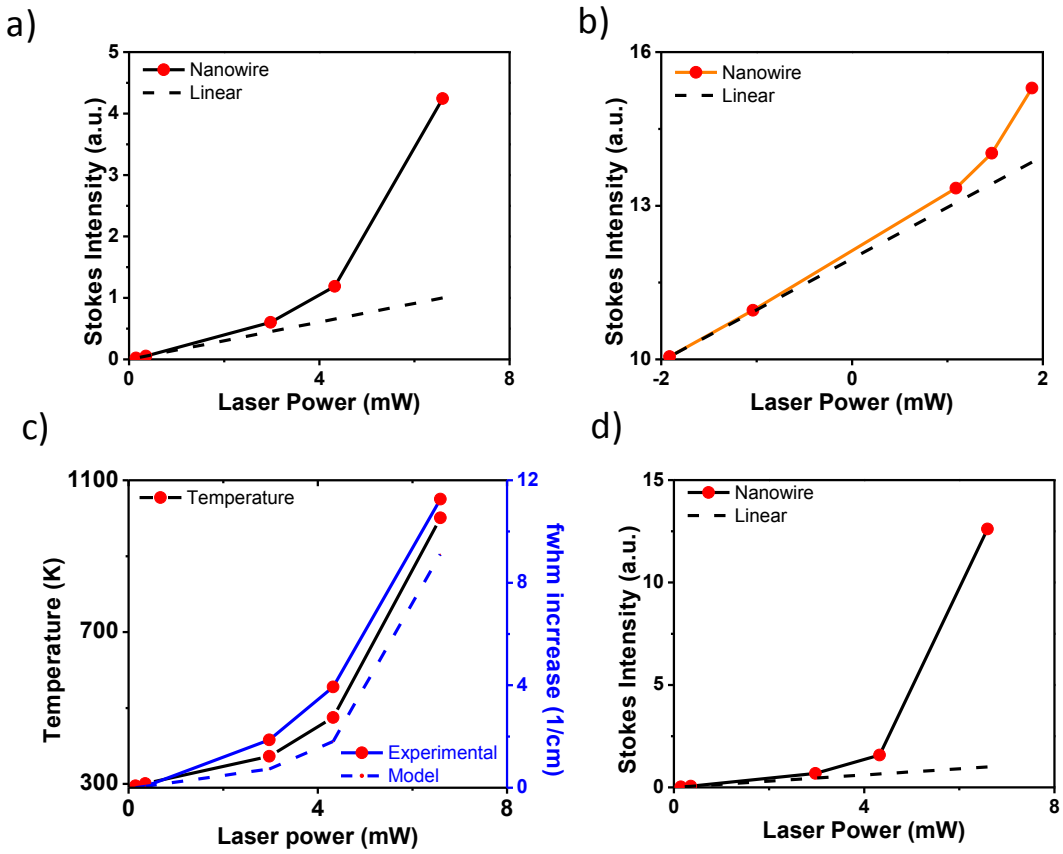

Figure 2.14: SRS in a bare nanowire of diameter 225 nm with a 660 nm pump: a) Pump power dependence of integrated Stokes intensity; b) a log-log plot of pump power dependence of Stokes intensity; c) Temperature (left vertical axis) and FWHM increase (right vertical axis) vs. pump power for the nanowire; d) Temperature corrected Stokes scattering intensity for silicon nanowire in figure 2.14a;

2.5: Concluding remarks on SRS on bare silicon nanowire

Raman scattering is directly proportional to the 4^{th} power of the pump frequency[17]. Thus the scattering cross section and by extension Raman gain at 532 nm should be higher compared to at 660 nm. In spite of this, stronger SRS is observed at 660 nm. This is because of two reasons. Firstly the diameter of resonant cavity at 660 nm pump is more than at 532 nm. This allows for larger power to be coupled into the cavity and also allows for a larger propagation length in the gain medium which would lead to a higher observed enhancement. Secondly the losses at 660 nm are much lower than at 532 nm which lead to an increase in SRS because of more power availability for SRS and because of lower heating.

While extremely high SRS was observed in bare nanowires (Raman scattering dependent on the third power of pump intensity) lasing was not achieved. This could be because of two reasons. Firstly the cavities have a quality factor of less than 100 which makes lasing incredibly difficult. A higher quality factor means that the photon would spend more time in the cavity and make higher number of round trips before leaving the cavity which would lead to more gain. Typical quality factors for silicon cavities in which Raman lasing was observed were of the order of 10^{6} [3] [33]. Even with bad quality factor cavities, lasing could potentially be achieved at higher pump powers as has been shown before[34]. But significant heating is observed at higher pump power which is detrimental to Raman scattering and also to the cavity itself if sufficiently high temperature is reached. The Raman lasers in silicon that have been built so far have been at 1.55 microns. At this wavelength the major loss mechanism is free carrier absorption

(FCA) by carriers generated by two photon absorption (TPA) from the pump[35] [36]. At 532 nm and at 660 nm the major loss mechanism is absorption. Total loss in silicon at 532 nm and at 660 nm is ~ eight orders of magnitude higher than at 1.55 μm (table 2.1). A significant increase in SRS was observed when the losses were brought down by a factor of only three. It is quite possible that performing similar measurement on resonant cavities at 1.55 μm may make the nanowire lase because of much lower losses.

$\lambda_{\mu m}$	α (cm^{-1})	β (cm^{-1})	α_{FCA} (cm^{-1})	**Total Losses**
1.550		7.50E-10	4.24E-05	4.24E-05
0.660	2.58E+03		2.25E+01	2.60E+03
0.530	7.85E+03		3.55E+01	7.89E+03

Table 2.1: Total cavity losses at different wavelengths

The calculations were done based on the equations given by [37]:

$$\alpha_{FCA} = \frac{1.45*10^{-17} * \lambda_{\mu m}^2 * \Delta N}{1.55^2} = \sigma * \Delta N \qquad (2.6)$$

$$\Delta N = \frac{\alpha * I_p * \tau_{eff}}{\hbar * \omega} + \frac{\beta * I_p^2 * \tau_{eff}}{2 * \hbar * \omega} \qquad (2.7)$$

where α, β and α_{FCA} refer to the one photon absorption, two photon absorption and free carrier absorption cross sections respectively, $\lambda_{\mu m}$ is the wavelength in microns. Loss associated with one photon absorption at 1.55 μm and with two photon absorption in the visible spectrum were assumes to be negligible compared to other losses at the respective wavelengths. The absorption, TPA and FCA coefficients were taken from [32] [38] and [37] respectively. In calculating FCA, carrier lifetime was assumed to be 10 ns, about the half

the value that what was reported for conventional rib waveguides[39], pump power was taken to be 10^6 W/cm^2,

Due to lack of experimental setup we were unable to perform measurements at this wavelength. As a result new cavities were synthesized by coating the nanowires with a thick metal (gold or silver) shell. While a metallic layer would not decrease the total cavity losses, it could decrease the cavity temperature by providing a thermal sink to the nanowires. Gold/silver have the lowest loss among all metals in the visible spectrum and both have extremely high thermal conductivity values[40] [41]; thus making them ideal candidates for a heat sink.

2.6: SRS on silicon-gold cavities

The silicon-gold cavities were fabricated as explained in section 2.3. Figure 2.3 shows a scanning electron microscopy image of a 360 nm gold coated silicon nanowire which was milled by using a focused ion beam to reveal the cavity cross section; showing the nanowire and the gold coating on top of it. It can be seen that gold forms a uniform thick layer on top of silicon which should enable good heat transport from silicon. Raman measurements were performed on silicon-gold cavities at 660 nm excitation with the incident electric field parallel (transverse magnetic, 'TM' polarization) to the nanowire long axis. Power dependent Raman spectra in the range 8E3 W/cm^2 to 3.8 E6 W/cm^2 done on a gold coated nanowire of size 235 nm are shown in figure 2.15a. Compared to bare nanowire, with an increase in laser power the red shift is the Raman peak is much lower implying that the increase in temperature is much lower because of better thermal

transport via the gold layer. Integrated intensity calculated by adding the area under the Raman peak revealed that the increase in Raman intensity was super linearly dependent on laser power (figure 2.15b). The dashed line in the figure is a linear extrapolation of the expected Stokes scattering at higher powers from the measured Raman scattering intensity at 80 μW. Measurements on the silicon nanowire cavity revealed the Stokes intensity to be increasing at a faster rate than the pump power, leading to non-linear-almost exponential increase in Stokes scattering intensity. A log-log plot revealed that the non-linearity, threshold for stimulated Raman scattering, starts at a power of 200μW (figure 2.15c). The slope of the log-log curve which was close to 1 at low powers becomes 4.23 at a pump power of 38 mW, indicating that at a pump power of 38mW, Stokes scattering is increasing with the fourth order of pump power. Thus because of the addition of gold layer much stronger SRS is seen in the silicon nanowire. The gold layer also leads to the disappearance of fano interactions in between phonons and charge carriers. Figure 2.15d shows the plot of asymmetry parameter 1/q vs. laser power. Even at the highest power of 3.8E6 W/cm^2, the value of 1/q is 2E-6. This value is constant across all the powers and represents the noise level in the system. If these were real numbers, then 1/q would have increased with an increase in power because of increased photoexcited carriers at higher powers, which is not the case. Gold acts as a good sink for electron and leads to quenching of the charge carries, decreasing the effective carrier lifetime in the process and thus serves the same purpose as that of application of a reverse bias voltage using a p-i-n junction employed while making Raman lasers [37]. The fact that the electric field in the cavity is stronger than in the bare nanowire enhances the

quenching effect. This reduces the scattering of charge carries from phonons to such an extent that fano asymmetric broadening is not observed in the Raman spectra.

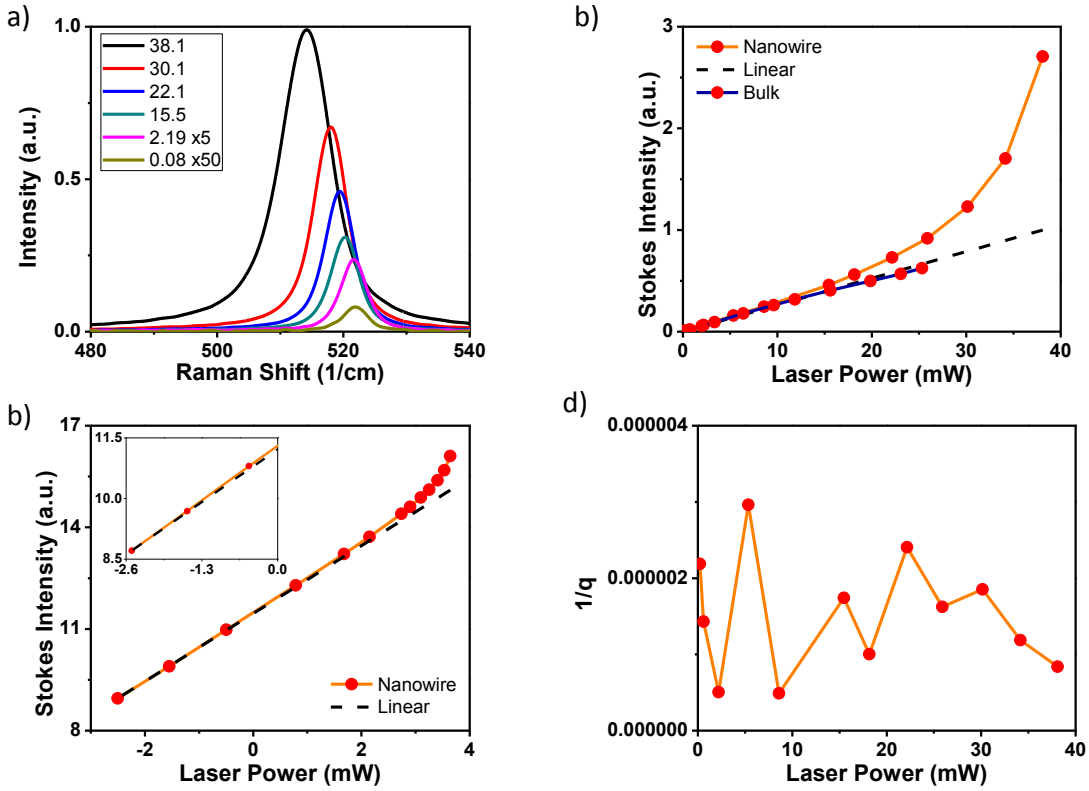

Figure 2.15: Stimulated Raman Scattering in gold coated silicon nanowire of diameter 235 nm with a 660 nm pump: a) Power dependent Stokes Raman spectra of the silicon nanowire of diameter 250 nm; b) Integrated Stokes intensity as a function of laser power; c)Log-log plot of integrated Stokes intensity as a function of laser power, inset is the zoomed in version of the same graph showing the onset of SRS ; d) Fano interactions parameter 1/q as a function of laser power

Calculations done using the FDTD methodology to simulate electric field intensity distribution inside the nanowire cavity indicated that the electric field was tightly confined in the cavity at the pump and at Stokes wavelength (figure 2.16a, golden curve). The maximum of electric field intensity is also strengthened by factors of over 10

and 6 relative to the incident electric field intensity. Similar calculations for bulk silicon (discussed earlier) revealed that maximum field intensity inside bulk silicon was only ~15% of the applied field intensity for both pump and Stokes field (figure 2.16a black curve) and the average electric field intensity was less than 10% of the applied field intensity. Since SRS is proportional to the product of pump field intensity as well as the Stokes field, the cavity confinement of electric field leads to an enhancement factor over 2000 for SRS in the gold coated silicon nanowire cavities compared to bulk silicon. Calculations of spatial distribution of electrical field intensity inside the cavity revealed the whispering gallery TM_{21} resonant with the cavity mode at pump (figure 2.16b) and at Stokes wavelength (figure 2.16c), with the electric field inside the silicon nanowire, leading to much stronger SRS because of the higher effective electric field experienced by the material. It must be noted that addition of gold leads to a threefold increase in field confinement in the cavity compared to bare nanowire because the thick gold film acts as a mirror reflecting the light back into the cavity at the silicon-gold interface.

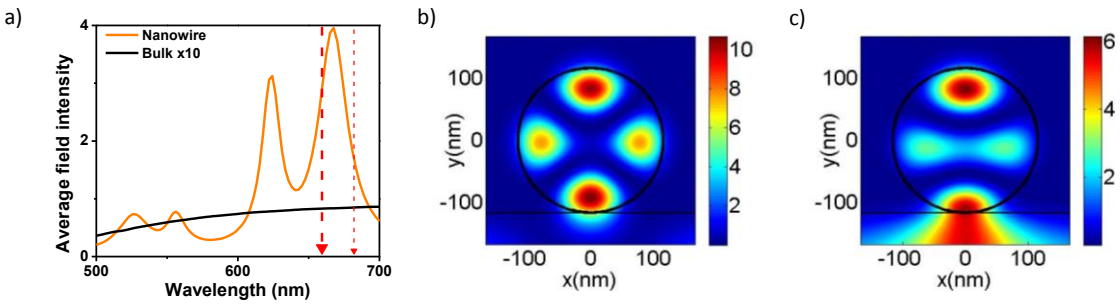

Figure 2.16: Mechanism of Stimulated Raman Scattering- gold coated silicon nanowire of diameter 235 nm with a 660 nm pump: a) Average electric field inside the cavity as a function of excitation wavelength. Vertical dash line represents the pump and the Stokes wavelength from left to right; b,c) electric field intensity distribution inside the silicon nanowire cavity at the pump wavelength (660 nm) and the Stoke's wavelength (683 nm). Black circles represent the nanowire. Horizontal line is the substrate-gold interface

Temperature calculations revealed that the temperature of this cavity was around 640K (figure 2.17a, left vertical axis) at a pump power of 3.8E6 W/cm^2, close to the eutectic temperature of silicon-gold system[42] but significantly lower than temperature in the bare nanowire. The FWHM values of these Raman peaks (figure. 2.17a, right vertical axis) were in good agreement with the values expected at the corresponding temperatures from the model proposed by Balkanksi et.al [13]. Up until this point, experimental values have always been larger than the model predicted FWHM values and this is the first time that they have been in agreement. The is because of two reasons: firstly the thermal heat sink allows for good heat transport removing any broadening associated with non uniform heating of the nanowire; secondly, absence of fano interactions also prevents asymmetric line broadening. Computational simulations of electric field confinement in the cavity based on the temperature dependent permittivity of silicon revealed that with an increase in temperature the field intensification (at pump and at Stokes) decreases and red shifts (figure 2.17b). Raman scattering intensity which depends on the product of pump and Stokes field intensity should decrease with temperature as result of poorer confinement which reduces to almost half of its value when temperature increases from 295K to 640 K (figure. 2.17b, inset). The empirical relation for temperature dependence of Stokes scattering intensity in bulk silicon as discussed earlier was used to estimate the temperature corrected Stokes intensity. These calculations revealed a much higher rate of increase in Stokes scattering with a ~ 400% (figure 2.17c) increase in scattering intensity and a slope of 5.71 in the log-log plot of Stokes intensity vs. laser power at a pump power of 38 mW (figure 2.17d) which is almost double the value of the slope in bare nanowires (albeit at higher powers).

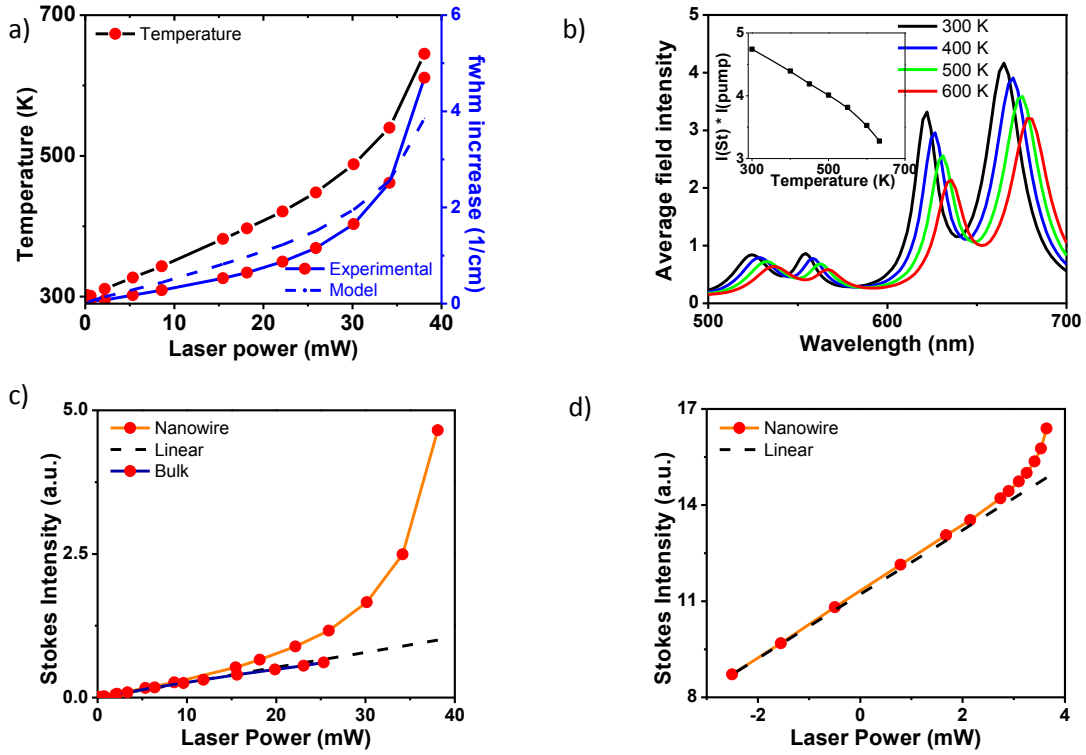

Figure 2.17: Effect of Temperature on Stimulated Raman Scattering- gold coated silicon nanowire of diameter 235 nm with a 660 nm pump: a): Temperature (left vertical axis) and increase in FWHM (right axis) of the cavity as a function of pump power. Inset shows the product of the electric field intensity at pump and at Stokes wavelength as a function of temperature; b) FDTD calculation of field confinement in the cavity as a function of temperature; c) Temperature corrected experimental integrated Stokes intensity as a function of laser power of silicon nanowire; d) Log-log plot of temperature corrected Stokes intensity vs. pump power

To investigate the wavelength and size distribution of cavity modes, calculations were done for average electric field intensity distribution inside silicon nanowire as a function of nanowire size and excitation wavelength for bare and gold coated wires. Figure 2.18a and figure 2.18b show the average field intensity inside the nanowire as a function of nanowire size and excitation wavelength in bare and metal coated wires

respectively in TM polarization. With an increase in cavity size a clear red shift in cavity mode resonance is observed. It is also observed that with an increase in wavelength the field confinement as a result of the mode increases. This is because of lower losses in silicon and in gold at larger wavelengths. The losses in silicon decrease with an increase in wavelength where as losses in gold are extremely low at 660 nm in gold and higher on either sides[40]. Moreover, gold leads to a stronger confinement of light inside the silicon nanowire, by acting as a mirror and preventing the light from leaking outside the cavity. The increase in confinement is typically three – five times depending on the excitation wavelength and the size of the nanowire. This stronger confinement should in general lead to stronger SRS as was also observed.

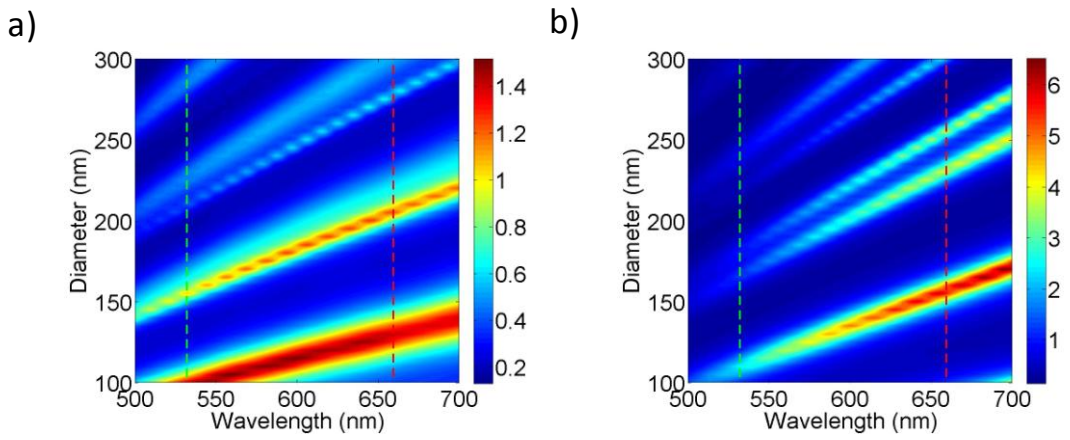

Figure 2.18: Wavelength and size distribution of average electric field intensity inside the silicon nanowire in TM polarization. a.) in bare silicon nanowire; b) in gold coated silicon nanowires. Green and red vertical dashed lines represent the position of the available pump wavelengths using which SRS experiments were conducted.

2.7 Estimation of gain coefficient

Using the model for pump and Stokes power evolution during Raman scattering developed by Jones et.al[37] calculations were done to estimate the Raman gain coefficient in silicon. Power at Stokes wavelength inside the cavity can be described as:

$$\frac{dP_s(z)}{dz} = -\alpha P_s(z) - \frac{2*\beta - g_r}{A_{eff}} * P(z) * P_s(z) - \sigma N(z) P_s(z) \qquad (2.8)$$

where P_s and P are powers of the Stokes wave and pump wave, z is the propagation distance, A_{eff} is the effective area of cross section and g_r is the Raman gain coefficient, z is the round trip distance and is equal to twice the nanowire diameter; A_{eff} is $1\mu m^2$. As a first order approximation pump depletion was neglected in the cavity. 100% reflection at the silicon-gold (gold coated nanowire) and at the silicon-silica (bare nanowire) interface has been assumed for the round trip. All losses in gold have also been ignored. At higher temperature, the absorption losses in silicon would increase but all the values have been taken at room temperature only. For intensity calculations total pump power has been used which is greater than the actual power coupled into the nanowire. From table 2.1 it can be seen that α_{FCA} and $\beta << \alpha$ at 532 nm and at 660 nm

This simplifies equation 2.8 to

$$\ln\left(\frac{P_{so}}{P_s}\right) = 2 * d * \left(\frac{g_r * P}{A_{eff}} - \alpha\right) \qquad (2.9)$$

Here $\ln(P_{so}/P_s)$ is the natural logarithm of the enhancement in Stokes power as a result of SRS. In a pump probe experiment, this would be the ratio of the output probe power with and without the pump. In experiments without the probe, this still represents the gain at Stokes power as a result of SRS but is calculated as the ratio of experimentally observed Stokes scattering intensity and the expected Stokes scattering intensity based on linear extrapolation of Stokes scattering intensity from low pump power. Such an analysis was also used by[2]. In all the calculations below, actual experimentally collected intensity was used instead of temperature corrected intensity. Using these calculations Raman gain coefficient of the order of 5E7 in bare wire and 10^7 in gold coated wires at 660 nm has been calculated. Previously a value of 9.5 cm/GW at 1.55 μm pump was reported for silicon[37]. This is the first instance of Raman gain being observed in the visible spectrum in silicon so a comparable value at 660 nm was not found. But given that the losses at 660 nm are ~ eight orders of magnitude higher than at 1.55 μm, it is almost remarkable that any SRS is observed at all. Still, these calculations, though approximate reveal 5-6 orders of magnitude increase in the gain coefficient of silicon. This is because of the strong confinement of light leading to extremely high electric field intensities in the nanowire cavities which cannot be attained in bulk cavities. Another interesting observation was that the gain coefficient in gold coated nanowire was lower than in bare nanowires in spite of higher field confinement in gold coated nanowires. This is most likely because of absorption losses of Stokes scattered field in gold. But, a steeper increase in Stokes scattering intensity is observed in gold coated wires at higher powers because of higher field confinement.

The gain coefficient values that have been calculated are not material constants but depend on the confinement of electric field inside the cavity and would thus be different for different cavity size and structures depending on the extent of confinement. These gain calculations, though approximate, explain the remarkable enhancement in Raman gain that can be achieved by confining the electric field modes inside the nanowire cavities.

2.8 Raman scattering in silicon-silver cavities and fano interactions

Cavities were also fabricated using silver instead of gold as the thermal sink. Silver has a lower imaginary part of permittivity compared to gold[40] and a higher thermal heat conductivity making it a better choice than gold. The eutectic temperature of silicon-silver system is also over 1110 K[43] which should make the silicon-silver cavity stable at higher temperatures compared to the silicon-gold cavity which may start getting damaged at temperatures close to 650 K. Raman measurements were done on these silver coated silicon nanowires in exactly the same way as was done with gold coated silicon nanowires.

While size of the individual wires was not determined, scanning electron microscopy was done on other nanowires from the same sample from which nanowires were taken for silver deposition. The results revealed that, a majority of wires were in the size range 210-240 nm. Raman measurements were done on multiple silver coated silicon wires to ensure that the trends observed were consistent and corresponded to that of wires in the size range 210-240 nm. Figure 2.19a shows the average electric field intensity

inside the silicon nanowire (coated with 360 nm silver) as a function of nanowire diameter and excitation wavelength. Figure 2.19b gives the size dependence of average field intensity inside the nanowire specifically at pump and at Stokes wavelength. They provide some insight into the expected electric field confinement inside the cavity.

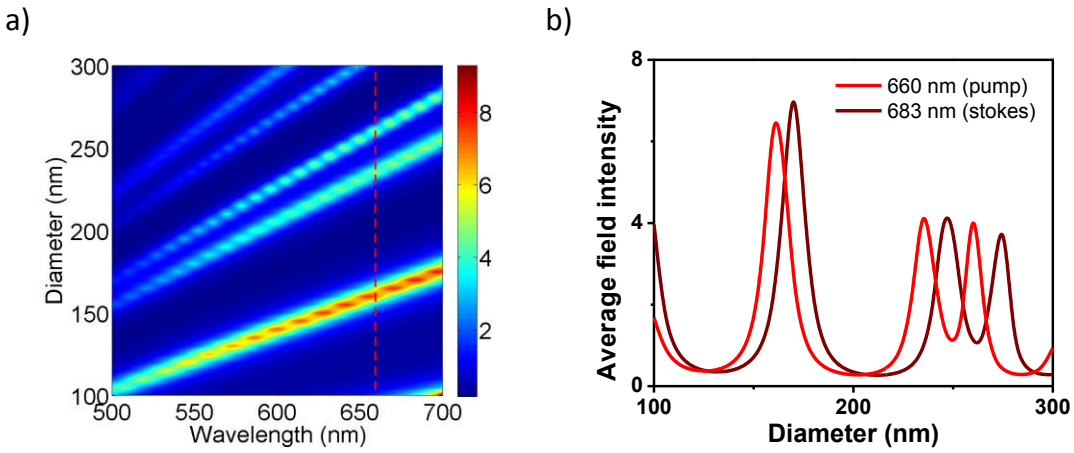

Figure 2.19: Electric field confinement in silver coated silicon nanowires: a) Wavelength and size distribution of average electric field intensity inside the silicon nanowire in TM polarization. The red dashed vertical line shows the position of pump; b) Diameter dependence of average electric field intensity at the pump and at Stokes wavelength.

Figure 2.20a and figure 2.20b show the power dependent anti Stokes and Stokes Raman spectra respectively. With an increase in pump power, an increase in asymmetric broadening is clearly observed. Figure 2.20c shows calculations for coupling constant, 1/q, at Stokes and at anti Stokes wavelength. The two values closely follow each other at all powers. At a pump power of 4E6 W/cm^2, 1/q value of 0.045 is observed, more than an order of magnitude higher than in bulk. At a pump power of 2.5E6 W/cm^2 (25 mW, figure 2.5), 1/q value in bulk is less than 10^{-3}, while it is greater than .01 in the silver

coated nanowire at the same power. This is because of much higher electric field confinement in the nanowire cavity. The increase in 1/q value with increase in power and similar nature of asymmetric broadening at Stokes and anti Stokes wavelength confirms that the fano resonance arises because of scattering of photoexcited charge carriers from the lattice. It is surprising that while coating gold lead to a quenching of fano interactions, coating silver does not lead to quenching. The most likely reason for this is the quality of silver film that is deposited. While the gold film was clean, it is possible that while depositing silver, a thin oxide layer may have formed at the silicon-silver interface. In such a case, the quenching of charge carriers would not take place. Instead the strong electric field intensity inside the cavity could lead to enhanced interactions in between the phonons and charge carriers leading to stronger fano resonance. Resonant bare nanowires could have shown similar 1/q numbers at higher powers but the faster rate of heating in them makes excitation at such high pump powers impossible without destroying the nanowire. Figure 2.20d shows the temperature and increase in FWHM values as a function of pump power. While with gold coated silicon nanowires there was good agreement in between experimental and model predicted FWHM values, much broader peaks are observed in silver coated silicon nanowires. Heating should be uniform in both the metal coated cavities and therefore this broadening is caused by the fano interactions in the silver coated film.

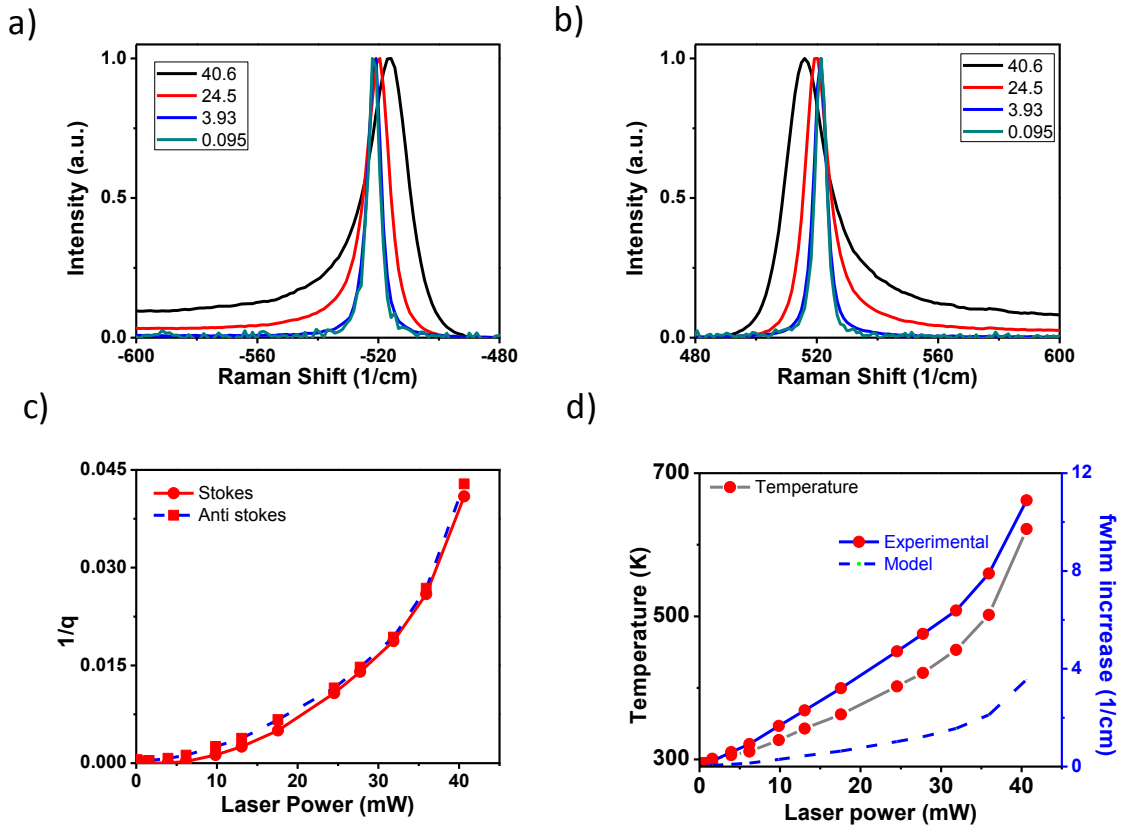

Figure 2.20: Raman scattering in silver coated silicon nanowire: a, b) Power dependent anti Stokes and Stokes Raman spectra; c) Fano interaction parameter as a function of laser power; d) Temperature (left vertical axis) and increase in FWHM (right vertical axis)as a function of laser power

Integrated intensity calculations (figure 2.21a) reveal that only a small enhancement in Stokes scattering intensity, lower than in the silicon-gold cavities, is observed. Even at a pump power of 4E6 W/cm^2, less than twofold enhancement in Stokes intensity is achieved. Figure 2.21b shows the plot of Stokes intensity vs. pump power in the log-log space. At a higher power of 4E6 W/cm^2, the slope of the curve is ~ 3, which is also lower than what is observed in gold coated cavities (>4 at pump power of 3.6E6 W/cm^2, figure 2.15). Among all the nanowires tested, this wire had the maximum enhancement in Raman scattering which is still lower than the enhancement observed in

gold coated cavities. It is quite likely that losses associated with scattering of charge carriers from phonons is leading to low SRS.

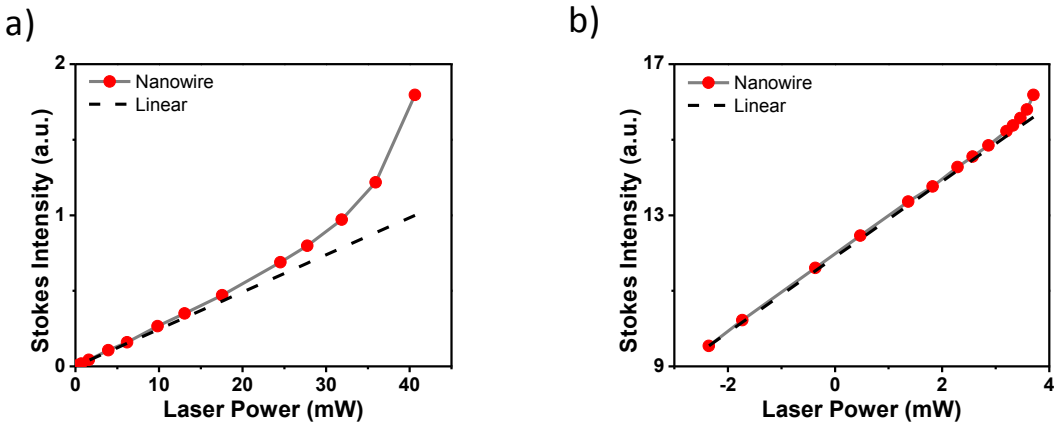

Figure 2.21: Stimulated Raman scattering in silver coated silicon nanowire: a) Integrated Stokes intensity as a function of pump power for the nanowire in figure 2.20; b) Log-log plot of integrated Stokes intensity vs. pump power for the same nanowire.

In some wires, saturation in fano interaction parameter is observed (figure 2.22). Neither such high coupling constants nor the saturation has ever been reported before in nanowires. While evolution of fano interactions in bare and metal coated nanowires is an interesting topic in itself, investigations were limited to enhancing SRS in the cavities.

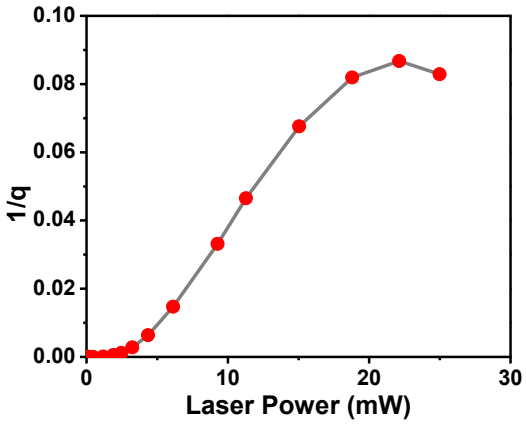

Figure 2.22: Fano asymmetry parameter 1/q vs. laser power for a silver coated silicon nanowire showing saturation in 1/q

2.9 A note on peaking narrowing during lasing

The onset of lasing is characterized by a sudden increase in intensity of emission and a gain associated peak narrowing. With huge increases in emission intensity have been observed in some nanowires, peak narrowing has been elusive. Competing with gain associated peak narrowing are a few processes which cause peak broadening. The most important contributor to peak broadening is the increase in temperature. At higher pump powers, due to increase in Raman scattering (which generates phonons) and absorption (which also generates phonons during non-radiative decay in indirect bandgap semiconductor), there is an increase in temperature of silicon nanowire as was shown. Because of higher lattice anharmonicity[44] at higher temperatures, the Raman emission becomes broader at higher temperatures, an effect that may be impossible to overcome. Higher pump powers may also lead to a certain degree of non uniform heating especially in bare nanowires which may lead to additional peak broadening. Moreover, comparison of increase in FWHM values in bare nanowires, gold coated nanowires and silver coated nanowires has revealed that fano interactions also lead to asymmetric peak broadening which would also make gain associated peak narrowing difficult to attain in nanowires which show fano interactions. In many cases (such as in figure 2.14), the jump in emission intensity was coincident with the increase in temperature and increase in peak width. It is possible that the nanowire was lasing at that time but due to the increase in temperature peak narrowing was not observed.

Keeping these factors in mind, it may be hard to achieve peak narrowing associated with lasing at least until the temperature of the system is kept under control.

2.10 SARS: Gain in anti-Stokes Raman scattering intensity

Stokes scattering generates phonons and leads to heating which is undesirable. Higher temperature attained during operation of Raman lasers is detrimental to the quality of emission[26]. Anti Stokes interactions, on the other hand, lead to phonon destruction and cooling of the system in the process. From that perspective, an anti Stokes laser would be extremely useful since, more the output of the laser would be, more heat would be taken away from the system. While there have been many reports on Stokes Raman gain and Stokes based Raman laser, very little work has been done on SARS (stimulated anti Stokes Raman scattering)[34]. One of the reasons for that is the low scattering cross section of anti Stokes scattering. At room temperature for silicon, anti Stokes intensity is only ~8% - 10% of Stokes intensity as has been shown in chapter 3.

Given that tuning the resonant cavity mode to the pump/Stokes wavelength, leads to an enhancement in Stokes scattering, it should also be possible to achieve gain in anti Stokes scattering since the processes are very similar. But before looking at some experimental data, it is important to understand the temperature dependence of anti Stokes scattering intensity since heating is a common occurrence in most of the cavities. There is no empirical model for anti Stokes intensity dependence on temperature available in literature. But the dependence of anti Stokes/Stokes ratio on temperature is reasonably well understood and has been widely used for temperature determination[45 46].

Using Stokes intensity's dependence on temperature[24] (figure 2.23a) and the anti Stokes/Stokes scattering intensity ratio dependence on temperature[23] (figure 2.23a), an

estimate of anti Stokes intensity's dependence on temperature can be made. Fig 2.23c shows this dependence that is obtained by multiplying the expressions for figure 2.23a and figure 2.23b. Note that, Stokes intensity – temperature dependence relation for 532 nm has been used and therefore the calculations for anti Stokes intensity give a slight overestimate for correcting experimental data with a 660 nm pump. Nevertheless, it can be seen that for a fixed pump power, with an increase in system temperature, the anti Stokes intensity first increases until ~ 700 K at which point it is about 2.25 times the intensity at 293 K. Above 700 K, the anti Stokes intensity starts to decrease again. This trend is the interplay of two factors: Stokes intensity dependence on temperature and the anti Stokes/Stokes ratio dependence on temperature. At lower temperature (<700 K), the increase in the ratio dominates over the decrease in Stokes scattering and thus the resultant effect is an increase in anti Stokes intensity. At higher temperature, the ratio starts to saturate and the increase is not large enough to compensate for the decrease in Stokes scattering and hence the anti Stokes intensity starts to decrease.

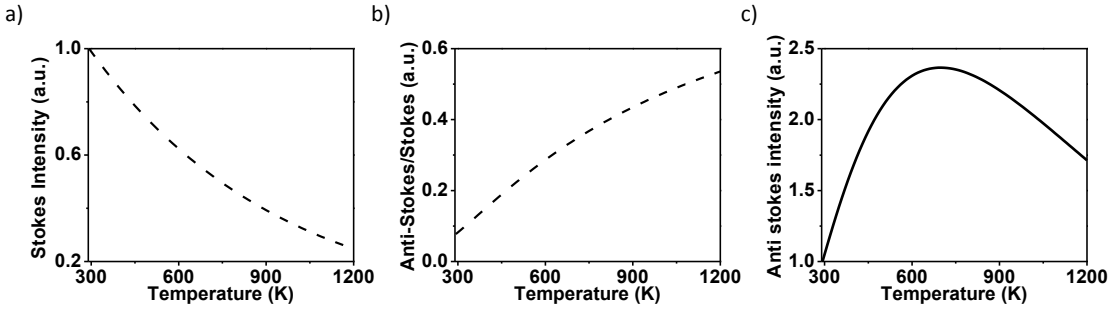

Figure 2.23: Dependence of anti Stokes intensity on temperature: a.) Stokes intensity vs. temperature with a 532 nm pump[24]; b) Anti Stokes/Stokes ratio vs. temperature[23]; c)Anti Stokes intensity as a function of temperature.

Fig. 2.24a shows the integrated anti Stokes intensity as a function of laser power for a gold coated wires of size 230 nm. A tenfold enhancement in anti Stokes intensity is seen at pump power of 3.8E6 W/cm^2 much higher than Stokes intensity enhancement in any of the wires before and also greater than 2.25 pointing towards non-linear processes contributing to anti Stokes scattering. Also, the Raman peaks did not show any fano character, consistent with the trend in gold coated wires. Temperature and FWHM calculations indicated that the cavity was heated to a temperature of ~ 640 K and the experimentally observed FWHM values were in close agreements with the values predicted by model. Temperature corrected anti Stokes scattering intensity still showed ~ fourfold enhancement in scattering intensity. Temperature corrected anti Stokes intensity should be linearly dependent on pump power since, at a constant temperature, in the absence of any non linear processes, spontaneous Raman scattering is linearly dependent. The fact that fourfold enhancement is seen is a definite indication of stimulated anti Stokes Raman scattering taking place in the system. Calculations for average electric field intensity inside the nanowire (figure 2.24d) revealed the presence of mode at the pump wavelength, extending to the anti Stokes wavelength. Because of this the average field intensity inside the nanowire is fourfold and twofold enhanced at the pump and at the anti Stokes wavelength, leading to strong anti stoke scattering. Higher cavity temperatures also aid anti Stokes scattering because of presence of more phonons in the excited state.

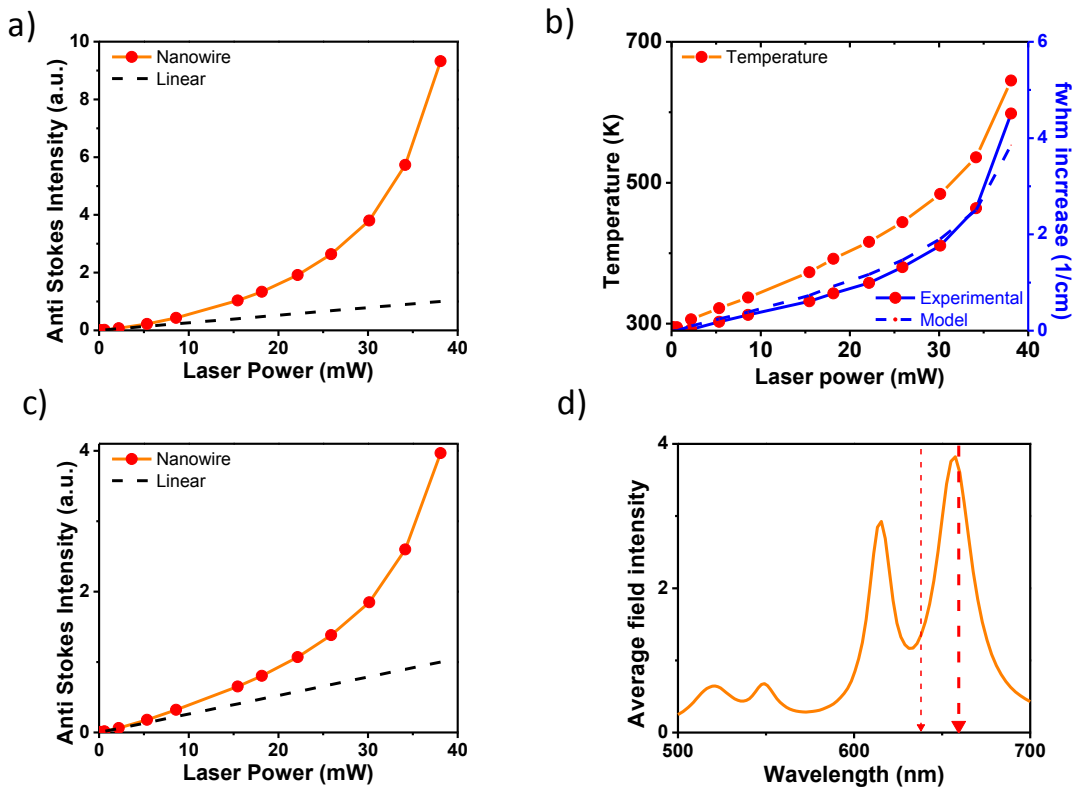

Figure 2.24: Stimulated anti Stokes Raman scattering in gold coated silicon nanowire of diameter 230 nm using a 660 nm pump: a) Power dependence of integrated anti Stokes intensity; b) Temperature (left vertical axis) and increase in FWHM (right vertical axis)as a function of laser power; c) Temperature corrected integrated anti Stokes intensity vs. pump power; d) Dependence of average electric field intensity inside the silicon nanowire of diameter 230 nm on wavelength. Vertical dash line represents the anti Stokes and the pump and wavelength from left to right.

The scattering cross section of anti Stokes scattering is much lower than that of Stokes scattering. In spite of that SARS is observed because of the tight confinement of electric field in the cavity. SARS in silicon nanostructures has never been reported before. It is interesting that cavities of similar size show SRS and SARS. This is because the cavity mode is broad enough to cover the pump wavelength, Stokes wavelength and anti Stokes wavelength leading to non-linearity on both sides. This type of cavities could be extremely important since, while the mode at Stokes side could be used to make a

Raman laser using SRS, enhancement on the anti Stokes side (SARS) could help in cooling the cavity. It may also be possible to make an anti Stokes laser from these cavities.

2.11 Conclusions and future directions

In conclusion, stimulated Raman scattering is attained in silicon nanowires by aligning the cavity mode with pump and Stokes wavelength. More than an order of magnitude enhancement in temperature corrected Stokes intensity is seen in bare nanowire cavities using a 660 nm pump; fivefold enhancement is observed in observed in metal coated cavities and in bare cavities at 532 nm. These enhancement values correspond to a gain value which is ~six orders of magnitude greater than in bulk at pump powers of the order of 10^6 W/cm^2. The reason for this high gain is the strong confinement of electric field modes inside the nanowire. Stimulated anti Stokes Raman scattering was also observed in nanowires when the cavity mode was aligned with the anti Stokes wavelength. This is the first report for SRS in homogeneous silicon nanostructures which have the potential to be monolithically integrated.

In spite of the high gain, peak narrowing (or lasing) was not observed. This could be because of two reasons: substantial heating was observed in nanowires due to absorption and stimulated Raman scattering and lattice anharmonicities lead to broadening of the Raman peak. Moreover in some cases, non uniform heating of the nanowire led to additional peak broadening. Secondly, scattering of photoexcited charge carriers from lattice led to asymmetric fano broadening. Coating a thick gold shell

reduced the fano interactions drastically and provided a good thermal sink for efficient heat loss which allowed the cavity to be pumped to higher powers. This led to observation of stronger instantaneous (higher slope of the log-log plot in metal coated nanowires compared to in bare nanowires) gain at higher pump power but losses in gold led to lower enhancement in SRS.

High temperature leads to a decrease in Raman scattering as well as a decrease in SRS. Therefore it is extremely important to have an efficient cavity heat management system without increasing the cavity losses. Between 532 nm and 660 nm, much larger Raman enhancement was observed at 660 nm. This is because of losses in silicon are ~ three times less at 660 nm than at 532 nm. Moreover no SRS was observed with a thick gold shell with a 532 nm pump even though SRS was observed in bare nanowires. This is because of the fact that d-band transitions in gold at 532 nm makes it much more lossy at 532 nm than at 660 nm leading to a decrease in observed Raman scattering.

Raman lasing was attained in silicon at 1.55 μm by making high quality factor cavities (10^6-10^{11}) and by minimizing the cavity losses. Our nanowire cavities typically have a quality factor of less than 100. Moreover, losses in silicon at 660 nm and at 532 nm are more than 8 orders of magnitude higher than at 1.55 microns. Comparing these factors and the fact that Raman scattering cross section is extremely low, it is almost incredible that any Raman gain is observed in the nanowire cavities. Nevertheless, decreasing the losses in silicon by only a factor of three, led to a threefold increase in SRS.

Below the bandgap of silicon losses in silicon would drastically decrease. Conducting measurements below the bandgap (where losses are drastically lower) in resonant cavities with the wave propagation distance along the nanowire long axis would increase the interaction length in the gain medium. This could potentially lead to lasing. Alternatively, methods to confine the silicon nanowire in another high quality factor cavity could also help in lasing. Lower losses would also keep the cavity temperature low, which would prevent deleterious effects of high temperature. Similar efforts towards optimizing the experimental conditions at the anti Stokes wavelength could lead to anti Stokes lasing. The advantage of anti Stokes lasing is that it would naturally act as cooling mechanism since anti Stokes scattering requires annihilation of a phonon which would prevent cavity heating. With proper cavity design, it may also be possible to achieve lasing at Stokes as well as anti Stokes wavelength, quite possibly in the same nanowire.

Because of lack of resources, these experiments could not be performed at the University of Pennsylvania. But the fact that a net Raman gain is observed in the nanowire cavities in the visible part of spectrum is very promising. This could potentially lead to the smallest Raman laser from a homogeneous silicon cavity having the lowest lasing threshold. Since nanowires are easy to synthesize and integrate into the existing microelectronics fabrication industry, this could lead to much better integration of optical technology into microelectronics industry leading to much faster device speeds and large energy and cost savings.

It would also be interesting to investigate the cause of strong fano resonance in silver coated cavities. Coating gold led to a dramatic decrease in fano interactions inside

silicon, to the extent that the fano coupling parameter (1/q) almost became 0. On the other hand coating silver enhanced these interactions (1/q ~ 0.1) and saturation in coupling factor was observed at pump powers of ~ 2E6 W/cm^2. It would be interesting to do Raman measurements with a reverse bias voltage applied across the silicon nanowire. Application of reverse bias has been shown to decrease the carrier lifetime[37] of photoexcited carriers. A decrease in carrier lifetime would decrease the fano interactions and hence the coupling factor (1/q). Dependence of 1/q on the applied reverse bias at a constant but high pump power could help better understand the mechanism of fano interactions and how to control them. Comparison of pump power and gate voltage dependent measurements could help in understanding the contributions of fano interactions in cavity heat generation and in decease of SRS. This could also help build a Raman laser on silver coated silicon nanowires.

---

[1] Sirleto, L., Ferrara, M.A., Nikitin, T. et.al. Giant Raman gain in silicon nanocrystals. Nature Communications **3** (1220), 1-6 (2012).

[2] Nikitin, T., Novikov, S. & Khriachtchev, L. Giant Raman gain in annealed silicon-rich silicon oxide films: Measurements at 785 nm. Applied Physics Letters **103**, 151110 (2013)

[3] Takahashi, Y. *et al.* A micrometre-scale Raman silicon laser with a microwatt threshold. *Nature* **498,** 470–4 (2013)

[4] Wu, J., Gupta, A.K., Gutierrez, H.R. et.al. Cavity-Enhanced Stimulated Raman Scattering from Short GaP Nanowires. Nanoletters **9** (9), 3252-3257 (2009)

[5] Zhang, B.P., Shimazaki, K., Shiokawa, T. et.al. Stimulated Raman scattering from individual single-wall carbon nanotubes. Applied physics letters **88**, 241101 (2006)

[6] Cho, C.-H., Aspetti, C. O., Park, J. & Agarwal, R. Silicon coupled with plasmon nanocavities generates bright visible hot luminescence. *Nat. Photonics* **7,** 285–289 (2013).

[7] Dhara, S., Mele, E. J. & Agarwal, R. Voltage tunable circular photogalvanic effect in silicon nanowires. Science **349,** 726-729 (2014).

[8] Raghunathan, V., Dimitropoulos, D., Claps, R. & Jalali, B. Raman induced wavelength conversion in scaled Silicon waveguides. *IEICE Electron. Express* **1,** 298–304 (2004).

[9] Aspetti, C.O., Cho, C., Agarwal, R. & Agarwal R. Studies of Hot Photoluminescence in Plasmonically Coupled Silicon via Variable Energy Excitation and Temperature-Dependent Spectroscopy. Nanoletters **14**(9), 5413-5422 (2014)

[10]Temple, P. A. & Hathaway, C. E. Multiphonon Raman Spectrum of Silicon. *Phys. Rev. B* **7,** 3685–3697 (1973).

[11] Magidson, V. & Beserman, R. Fano-type interference in the Raman spectrum of photoexcited Si. *Phys. Rev. B* **66,** 1–6 (2002).

[12] Gupta, R., Xiong, Q., Adu, C. K., Kim, U. J. & Eklund, P. C. Laser-induced fano resonance scattering in silicon nanowires. *Nano Lett.* **3,** 627–631 (2003).

[13] Balkanski, M., Wallis, R.F. & Haro, E. Anharmonic effects in light scattering due to optical phonons in silicon. Physical Review B 28 (**4**), 1929-1934 (**1983**)

[14] Balkanski, M., Jain, K. P., Beserman, R. & Jouanne, M. Theory of interference distortion of Raman scattering line shapes in semiconductors. *Phys. Rev. B* **12,** 4328 (1975).

[15] Cerdeira, F. & Cardona, M. Effect of Carrier Concentration on the Raman Frequencies of Si and Ge. *Phys. Rev. B* **5,** 1440 (1972).

[16] Sze, S.M. & Kwok K.N. Physics of semi conductor devices, third edition. (2006).

[17] Boyd, R.W. Nonlinear optics. Third Edition (2008)

[18] Jouanne, M., Beserman, R., Ipatova, I. & Subashiev, A. Electron-phonon coupling in highly doped n type silicon. *Solid State Commun.* **16,** 1047–1049 (1975)

[19] Liang D. * and Bowers J.E.; Recent progress in lasers on silicon; Nature Photonics **4**; (2010**)**

[20] Piscanec, S. *et al.* Raman spectroscopy of silicon nanowires. *Phys. Rev. B* **68,** 2–5 (2003).

[21] Adu, K. W., Gutiérrez, H. R., Kim, U. J. & Eklund, P. C. Inhomogeneous laser heating and phonon confinement in silicon nanowires: A micro-Raman scattering study. *Phys. Rev. B - Condens. Matter Mater. Phys.* **73,** 1–9 (2006).

[22] Temple, P. A. & Hathaway, C. E. Multiphonon Raman Spectrum of Silicon. *Phys. Rev. B* **7,** 3685–3697 (1973).

[23] Hart, T., Aggarwal, R. & Lax, B. Temperature Dependence of Raman Scattering in Silicon. *Phys. Rev. B* **1,** 638–642 (1970).

[24] Compaan, A., Lee, M. & Trott, G. Phonon populations by nanosecond-pulsed Raman scattering in Si. *Phys. Rev. B* **32,** 6731–6741 (1985).

[25] Compaan, a & Trodahl, H. Resonance Raman scattering in Si at elevated temperatures. *Phys. Rev. B* **29,** 793–801 (1984).

[26] Lux, O. *et al.* Stimulated Raman scattering and Raman laser operation in silicon single crystals at low temperatures. *Laser Phys. Lett.* **9,** 858–867 (2012).

[27] Khachadorian, S., Scheel, H., Colli, A., Vierck, A. & Thomsen, C. Temperature dependence of first- and second-order Raman scattering in silicon nanowires. *Phys. Status Solidi* **247,** 3084–3088 (2010).

[28] Venkateswarlu, K. Temmperature Dependence of the intensities of Raman lines. Nature **159**, 96-97 (1947)

[29] Jellison, G. E., Lowndes, D. H. & Wood, R. F. Importance of temperature-dependent optical properties for Raman-temperature measurements for silicon. *Phys. Rev. B* **28,** 3272–3276 (1983).

[30] Jellison, G. E. & Burke, H. H. The temperature dependence of the refractive index of silicon at elevated temperatures at several laser wavelengths. *J. Appl. Phys.* **60,** 841–843 (1986).

[31] Jellison, G. E. & Modine, F. a. Optical functions of silicon at elevated temperatures. *J. Appl. Phys.* **76,** 3758–3761 (1994).

[32] Jellison, G. E. & Modine, F. a. Optical constants for silicon at 300 and 10 K determined from 1.64 to 4.73 eV by ellipsometry. *J. Appl. Phys.* **53,** 3745–3753 (1982).

[33] Rong, H., Kuo, Y., Xu, S. et.al. Monolithic integrated Raman silicon laser. Optics express **14** (15), 6705-6712 (2006)

[34] Wang, C. *et al.* Extracavity pumped $BaWO_4$ anti-Stokes Raman laser. *Opt. Express* **21,** 26014 (2013).

[35] Rong, H., Liu, A., Nicolaescu, R. & Paniccia, M. J. Raman gain and nonlinear optical absorption measurements in a low-loss silicon waveguide. *Appl. Phys. Lett.* **85,** 2196–2198 (2004).

[36] Liang, T. K. & Tsang, H. K. Role of free carriers from two-photon absorption in Raman amplification in silicon-on-insulator waveguides. *Appl. Phys. Lett.* **84,** 2745–2747 (2004).

[37] Jones, R. *et al.* Net continuous wave optical gain in a low loss silicon-on-insulator waveguide by stimulated Raman scattering. *Opt. Express* **13,** 519–525 (2005).

[38] Bristow, A. D., Rotenberg, N. & van Driel, H. M. Two-photon absorption and Kerr coefficients of silicon for 850–2200 nm. *Appl. Phys. Lett.* **90,** 191104 (2007).

[39] Liu, A., Rong, H., Paniccia M. et.al Net optical gain in a low loss silicon-on-insulator waveguide by stimulated Raman scattering. Optics Express **12** (18), 4261-4268 (2004)

[40] Johnson, P.B. & Christy, R.W. Optical constants of noble metals. Phys. Rev. B **6**, 4370–4379 (1972).

[41] Palik, E. D. Handbook of Optical Constants of Solids. (Academic,1998).

[42] Abouie, M., Liu, Q. & Ivey, D. G. Eutectic and solid-state wafer bonding of silicon with gold. *Mater. Sci. Eng. B* **177,** 1748–1758 (2012).

[43] Arita, K., Fujiwara, K., Tsurumi, S. & Yamauchi, G. Eutectic Silver-Silicon Internally Oxidized Contacts. *Components, Hybrids, Manuf. Technol. IEEE Trans.* **4,** 122–127 (1981).

[44] Ipatova, I. P., Maradudin, A. A. & Wallis, R. F. Temperature dependence of the width of the fundamental lattice-vibration absorption peak in ionic crystals. II. Approximate numerical results. *Phys. Rev.* **155,** 882–895 (1967).

[45] Tsu, R. & Hernandez, J. G. Temperature dependence of silicon Raman lines. *Appl. Phys. Lett.* **41,** 1016–1018 (1982).

[46] Doerk, G. S., Carraro, C. & Maboudian, R. Temperature dependence of Raman spectra for individual silicon nanowires. *Phys. Rev. B* **80,** 073306 (2009).

CHAPTER 3: Cavity effects on Bose Einstein Distribution of phonons

3.1 Motivation

In the previous chapter enhancement of Stokes and anti Stokes scattering by cavity mode engineering was discussed. It would be interesting to compare the relative enhancement of anti Stokes and Stokes scattered field. More specifically, is it possible to tune the relative magnitudes of Stokes and anti scattering by cavity engineering and what is the effect of pump power and temperature on this ratio.

The ratio of anti Stokes to Stokes scattering is a measure of relative populations of bosons in excited and ground state respectively and has been extensively used to determine the temperature of the system[1] [2] [3]. Lauhon et.al [4] performed experiments on diameter dependence of Raman Stokes scattering intensities of silicon nanowires, in which they briefly mentioned that the anti Stokes to Stokes scattering intensity ratio should not be used to determine temperature of the nanowire without a diameter dependent term; although no experimental data or calculations were shown to corroborate this. The possibility of tuning the anti Stokes to Stokes scattering ratio at room temperature by cavity engineering seems extremely interesting. But before exploring these effects, it is important to review the basics and the equilibrium distribution of phonons in bulk silicon.

3.2 Bose Einstein Distribution and Temperature

It is important to differentiate the Bose-Einstein distribution of phonons from the ratio of anti-Stokes and Stokes scattered Raman intensities. Bose Einstein distribution/statistics describe the distribution of bosons (phonons) in the excited state as a function of total system energy or temperature. At a lower temperature, the energy of the system is low and hence more phonons occupy ground state. At a higher temperature, because of higher system energy, more phonons occupy the excited state. Thus the relative distribution of phonons in ground state to the particles in excited state can be used to determine the temperature of the system. Stokes scattering happens when a phonon in the ground state interacts with a photon to transition to an excited state, generating a photon with a slightly lower energy in the process. Anti Stokes scattering happens when a phonon in the excited state interacts with a photon to relax back to ground state, generating a photon of slightly higher energy in the process. Aside from some frequency dependent factors (discussed in the next paragraph) a photon is equally likely to interact with the phonons in the ground state and in the excited state. Therefore, the ratio of anti Stokes scattering to the ratio of Stokes scattering is equal to the ratio of populations to phonons in excited state to phonons in ground state.

Since Raman scattering and absorption which is frequency dependent are competing processes, Raman scattering is also affected by change in frequency. Besides different works have suggested different frequency (of scattered light) dependence of Raman scattering cross section. Equations 3.1 and 3.2 explicitly discuss two of the possible relations. Based on these parameters, various relations for scattering intensities

(Stokes and anti Stokes) and Bose Einstein distribution have been proposed some of which are mentioned below:

$$\frac{I_{AS}}{I_{St}} = \left(\frac{\omega_{AS}}{\omega_{St}}\right)^4 \exp\left(\frac{-\hbar\omega_o}{K_B T}\right)^5 \quad (3.1)$$

$$\frac{I_{AS}}{I_{St}} = A * \left(\frac{\omega_{AS}}{\omega_{St}}\right)^3 \exp\left(\frac{-\hbar\omega_o}{K_B T}\right)^6 \quad (3.2)$$

$$\frac{I_{AS}}{I_{St}} = F * \exp\left(\frac{-\hbar\omega_o}{K_B T}\right)^{7\,8} \quad (3.3)$$

$$\frac{I_{AS}}{I_{St}} = 1 * \exp\left(\frac{-\hbar\omega_o}{K_B T}\right)^9 \quad (3.4)$$

Where the subscript AS, St and p refer to anti Stokes and Stokes and pump, I is the scattering intensity, ω is the frequency, ω_o is the Raman shift, ħ is the Planck's constant, K_B is Boltzmann constant, T is the system temperature, and F is wavelength dependent constant and typically close to 1 (values in between 0.8 and 0.97 have been suggested in various studies). While a variety of relations have been suggested, there is no consensus as to which of these relations is correct and experimental proof has been shown to support each one of them.

For silicon the room temperature value (295 K) of the exponential term is 0.0774. For a 660 nm pump, using the equation 3.1-3.4, the range over which I_{AS}/I_{St} could vary should be 0.062 - 0.101.

3.3 Experimental details and measurements in bulk silicon

To investigate the effect of cavity size, cavity structure structure and wavelength on anti Stokes to Stokes scattering ratio, Raman measurements were performed on samples at room temperature using very low pump powers. The method of collecting data is exactly the same as described in chapter 2. Low powers ensured that there was no heating in the sample. Measurements were made at two - three different powers to ensure that there was no heating which would have been reflected by a change in the Raman shift. Measurements were performed on bare and gold coated nanowires with diameters ranging from 60 nm to 400 nm using both the pump wavelengths to check the wavelength dependence as well. To check the effect of cavity mode on the same nanowires, measurements were made on the same nanowire before and after coating gold using both the wavelengths. Procedure for doing scanning electron microscopy on bare and metal coated wires has already been described in chapter 2. Following the nanowire diameter determination, FDTD calculations were done to calculate the average electric field intensity inside the nanowire described in the same way in chapter 2. From these FDTD calculations ratio of average electric field intensity inside the nanowire at the anti Stokes wavelength and at the anti Stokes wavelength was calculated and compared to experimentally observed ratios of anti Stokes and Stokes intensity. Power dependent measurements on various wires were also conducted to investigate the dependence of anti Stokes to Stokes scattering ratio on the temperature of the cavity. Cavity temperature was calculated by using the change in Raman shift methods described earlier. For a 660 nm pump equation 3.1 and 3.2 are reduced to:

Repeated measurements performed on multiple silicon wafers at room temperature and at very low pump powers, typically in between 5E3 ~ 8E3 W/cm, using the 532 nm and the 660 nm pumps have revealed the anti Stokes to Stokes scattering ratio to be .080 and 0.098 respectively. While ratio differs for different pump wavelength it was consistent for multiple measurements using the same pump. From FDTD calculation ratio of average electric field inside the nanowire at the anti Stokes to that at Stokes was calculated to be 0.760 for the 532 nm pump and 0.950 for the 660 nm pump. The results have been summarized in table 3.1. Relatively lower electric field confinement at the anti Stokes wavelength (to Stokes field) with a 532 nm pump leads to a relatively lower anti Stokes scattering (to Stokes scattering) at 532 nm.

Wavelength (nm)	Experimental	FDTD calculations
532	0.080	0.761
660	0.098	0.950

Table 3.1: Anti Stokes to Stokes ratios in bulk silicon at different wavelengths. Experimental values are ratios of experimentally measured scattering intensities at anti Stokes and Stokes wavelength. FDTD calculations refer to the ratio of average electric field intensity inside the nanowire at the anti Stokes and Stokes wavelength.

To make a fair comparison across measurements for different cavities and at different wavelengths, all the measurements and FDTD calculations in nanowires were normalized by the corresponding number for bulk silicon. All experimentally measured anti Stokes/Stokes scattering ratios using the 660 nm pump were divided by the corresponding value for bulk (0.098). All ratios of average electric field intensity inside the nanowire at anti Stokes to Stokes wavelength with a 660 nm pump from FDTD

calculations were divided by the corresponding value for bulk (0.950). The same was done measurements and calculations at 532 nm. Based on these normalizations, two new quantities can be defined as following:

$$Theroretical\_ratio = \frac{\left(\frac{(E.E)_{anti\_stokes}}{(E.E)_{stokes}}\right)_{nanowire}}{\left(\frac{(E.E)_{anti\_stokes}}{(E.E)_{stokes}}\right)_{bulk}} \tag{3.5}$$

$$Experimental\_ratio = \frac{\left(\frac{(I)_{anti\_stokes}}{(I)_{stokes}}\right)_{nanowire}}{\left(\frac{(I)_{anti\_stokes}}{(I)_{stokes}}\right)_{bulk}} \tag{3.6}$$

where E.E is the average electric field intensity (at Stokes or anti Stokes wavelength) inside silicon obtained from FDTD calculations and I is the experimental scattering intensity at the anti Stokes or Stokes wavelength. It must be noted that these ratios represent only the relative electric field intensity and relative scattering intensities and must not be confused with the absolute electric field intensity or the absolute scattering intensity.

The value of 1 for theoretical ratio and experimental ratio, thus correspond to the value for bulk silicon. Values greater than 1 would correspond to a case where compared to bulk, the ratio of anti Stokes to Stokes scattering (or average electric field inside the nanowire) is higher in the nanowire. Values less than 1 would correspond to the case where compared to bulk, the ratio of anti Stokes to Stokes scattering (or electric field

intensity inside the nanowire) is lower in the nanowire. This helps compare the average enhancement/reduction in electric field intensity ratios in nanowire and its corresponding effect on enhancement/reduction in experimentally observed scattering intensities.

3.3 Anti Stokes – Stokes intensity ratios in silicon nanowire

Figure 3.1 shows the anti Stokes and Stokes Raman scattering spectra for a bulk silicon sample, and 2 nanowires of diameters 220 nm and 280 nm respectively, taken with a 660 nm pump. Each of the three spectra have been normalized to the maximum of corresponding Stokes spectrum so that the anti Stokes to Stokes ratio can directly be read from the vertical axis. The corresponding ratios of anti Stokes to Stokes intensity are 0.098, 0.058 and 0.342 respectively and have been summarized in table 3.2. The three silicon samples are identical in every way and have been measured under exactly same conditions at room temperature and suing the same pump wavelength. The only difference is in the diameter of silicon nanowires. Yet the three samples have different anti Stokes to Stokes scattering intensity ratios. It is unlikely that the phonon population itself is changing since that is determined only by the energy (temperature) of the system.

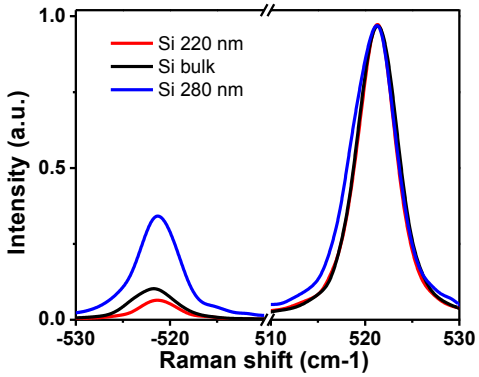

Figure 3.1: Anti Stokes and Stokes Raman spectra of 3 silicon samples: bulk, nanowires of diameter 220 nm and 280 nm collected using a 660 nm pump. The three spectra have been normalized with the maximum of Stokes intensity.

	anti Stokes/Stokes intensity ratio
Silicon nanowire 220 nm	0.058
Bulk silicon	0.098
Silicon nanowire 280 nm	0.342

Table 3.2: Anti Stokes/Stokes intensity ratio for three silicon samples at room temperature using a 660 nm pump. The numbers adjacent to the nanowires are the diameters of the nanowire

To better understand the nature of this discrepancy, average electric field intensity and the spatial distribution of electric field intensity inside the three samples (nanowires of respective sizes and bulk silicon) were calculated as a function of wavelength using FDTD simulations. Figure 3.2 presents the spatial electric field intensity profiles at the anti Stokes (a, c) and Stokes wavelength (b, d) for silicon nanowires of diameter 220 nm (a, b) and 280 nm (c, d). It can be seen that for the nanowire of diameter 220 nm, the electric field mode is more strongly confinement (more intense electric field intensity inside the nanowire) at the Stokes wavelength than at the anti Stokes wavelength, which should lead to a stronger average electric field intensity value at the Stokes wavelength. The situation is reverse in the nanowire of diameter 280 nm. The electric field intensity inside the nanowire is more intense at the anti Stokes wavelength than at the Stokes

wavelength which should lead to a stronger average field intensity value at the anti Stokes wavelength.

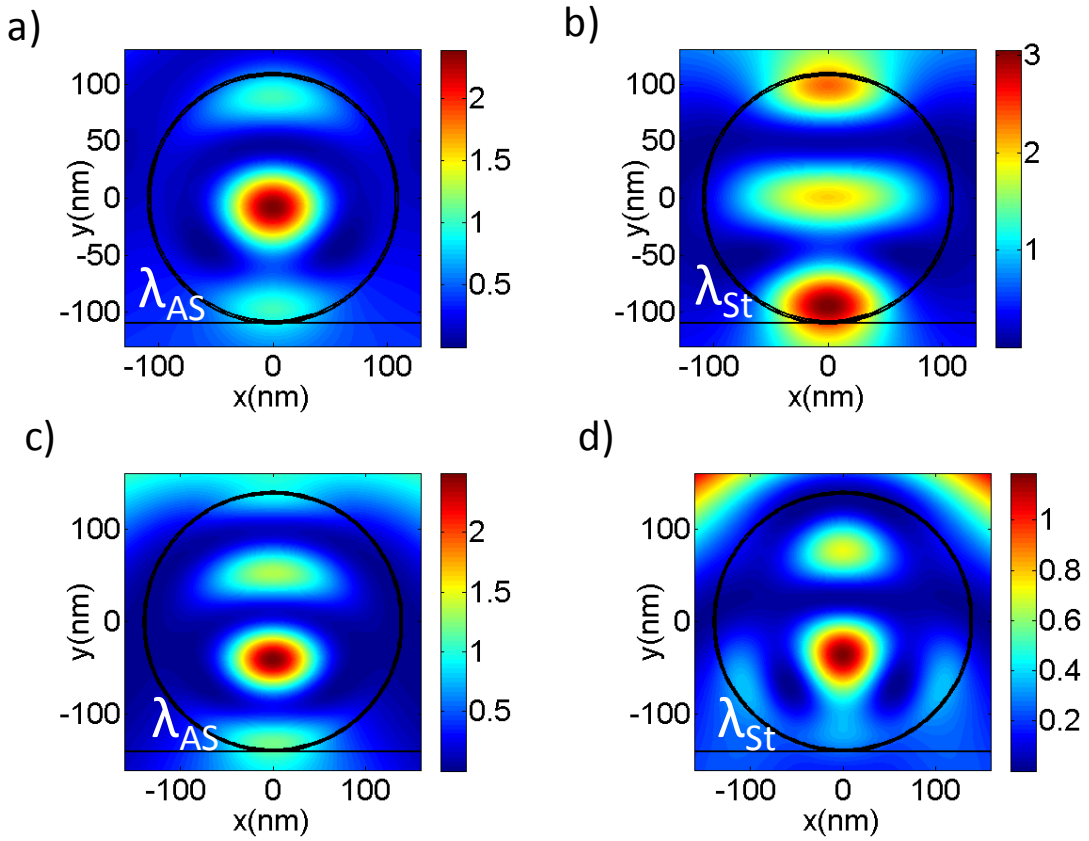

Figure 3.2: Spatial electric field intensity profile inside the nanowires at: a, b) anti Stokes and Stokes wavelength for the silicon nanowire of diameter 220 nm; c, d) anti Stokes and Stokes wavelength for the silicon nanowire of diameter 280 nm.

Average electric field intensities inside the silicon cavity (bulk and nanowires) as a function of wavelength have been shown in figure 3. The field intensity profile inside the bulk sample is almost independent of wavelength since there are no cavity modes in bulk silicon (ratio of average field at intensity at anti Stokes and Stokes field equals 0.950). The small difference is because of change in permittivity of silicon as a function

of wavelength. For the nanowire of size 280 nm, the average electric field intensity inside the nanowire is stronger at anti Stokes frequency than at Stokes wavelength. This higher confinement of anti Stokes field intensity relative to Stokes field intensity inside the nanowire leads to relatively stronger scattering at the anti Stokes wavelength than at the Stokes wavelength leading to a higher anti Stokes to Stokes scattering ratio than in bulk. Exactly opposite happens with the silicon nanowire of diameter 220 nm. The average electric field intensity inside the nanowire is stronger at Stokes wavelength than at anti Stokes wavelength leading to relatively stronger scattering at Stokes wavelength than at anti Stokes wavelength and lower anti Stokes to Stokes ratio than in bulk.

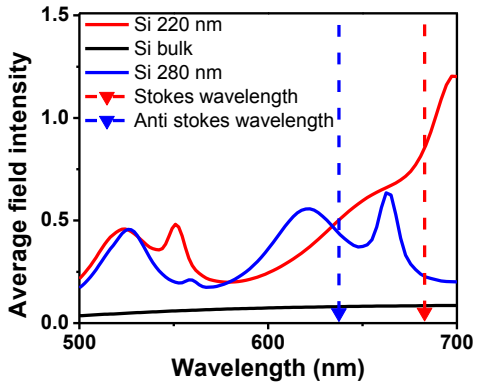

Figure 3.3: Average electric field intensity inside the silicon as a function of wavelength for bulk silicon and two nanowires of diameters 220 nm and 280 nm.

Theoretical and experimental ratios as defined in section 3.2 were calculated for the two nanowires. Table 3.3 summarizes the results of these calculations for both the nanowires and bulk silicon. It can be seen that a theoretical ratio greater than 1 leads to an experimental ratio greater than 1 and a theoretical ratio less than 1 leads to an experimental ratio less than 1.

	Theoretical ratio	Experimental ratio
Si 220 nm	0.62	0.81
Bulk	1	1
Si 280 nm	2.03	3.50

Table 3.3: Comparison of calculations for ratio of average electric field intensity in the nanowire at anti Stokes and Stokes wavelength with the ratio of experimental scattering intensity at anti Stokes and Stokes wavelength for silicon nanowires of diameter 220 nm and 280 nm and for bulk silicon. The values have been normalized with the corresponding bulk values.

Figure 3.4 shows the dependence of average electric field intensity at anti Stokes wavelength and at Stokes wavelength as a function of nanowire diameter. Diameter dependence of theoretical ratio can be obtained by dividing the blue curve (anti Stokes wavelength) with the red curve (Stokes wavelength) and then dividing that by the corresponding ratio for bulk silicon (0.950).

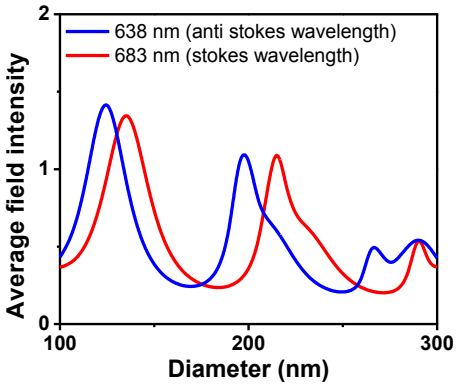

Figure 3.4: Average electric field intensity at anti Stokes (638 nm) and Stokes (683 nm) wavelength inside the silicon nanowire as a function of nanowire diameter.

3.4 Discussion

Changing the nanowire diameter changes the relative confinement of electric field intensity inside the nanowire at the anti Stokes and Stokes wavelength (theoretical ratio ≠1) which leads to a change in the density of state of photons at anti Stokes and Stokes wavelength[10]. This changes the way, photons interact with phonons resulting in different ratios of Raman scattering at the anti Stokes and Stokes wavelength (experimental ratio ≠ 1). In bulk silicon the ratio of confinement of electric field intensity is ~ 1 at 660 nm excitation. The direction and deviation of theoretical ratio away from 1 (stronger confinement of one of Stokes or anti Stokes field than the other) inside the nanowire directly correlates with the deviations of experimental ratio (relatively stronger Raman scattering at one of Stokes or anti Stokes field than the other). It is interesting that there is no additional external electric field (probe) at either Stokes or anti Stokes wavelength in the cavity and the only electric field generated will be from Raman scattering itself after the photon interacts with phonon. In other words, changing the density of state of photon that will be generated after the pump photon interacts with a phonon, the said interaction between the pump photon and phonon can be altered. The pump field should affect Stokes and anti Stokes scattering equally and should not cause any deviations of experimental ratio away from 1. This effect is seen even at extremely low pump intensities ($<10^4$ W/cm^2) so it unlikely that it is caused by any other non linear process.

To test this hypothesis, Raman measurements were performed under exactly similar conditions (room temperature, low power, 660 nm pump) on multiple nanowires of varying diameter in the range 100 nm to 300 nm. For each of these wires, theoretical

ratio and experimental ratio, as defined in section 3.3, were calculated. The results are shown in figure 3.5. Horizontal axis represents the diameter of the nanowire. The left vertical axis (in black) represents the experimental ratio and data for various nanowires is represented by circles. Depending on the diameter, nanowires have experimental ratio greater than or less than 1 pointing to either a relative (to bulk silicon) enhancement or reduction in the ratio of anti Stokes scattering to Stokes scattering. The right vertical axis (in red) represents the theoretical ratio. Calculations for nanowires of different diameters have been shown by a continuous plot highlighting the dependence of increase/decrease in the theoretical ratio on the nanowire diameter. The scales for the two vertical axes have been set up in such a way so that the 1 for each of them is coincident representing the value for bulk silicon which is shown in the graph by the black dashed line.

As can be seen in figure 3.5, a very good match in between experimentally observed ratios and theoretically calculated ratios is observed. If for a particular nanowire diameter, the FDTD calculations predict that the ratio of average electric field intensity at anti Stokes wavelength to Stokes wavelength is twice the value for bulk. Then the experimental anti Stokes to Stokes scattering intensity ratio is twice the corresponding value in bulk. Conversely, if the FDTD predict a lower ratio, then the same lower ratio is observed experimentally as well. This agreement in between theoretical and experimental ratios was found to hold true for the entire range of nanowire diameters on which experiments were performed (100 nm to 300 nm), confirming the validity of the hypothesis.

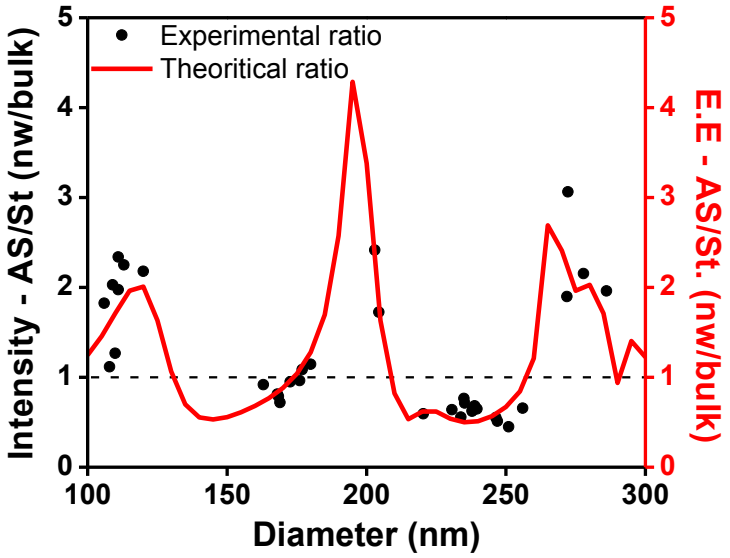

Figure 3.5: Comparison of experimental ratios (left vertical axis) and theoretical ratios (right vertical axis) (as defined in section 3.2). Left vertical axis: Dependence of anti Stokes to Stokes scattering ratio (relative to bulk) on nanowire diameter; Right vertical axis: Dependence of ratio of average electric field confinement at anti Stokes to Stokes wavelength (relative to bulk) on nanowire diameter.

AS and St refer to the anti Stokes and Stokes wavelength, Intensity refers to the experimentally observed scattering intensity, E.E refers to the average electric field intensity inside the nanowire, nw refers to nanowire.

3.5 Measurements in silicon-gold cavities

This is the first report of tuning the interactions of phonons with photons by changing the nanowire diameter which leads to a change in the photon density of states. In order to check the validity of this hypothesis to different cavity structures and different wavelengths, diameter dependent measurements were carried on silicon nanowires coated with a thick gold layer (~1.5 times the diameter of silicon nanowires) with a 660 nm pump and a 532 nm pump.

Deposition of gold changes the field confinement in the cavity and changes the position of resonant modes. Deposition of a metal also changes the carrier lifetime and carrier dynamics as has been shown previously[11]. If the ratio of scattering intensity is dependent only on the relative electric field confinement at the anti Stokes and Stokes wavelength, there should still be a good agreement in between experimental ratios and theoretical ratios. Figure 3.6a shows the dependence of anti Stokes - Stokes ratio on diameter of silicon nanowire for measurements in the diameter range of 50 nm to 360 nm. Similar to figure 3.5, the left vertical axis (in black) represents the ratio of experimentally observed anti Stokes – Stokes scattering intensity normalized for the same ratio in bulk (experimental ratios). The right vertical axis (in red) shows results of FDTD calculations for the ratio of average electric field intensity at the anti Stokes wavelength and the Stokes wavelength normalized to the same ratio for bulk (theoretical ratios). The theoretical ratios in the gold coated cavities are a little higher than in bare nanowires. This is because of the fact that coating gold leads to stronger confinement of electric field intensity inside the nanowire which leads to more skewed ratios. The figure shows that the agreement in between the experimental and theoretical ratios is very good over the entire range of nanowire diameter. Although a wide of ratio of anti Stokes to Stokes scattering intensity (normalized to bulk) has been observed (from ~0.35 to greater than 4.5), extreme scattering intensity ratios such as 10 were not observed. Although it is possible that measurements on more nanowires would reveal at least some wires to have extreme ratios, is could also be because of the fact that the theoretical calculations represent a highly ideal system which is not the case experimentally. Nevertheless, the

agreement in between the theoretically calculated ratios and experimentally observed ratios is very good.

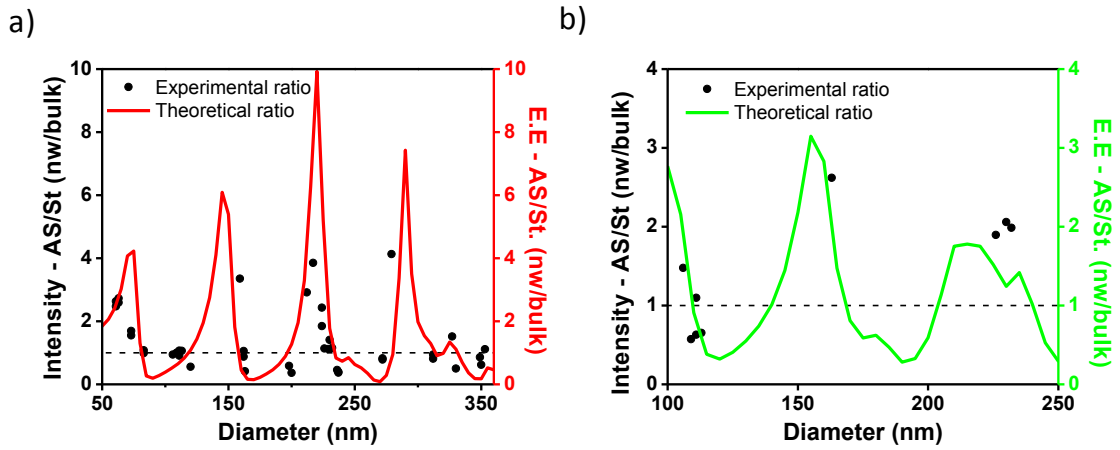

Figure 3.6: Comparison of experimental ratios (left vertical axis) and theoretical ratios (right vertical axis) (as defined in section 3.2 in gold coated silicon nanowires at a) 660 nm; b) and at 532 nm.

Left vertical axis: Dependence of anti Stokes to Stokes scattering ratio (relative bulk) on nanowire diameter; Right vertical axis: Dependence of ratio of average electric field confinement at anti Stokes to Stokes wavelength (relative to bulk) on nanowire diameter. AS and St refer to the anti Stokes and Stokes wavelength, Intensity refers to the experimentally observed scattering intensity, E.E refers to the average electric field intensity inside the nanowire, nw refers to nanowire.

Measurements were also carried out on similar cavities with a 532 nm pump to ensure that the hypothesis is valid at multiple wavelengths. At 532 nm, the ratio of anti Stokes to Stokes average electric field intensity are much lower than at 660 nm. This is because of the fact that higher losses in silicon and in gold lead to lower confinement (average electric field values) of electric field intensity inside the nanowire which makes the ratios less extreme. Good agreement similar to at 660 nm in experimentally measured and theoretically calculated ratios is observed (figure 3.6b).

Measurements were also carried at in the silicon-gold cavities with 660 nm pump in TE polarization (figure 3.7). While more polarization dependent measurements need to be done to get a clearer picture, it appears that at least in some cases, theoretical and experimental values may not agree.

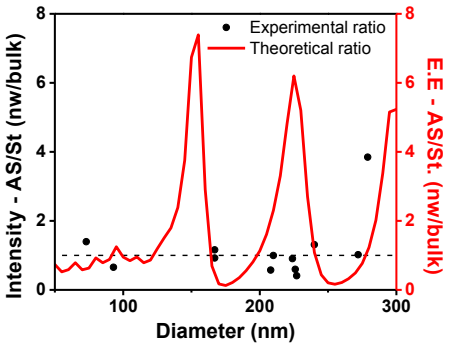

Figure 3.7: Comparison of experimental ratios (left vertical axis) and theoretical ratios (right vertical axis) (as defined in section 3.2 in gold coated silicon nanowires in TE polarization at 660 nm;

To prove that the anti Stokes/Stokes ratio depends on the relative confinement of modes in the nanowire and not on the intrinsic nanowire diameter, measurements were carried out on the same nanowire before coating gold using a 660 nm pump or after coating a thick gold layer (~1.5 times the thickness of nanowire) using a 660 nm or a 532 nm pump. For multiple nanowires either some of all of the three measurements were carried out. These measurements are important because for the same nanowire, depending on the combination of cavity (bare or gold coated silicon nanowire) and pump wavelength (532 nm or 660 nm), cavity modes will be different. This will change the relative confinement of average electric field intensity at Stokes and at anti Stokes wavelength, which should lead to different anti Stokes to Stokes scattering intensity ratios experimentally for the same nanowire. Figure 3.8 shows the data of four such nanowires in the diameter range 100 nm to 250 nm. Data for more nanowires was

collected to ensure consistency of trends but has been left out for the sake of redundancy. The figure shows the results for multiple nanowires plotted according to the method described in figures 3.5 to 3.7 except here only 1 vertical axis has been used for simplicity. The three continuous curves represent the theoretically calculated ratios of average electric field intensity inside the nanowire at anti Stokes and at Stokes wavelength (relative to bulk silicon) at three cavity-wavelength combinations. Accordingly the black, red and green curves represent data for bare nanowire with a 660 nm pump, gold coated nanowire with a 660 nm and gold coated nanowire at 532 nm respectively. The circles represent the experimentally observed ratios of scattering intensities. The color coding for circles is the same as for solid curves. For all the four nanowires, the circles are almost coincident with the curves for the corresponding colors pointing to a good agreement in experimental ratios and theoretical ratios. The same wire, depending on the relative confinement of mode at the anti Stokes and Stokes field leads to different anti Stokes to Stokes scattering intensity ratios.

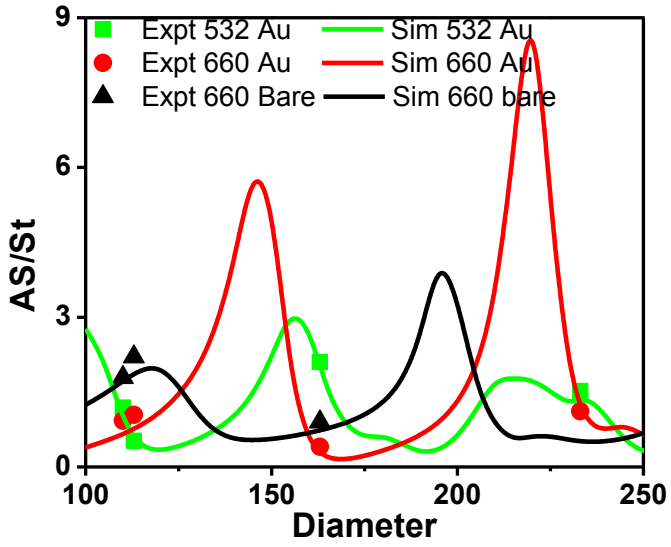

Figure 3.8: Comparison of scattering intensity ratios (relative to bulk) in the same nanowire with different mode confinement at Stokes and anti Stokes wavelength.

Expt refers to the experimental scattering intensity data. Sim refers to the theoretical calculations for ratio of average electric field intensity inside the nanowire at anti Stokes to Stokes wavelength. AS/St ratio refers to the corresponding ratios at anti Stokes and Stokes wavelength. Au refers to gold coated silicon nanowire, bare refers to bare silicon nanowire without gold

Experiments have been performed on a wide range of nanowire diameters (50 nm to 360 nm), using multiple wavelengths (532 nm and 660 nm) and using different cavity structures (bare and gold coated silicon nanowires). The good agreement in between experimental ratios and theoretical ratios lends credibility to the hypothesis that the scattering of one of anti Stokes or Stokes scattering relative to the other can be enhanced by tuning the cavity resonant mode with the desired wavelength. It is the relative tuning of the modes that is important and not the absolute tuning of either of the modes. Tuning both the modes in equally good or equally bad manner would not change the ratio of anti Stokes – Stokes scattering intensity, although it would change the absolute scattering of

Stokes or anti Stokes. These effects are observed at room temperature and at extremely low pump powers where it may be difficult for any non linear effects to make a significant contribution.

3.6 Variance of anti Stokes/Stokes ratio on temperature

To check the temperature dependence of anti Stokes to Stokes scattering ratio, measurements were carried out on multiple nanowires at high pump powers to induce heating. If the anti Stokes to Stokes scattering intensity ratio in a nanowire increases proportionally to the increase in phonon population in bulk silicon at higher temperature, it would confirm that cavity mode confinement alters the interactions in between photons and phonons at the very fundamental level. It would be particularly interesting to investigate the possibility of achieving higher anti Stokes scattering intensity than Stokes scattering intensity.

To make this comparison it is important to first estimate the temperature dependence of anti Stokes to Stokes scattering intensity ratio in bulk silicon. This can be extracted from the relation in between Bose Einstein distribution and anti Stokes to scattering intensity ratio from the expressions available in literature. By comparing the experimentally measured anti Stokes to Stokes scattering ratio at room temperature using a 660 nm pump for bulk silicon with equations 3.1-3.3 the following expressions can be attained

$$\frac{I_{AS}}{I_S} = 1.313 * \exp\left(\frac{-\hbar\omega_i}{K_B T}\right)^{+} \qquad (3.1b)$$

$$\frac{I_{AS}}{I_S} = 1.241 * \exp(\frac{-\hbar\omega_i}{K_B T})^{\&}; \quad (3.2b)$$

$$\frac{I_{AS}}{I_S} = 1.241 * \exp(\frac{-\hbar\omega_o}{K_B T}); \quad (3.3c)$$

where A in equation 3.2 is set to 1.011, experimental constant F in equation 3.3 is set to 1.241. Since equations 3.1 and 3.4 cannot be made to agree with the experimental results in bulk silicon at room temperature and equation 3.2 and 3.3 give the same dependence of anti Stokes to Stokes scattering on temperature, equation 3.2b (or 3.3b) is used to estimate the anti Stokes to Stokes scattering intensity in bulk silicon at temperature T that is calculated from the change in Raman shift method described in section 2.3. From these calculations, a quantity called phonon population ratio is defined which is the extent of increase in ratio of phonon population in excited state with respect to ground state at higher temperature normalized to the ratio at room temperature. It can be calculated by dividing the expression for equation 3.2 (or 3.3) at a temperature T, to the same at room temperature:

$$\frac{(\frac{I_{AS}}{I_S})_T}{(\frac{I_{AS}}{I_S})_{295K}} = \frac{[1.241 * \exp(\frac{-\hbar\omega_o}{K_B T})]_T}{[1.241 * \exp(\frac{-\hbar\omega_o}{K_B T})]_{295K}} \quad (3.7)$$

which reduces to:

$$\frac{(\frac{I_{AS}}{I_S})_T}{(\frac{I_{AS}}{I_S})_{295K}} = \frac{[\exp(\frac{-\hbar\omega_o}{K_B T})]_T}{[\exp(\frac{-\hbar\omega_o}{K_B T})]_{295K}} \quad (3.8)$$

It can be inferred that the relative increase in phonon population in excited state at a temperature T compared to at room temperature (*phonon population ratio*) is equal to the ratio of anti Stokes to Stokes scattering intensity (*AS/St*) at temperature T to the corresponding value at room temperature (295 K).

A comparison was made for the phonon population ratios of nanowires, calculated from the experimental data and the phonon population ratios for bulk silicon, estimated from calculated anti Stokes to Stokes scattering intensity ratios from equation 3.2b (or 3.3b). It is important to know what this comparison would look like for bulk silicon but since it was not possible to heat bulk silicon to high temperatures, a nanowire with anti Stokes to Stokes ratio similar to the bulk value was selected for the same. The results for anti Stokes to Stokes scattering intensity shown in figure 3.9 reveal a good agreement in the experimental anti Stokes to Stokes scattering intensity ratios and the estimated ratios from corresponding temperatures using the Bose Einstein distribution. At a temperature of ~ 500 K, based on the Bose Einstein distribution the AS/St ratio for bulk should be ~ 0.27. The corresponding experimental ratio is 0.31 which is in reasonably good agreement, given the different models involved in doing the calculations and estimating the ratios. Figure 3.9b shows the experimentally observed phonon populations ratio for the nanowire and the estimate for bulk at different temperatures. At a temperature ~ 500 K, based on the Bose Einstein statistics, the ratio of phonons is the excited state relative

to ground state should be about 2.7 times the corresponding ratio at 295 K. Experimentally this number was measured to be 3.1 which is in reasonably good agreement with the number from Bose Einstein statistics given the fact multiple models exist for this comparison (AS/St. scattering intensity vs. Bose Einstein statistics) with neither one of them being able to explain all the experimental results.

It may be possible to devise a new statistical distribution model which better agrees with the experimental data such as including temperature dependent absorption values but that is not the objective of this comparison. More extensive models for this comparison exist in literature and can be found in the following references[12 13]. The slight disagreement at higher temperatures could also be because of the fact that with a temperature change, the permittivity of silicon changes (also absorption) which changes the confinement of electric field intensity inside the nanowire cavities which would change the scattering intensities at Stokes and at anti Stokes wavelength leading to slightly different ratios. Wavelength dependent absorption values also change with temperature which would change the proportion of Raman scattering. The two graphs may look trivial at the moment but this is because a nanowire with a behavior similar to bulk silicon was selected to establish the trend of phonon population ratio and anti Stokes to Stokes scattering intensity.

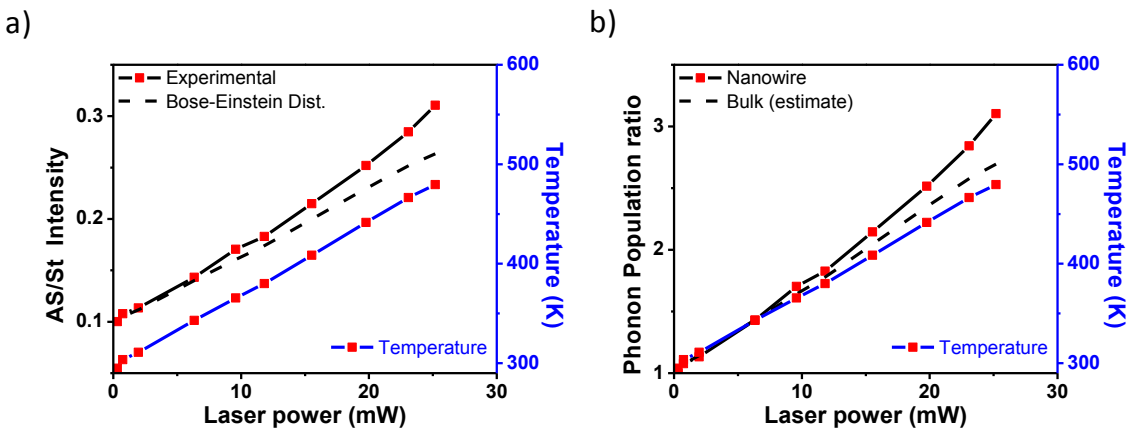

Figure 3.9: Comparison of a) anti Stokes to Stokes scattering intensity ratio (AS/St intensity); and b) phonon population ratio; at elevated temperature for a nanowire with bulk like anti Stokes to Stokes scattering intensity ratio

Figure 3.10 shows the similar comparison for a bare silicon nanowire of diameter 330 nm. The simulations predict relatively stronger enhancement at the anti Stokes wavelength. Accordingly, at room temperature a ratio of 0.28 for AS/St scattering intensity is observed which is much higher than the corresponding value in bulk. At a temperature of 470 K at which the bulk value for AS/St scattering ratio is 0.25, the ratio for the nanowire is 1 (figure 3.10a). At this point, the scattering at anti Stokes wavelength is equal to the scattering at Stokes wavelength. Such high values of AS/St scattering have never been reported before. While there is a mismatch in between anti Stokes to Stokes scattering intensity ratios, figure 3.10 shows that there is a relatively good agreement in the phonon population ratios measured experimentally and those estimated from Bose Einstein statistics.

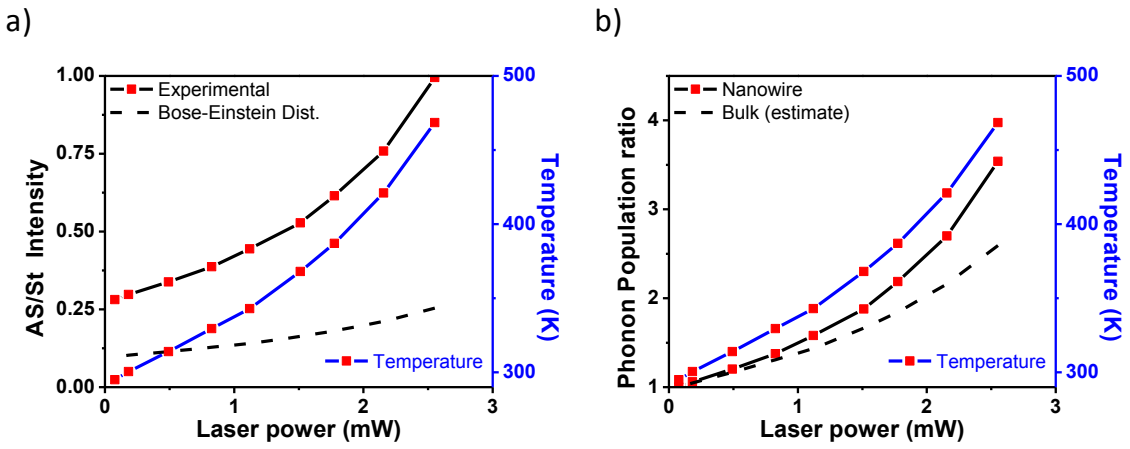

Figure 3.10: Comparison of a) anti Stokes to Stokes scattering intensity ratio (AS/St intensity); and b) phonon population ratio; at elevated temperature in a bare silicon nanowire of diameter 330 nm.

Good agreement is also observed in silicon nanowire coated with a thick gold shell (~1.5 times the diameter). Figure 3.11a and 3.11b show the data for one such silicon nanowire of diameter 60 nm. Although at a temperature of 580 K, the AS/St scattering intensity ratios measured experimentally and estimated from Bose-Einstein statistics are 0.85 and 0.35 respectively (figure 3.11a), very good agreement is observed in the phonon population ratios. These values for phonon population ratios at 580 K are 0.53 and 0.57 from experimental measurements and from Bose-Einstein's distribution respectively. In fact, for the entire temperature range and across all laser powers the experimentally determined phonon population ratios and those estimated from Bose-Einstein statistics are very similar (figure 3.11b).

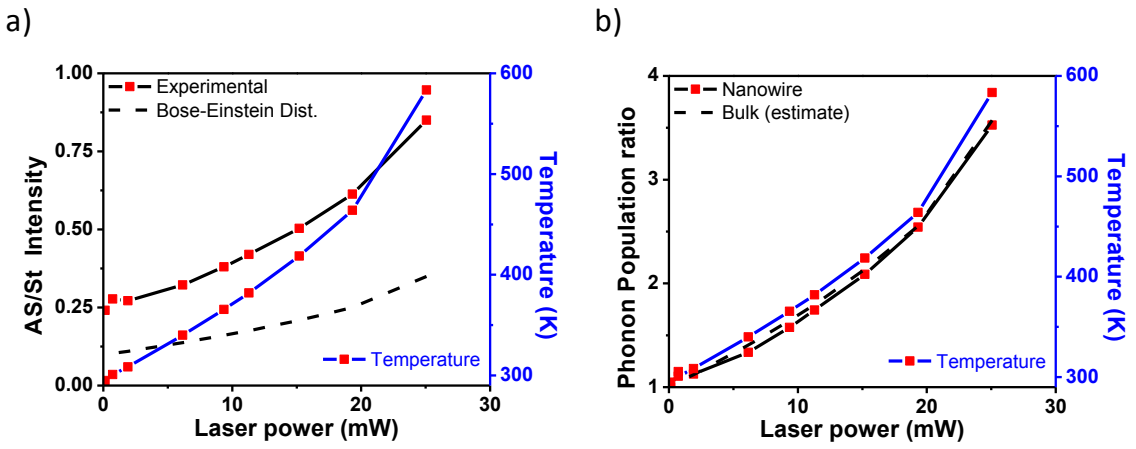

Figure 3.11: Comparison of a) anti Stokes to Stokes scattering intensity ratio (AS/St intensity); and b) phonon population ratio; at elevated temperature, in a silicon nanowire of diameter 60 nm, coated with a thick gold shell

Similar experiments were conducted on multiple nanowires with different levels of enhancement in AS/St ratio at room temperature which showed good agreement in phonon population ratios irrespective of the values of actual AS/St intensities. Even the most extreme cases which are presented here (experimental AS/St scattering intensity ratio approaching 1) show good agreement. Measurements performed on nanowires which showed a reduction in AS/St scattering intensity at room temperature revealed similar results. Figure 3.12 shows the results for a bare nanowire of diameter 234 nm (a and b) and a gold coated nanowire of diameter 190 nm (c and d). In the bare nanowire, data was collected up to a temperature of ~ 1000 K. At room temperature the AS/St scattering ratio is only 0.058 and at a temperature of 1000 K, the AS/St scattering intensity ratio is 0.32 while according to Bose-Einstein distribution calculations, it should be 0.61. In spite of this mismatch in between experimental and estimated AS/St

intensities, good agreement is observed in the phonon population ratios for the entire temperature range. Similarly in the gold coated nanowire, even though the room temperature value of AS/St scattering intensity is 0.37, much lower than the value of bulk (0.98), good agreement is observed in experimentally observed and estimated phonon population ratios.

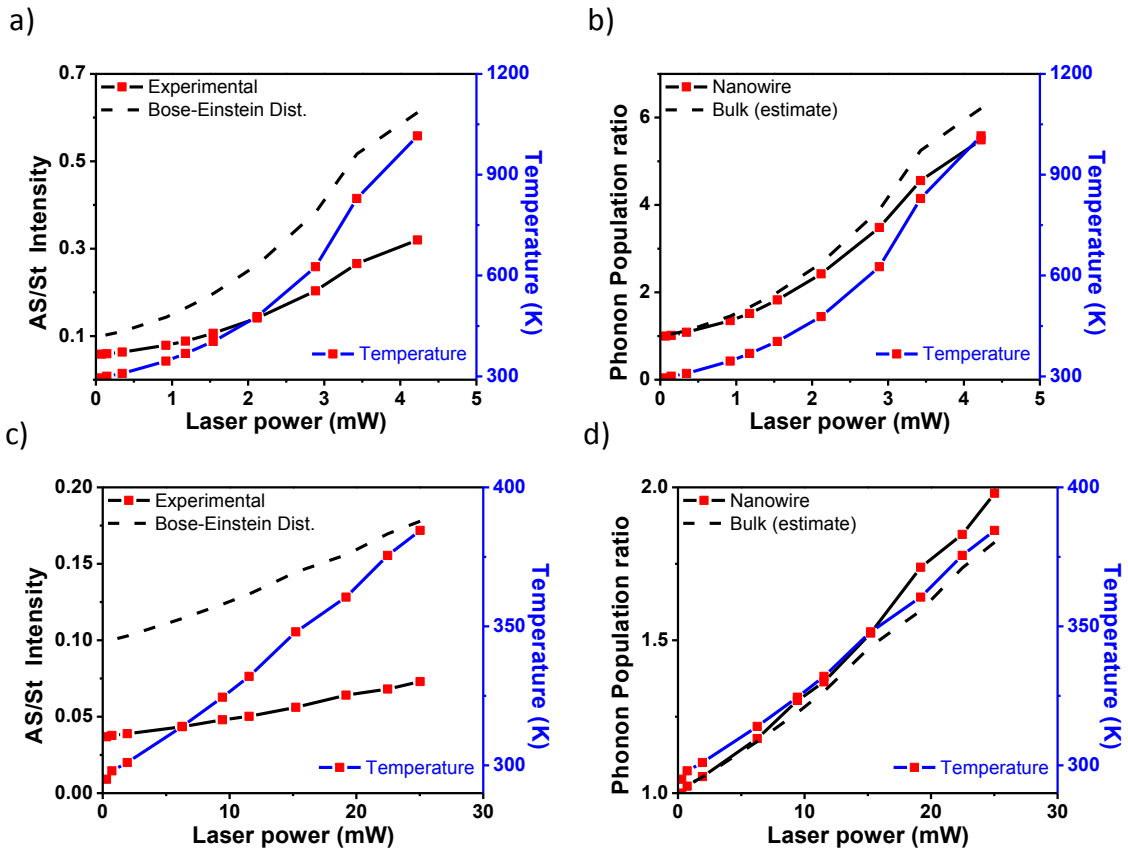

Figure 3.12: Comparison of a) anti Stokes to Stokes scattering intensity ratio (AS/St intensity); and b) phonon population ratio; at elevated temperature, in a silicon nanowire of diameter 234 nm; c-d) similar comparison for a silicon nanowire of diameter 190 nm coated with a thick gold shell

Experiments were conducted to explore the possibility of "population" – inversion; a state in which the population of phonons in the excited state is greater than the population of phonons in ground state. While physically it is not possible to achieve this for phonons, it may be possible to at least have a system in which anti Stokes scattering is greater than Stokes scattering. This was observed in a bare silicon nanowire (figure 3.14) at temperatures of ~ 650 K and above and at pump powers as low as 2E5 W/cm^2. Since anti Stokes scattering is greater than Stokes scattering, more phonons are annihilated than generated during the Raman process. This should lead to cooling of the nanowire. But because of absorption and other losses, which only generate phonons, a net decrease in the temperature of the system was not observed. The ratio drops at a pump power of 3.8E5 W/cm^2 most likely because the nanowire is damaged which leads to cavity destruction and changes the confinement of electric fields inside the nanowire leading to a change in the AS/St scattering intensity ratio.

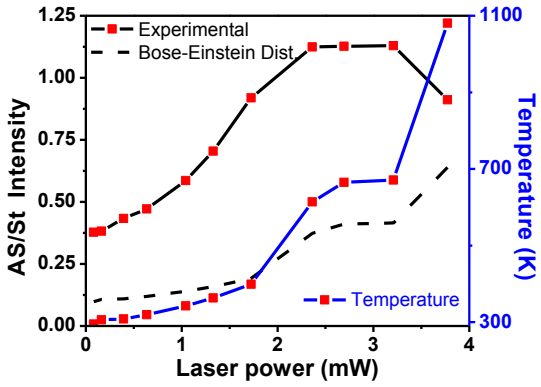

Figure 3.13: "Population"-inversion: Anti Stokes to Stokes scattering intensity ratio (AS/St intensity) showing greater intensity of anti Stokes scattering than Stokes scattering.

Note that it is possible to achieve "population"-inversion in many nanowires and many were shown to attain a state in which anti Stokes scattering was equal or almost

equal to Stokes scattering. But because of certain experimental constrains on availability of pump power, it was only be observed in a few nanowires. In certain cases, the nanowire temperature rose drastically (as in figure 3.13) which led to a destruction of cavity before "population"-inversion could be attained. Further experiments in gold coated nanowires using a higher pump power should reveal more instances of "population" inversion.

3.7 Concluding remarks and future work

In conclusion cavity engineering of anti Stokes – Stokes scattering intensity ratio has been shown. By changing the cavity size, variations by over a factor of ten have been observed (0.035-0.45) in the room temperature anti Stokes to Stokes scattering ratio. Nanowire diameter, excitation wavelength and cavity structure dependent measurements have confirmed that this ratio depends on the relative confinement of the anti Stokes and Stokes electric field intensity inside the cavity. A higher confinement of anti Stokes electric field intensity inside the nanowire (relative to Stokes electric field intensity) leads to higher relative (to Stokes scattering) emission of the anti Stokes scattering. Thus it is possible to enhance phonon-photon interactions by simply increasing the density of states (in the cavity) at the wavelength at which the new photon is expected to be emitted. While the absolute Stokes and anti Stokes scattering intensity also depend on the confinement of pump intensity, the ratio is completely independent of the confinement of the pump electric field inside the cavity.

Tuning of photon-phonon interaction using the cavity mode alignment has never been reported before. While this is very interesting purely as a scientific phenomenon, it could also be extremely critical in mitigating system heat and hence in the design of Raman lasers. During operation of Raman lasers, phonons are constantly being generated which lead to heating of the gain medium. This heating has detrimental effects on the quality of emission[14]. Since anti Stokes scattering leads to destruction of a phonon and hence cooling, it provides a natural mechanism for cooling of the gain medium. A Raman laser cavity which also has a strong confinement at the anti Stokes wavelength would also have enhanced anti Stokes emissions and would be heated to a lesser degree in the process.

High temperature measurements reveal that the tuning of anti Stokes-Stokes scattering intensity ratio on cavity mode is independent of the pump power and the system temperature. In other words the ratio continues to stay tuned even at elevated temperatures. This tuning ratio is important to understand and estimate from the application perspective of temperature determination from anti Stokes to Stokes ratio. The cavities can even be tuned to reach a state in which emission at anti Stokes wavelength is greater than the emission at Stokes wavelength leading to a net cooling effect in the cavity. While at above bandgap temperatures, due to high absorption related losses, net cooling was not observed, the cooling capacity of such systems is worth investigating with below bandgap excitation. Moreover when anti Stokes emissions is greater than Stokes emissions, the system is in a state of "population" inversion which was described as an important consideration for building an anti Stokes Raman laser[15].

Future FDTD simulations to predict cavities which can attain "population inversion" at lower temperatures and experiments on such cavities could reveal interesting results. The applications of optical cooling in silicon are immense given the demand of more energy efficient silicon based devices and understanding photon-phonon interactions is the key to achieving it

---

[1] Fang Z., Zhen Y., Halas N.J. et.al; Evolution of Light-Induced Vapor Generation at a Liquid-Immersed Metallic Nanoparticle; Nanoletters 13(4), 1736-1742 (**2013**)

[2] Balkanski, M., Wallis, R.F. & Haro, E. Anharmonic effects in light scattering due to optical phonons in silicon. Physical Review B 28 (4), 1929-1934 (1983)

[3] Compaan, A., Lee, M. & Trott, G. Phonon populations by nanosecond-pulsed Raman scattering in Si. *Phys. Rev. B* **32,** 6731–6741 (1985).

[4] Lopez, F. J. *et al.* Diameter and Polarization-Dependent Raman Scattering Intensities of Semiconductor Nanowires Diameter in single tapered silicon . (2012). doi:10.1021/nl204537d

[5] Fujimori, H., Kakihana, M., Ioku, K., Goto, S. & Yoshimura, M. Advantage of anti-Stokes Raman scattering for high-temperature measurements. *Appl. Phys. Lett.* **79,** 937–939 (2001).

[6] Doerk, G. S., Carraro, C. & Maboudian, R. Temperature dependence of Raman spectra for individual silicon nanowires. *Phys. Rev. B* **80,** 073306 (2009).

[7] Jellison, G. E., Lowndes, D. H. & Wood, R. F. Importance of temperature-dependent optical properties for Raman-temperature measurements for silicon. *Phys. Rev. B* **28,** 3272–3276 (1983).

[8] Gupta, R., Xiong, Q., Adu, C. K., Kim, U. J. & Eklund, P. C. Laser-induced fano resonance scattering in silicon nanowires. *Nano Lett.* **3,** 627–631 (2003).

[9]Hart, T., Aggarwal, R. & Lax, B. Temperature Dependence of Raman Scattering in Silicon. *Phys. Rev. B* **1,** 638–642 (1970).

[10] Cho, C.-H. *et al.* Tailoring hot-exciton emission and lifetimes in semiconducting nanowires via whispering-gallery nanocavity plasmons. *Nat. Mater.* **10,** 669–675 (2011).

[11] Cho, C.-H., Aspetti, C. O., Park, J. & Agarwal, R. Silicon coupled with plasmon nanocavities generates bright visible hot luminescence. *Nat. Photonics* **7,** 285–289 (2013).

[12] Lo, H. W. & Compaan, a. Raman measurement of lattice temperature during pulsed laser heating of silicon. *Phys. Rev. Lett.* **44,** 1604–1607 (1980).

[13] Tsu, R. & Hernandez, J. G. Temperature dependence of silicon Raman lines. *Appl. Phys. Lett.* **41,** 1016–1018 (1982).

[14] Vermeulen, N., Debaes, C., Muys, P. & Thienpont, H. Mitigating Heat Dissipation in Raman Lasers Using Coherent Anti-Stokes Raman Scattering. *Phys. Rev. Lett.* **99,** 093903 (2007).

[15] Vermeulen, N., Debaes, C. & Thienpont, H. Coherent anti-stokes Raman scattering in Raman lasers and Raman wavelength converters. *Laser Photonics Rev.* **4,** 656–670 (2010).

CHAPTER 4: Enhanced heating and localized surface plasmonic activity in silicon-gold nanocavity

4.1 Motivation

Chapters 2 and 3 discussed the effects of confining electric field modes inside silicon nanowires on nonlinear optical properties of silicon. At high pump powers, heating was observed. While the focus earlier was to design methods to reduce cavity heating, this chapter focuses on optimizing the cavity design to enhance the degree of excitation of localized surface plasmon modes in gold from the evanescent field inside the nanowire, and achieving high cavity temperature in the process.

Recently Halas et.al showed solar vapor generation using nanoparticles at ambient temperature[1 2 3]. Irradiating focused sunlight on gold nanoparticles (silica-gold core-shell structures) led to heat generation due to excitation of localized surface plasmons (LSP). The amount of heat generation was directly proportional to the degree of LSP excitation which was directly proportional to the intensity of sunlight (electric field) irradiated on the nanoparticles. Thus using focussed sunlight led to stronger electric field intensities inside the nanoparticles leading to stronger heat generation. In another experiment irradiating gold nanoparticles with a laser led to extremely high localized heating and high temperatures which promoted the growth of various nanostructures such as semiconductor nanowires and carbon nanotubes[4 5]. These reactions were carried out at room temperature and used small gold nanoparticles of the size of a few tens of

nanometers. Thus it was possible to perform high temperature reactions at ambient temperature leading to a decrease in energy requirements. Plasmonic heating (and/or hot electrons from plasmons) has also been shown to increase the rate of chemical reactions while irradiating from a laser or a UV/visible lamp[6] [7]. The principle behind the enhancement is similar, with light exciting plasmons in the metallic nanoparticles, which led to enhancement of the reaction rate either because of heat generation or because of generation of hot electrons from plasmons.

The success of these experiments depended on the degree of plasmon excitation which depends on the intensity of electric field irradiant upon the plasmonic nanoparticles. The experiments discussed above used either an inactive core (such as silica) or simple nanoparticles without the use of cavity engineering to enhance the plasmonic interactions such that higher degree of plasmon excitation and higher temperatures could be attained at much lower irradiation powers (laser or UV/visible lamp). Use of a high refractive index material as a core could lead to high electric field intensities inside the core (as was shown in chapters 2 and 3) and in the metal nanoparticle outside because of evanescent field extending into the nanoparticle from the nanowire.

The following chapter will focus on demonstrating a new method to tune and enhance the plasmon resonance properties of metals (gold) using novel semiconductor-metal nanowire cavity which is heated to high temperatures at cavity mode resonance. Using the combined effect of a high refractive index core enhanced by an effective metallic cavity and the LSPs in gold, temperature close to 1000K can be attained in these

cavities at a pump power as low as ~5.7E5 W/cm^2, which is highest reported temperature for any plasmonic system. Because of the resonant enhancement effect of cavity, the absorption inside the cavity is stronger than the sum of absorption values inside the individual components of the cavity if excited separately: a bare silicon nanowire and a hollow gold shell. The silicon core gives the additional advantage of accurate temperature measurement capabilities and the ability to control the plasmon resonance of gold even at high temperatures. Since gold is known to anneal at high temperature[8], the ability to control plasmon resonance wavelength could be particularly useful.

New silicon-gold cavities structures were designed and investigated to enhance their potential to achieve high temperature at lowest possible pump power. The mechanism of heat generation was investigated and methods to tune it to different wavelengths were explored.

4.2 Sample preparation and Experimental

Silicon nanowires procured from Sandia National Laboratories were transferred onto a cover glass slip. The silicon nanowires had a 2 nm thick native oxide layer on the surface[9]. Experiments were either conducted on bare nanowires or depending on the experiment, either a 10/150 nm gold or a 10 nm Ti layer was deposited on these wires using electron beam deposition (PVD 75, Kurt J. Lesker Company) at a low deposition rate of 0.2 Å s-1 for the first 10 nm and 1.0 Å/s for the remaining film (if applicable). Figure 4.1 shows the SEM image of a representative nanowire. Experiments were performed on nanowires in the diameter range 100 nm to 250 nm. To measure the

diameter of the nanowires, a thin (less than 10 nm) gold/palladium layer was sputter coated onto the sample and high resolution scanning electron microscopy (JOEL 7500F) was performed. Experiments were also performed on a bare bulk silicon wafer and a silicon wafer coated with 10 nm gold to compare the results with those of a nanowire/cavity.

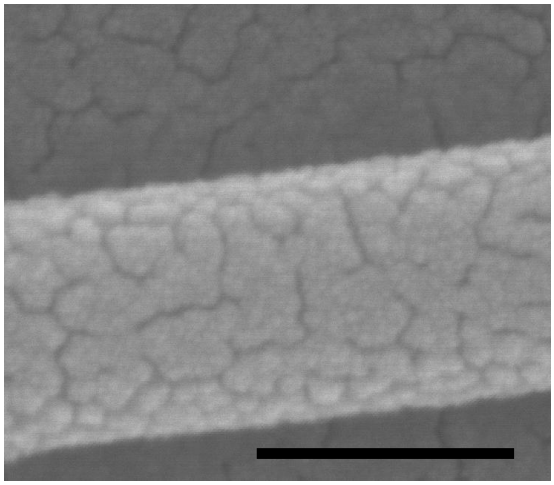

Figure 4.1: Scanning electron microscopy (SEM) image of a gold coated silicon nanowire (scale bar: 200 nm)

Raman spectroscopy was performed in the same way described in section 2.3 at 532 nm and 660 nm excitation. For bare nanowires and nanowires with a thin metallic shell, the cavity was excited from the nanowire size. With a thick metal the cavity was excited through the cover glass slip. Power dependent measurements were carried out with the power ranging from 5E3 W/cm^2 to 6E5 W/cm^2. Experiments were performed with the polarization of the incident electric field either parallel (TM polarization) or perpendicular (TE polarization) to the nanowire long axis (cavity schematic in figure 4.2).

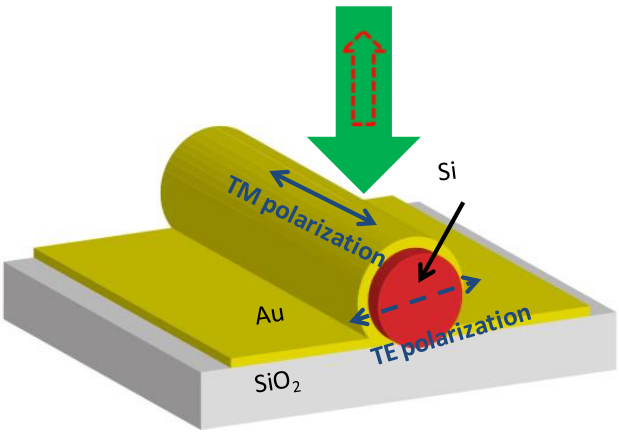

Figure 4.2: Schematic of cavity. Green and red arrows indicate direction of K vector of incident wave and back scattered Raman wave respectively, solid and dashed black arrows indicate direction of polarization of electric field of incident light in transverse magnetic (TM) and transverse electric polarization (TE) respectively.

Temperature of the nanowire was calculated by measuring the temperature dependent change in Raman shift of silicon as a function of pump power (details in section 2.3). The energy of Raman active longitudinal optical phonon of silicon decreases with an increase in temperature (phonon softening) at a rate of 2.73μeV/K at 295K (higher rate at higher temperature)[10] which has been demonstrated to provide a robust method for temperature calculation of the system from the change in Raman shift[11]. For recording the Raman spectra of bulk silicon, an ultra fine resolution grating with a resolution of 0.05 cm^{-1} was used to detect potential small changes in temperature.

Procedure for numerical calculations has already been explained in section 2.3. From the spatial distribution of electric field in the cavity, cavity absorption was calculated using the following expression:

$$Absorption = \frac{1}{2} * \omega * |E|^2 * (\varepsilon'') \qquad (4.1)$$

where ω is the frequency, Ɛ'' is the imaginary part of the permittivity of material at ω and E is the Electric field. Native oxide layer thickness was set to 2 nm in designing cavity structure for simulations.

Photocatalysis experiments were performed in collaboration with Dr. Matteo Cargnello in Prof. Chris Murray's group at the University of Pennsylvania. For performing these measurements, samples of silicon NWs were deposited on cover glass slides (18x18 mm, Fisher Scientific) and coated with a 10 nm gold film. Titania nanostructures were prepared from $TiCl_4$ in the presence of oleylamine and oleic acid according to[1213]. Solutions of these structures in hexanes/octane 8/2 v/v at concentrations of 5 mg mL^{-1} were drop-casted directly onto the substrate containing the cavity by reducing the evaporation rate by covering the substrate. Control samples were prepared by depositing a 10 nm gold film on the glass slide without the silicon nanowires followed by deposition of the titania nanostructures. Samples were dried overnight before further use. To perform photocatalysis, these films were immersed in a 4 mL of a 1/1 v/v solution of water/ethanol and tested in a semi-batch photoreactor under irradiation of a 300 W Hg/Xe lamp equipped with a water IR filter to remove the heat. Gaseous products were transported to a gas-chromatograph (Buck Scientific) by a flow of nitrogen, and hydrogen and other gaseous species were separated using a Shin Carbon column (Restek) and detected using a thermal conductivity detector and nitrogen as inert carrier gas. Cavity schematic is shown in figure 4.3

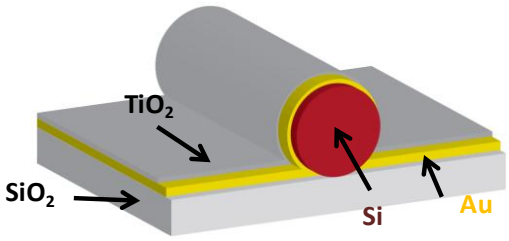

Figure 4.3: Schematic of cavity for photocatalysis experiments

4.3 Optical measurements on a silicon wafer

Figure 4.4 a and b show the power dependent Raman spectra obtained from a bare silicon wafer and a silicon wafer coated with 10 nm gold respectively with 532 nm excitation. While Raman spectrum was collected at multiple powers, only the spectra at lowest and highest powers have been shown here. There was no change in Raman shift in bare silicon wafer at powers up to 1.2E6 W/cm^2 (highest possible pump power) implying that there was no change in the temperature of silicon wafer upon laser irradiation. This is because of the large size of silicon wafer which would require a large amount of power to show any heating. Measurements carried out on 10 nm gold coated silicon wafer revealed a small change of 0.2 cm^{-1} in the Raman spectra at the highest and the lowest power. This shift corresponds to a temperature increase of 10 K in the silicon wafer. While this change may appear small, it is brought about by an extremely thin 10 nm gold layer (particles in the film) and points to the presence of localized heat generated by the gold film.

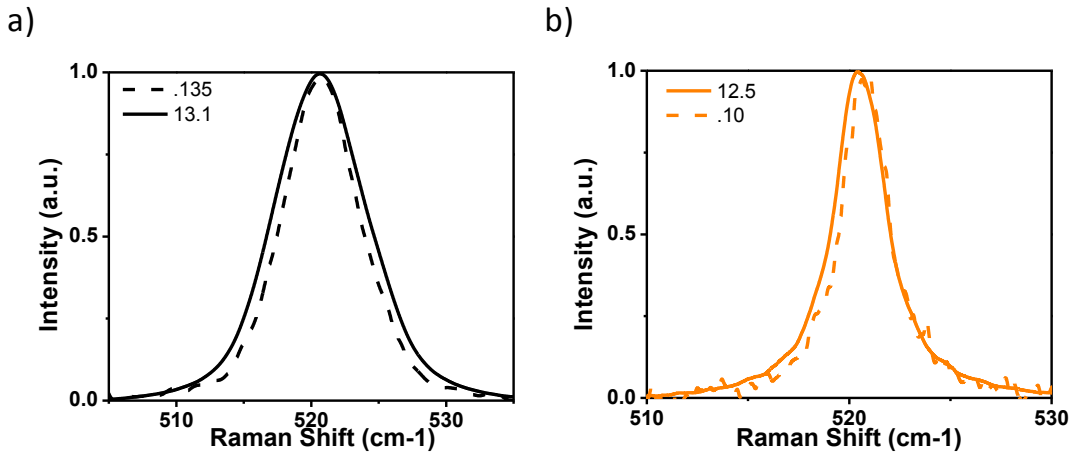

Figure 4.4: a-b) Power dependent Raman spectra using a 532 nm pump of a) Bare silicon wafer; b) Silicon wafer coated with 10 nm gold. Legend indicates pump power in mW.

4.4 Optical measurements on silicon nanowires

To test the enhancement in heating brought about by silicon-gold resonant cavity structures; a cavity was fabricated by coating a 10 nm gold layer on silicon nanowire placed on a glass substrate. The 10 nm thick gold film breaks into small particles with an interparticle separation of ~ 5 nm as can be seen in the scanning electron microscopy (SEM) image in figure 4.1. The amount of cavity heating which is also directly related to the degree of plasmonic excitation was assessed by calculating the temperature of the silicon core by measuring the change in temperature dependent phonon energy of silicon via Raman scattering[14] (ref. and citations). Power dependent Raman measurements on a bare silicon nanowire of diameter 100 nm (fig. 4.5) revealed that with an increase in laser power, Raman shift decreased in energy suggesting an increase in temperature of the silicon nanowire.

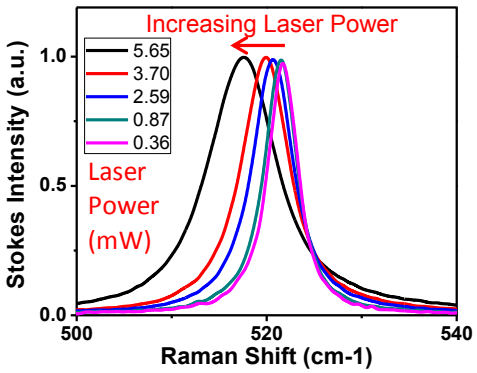

Figure 4.5: Raman spectra of a bare silicon nanowire (100 nm diameter) at different incident powers using 532 nm wavelength in the TM polarization.

The change in the phonon energy (Raman shift) of the silicon nanowire as a function of laser power was fitted with the Raman shift vs. temperature model proposed by Balkanski et.al[10] to obtain the temperature of the silicon nanowire as a function of laser power. These temperature calculations (figure 4.6a) from the Raman spectra of bare silicon nanowire revealed that a peak temperature of ~ 500K was achieved in the TM polarization (solid black curve) at a laser power of 5.7E5 W/cm^2. Raman measurements performed on the same nanowire after coating a 10 nm gold film revealed that there was a dramatic increase in temperature of the system and a peak cavity temperature of 1000 K was observed in TM polarization at the same laser power of 5.7E5 W/cm^2 (figure 4.6a, solid golden curve). Compared to previous reports in metal-semiconductor structures in which indirect estimates of potential temperatures achieved during plasmonic excitation using either the rate of chemical reactions or analytical calculations[15 16 17 18] have been made, use of silicon in this work provides a method to directly measure the temperature. To understand this enhanced heating effect, absorption spectra of bare and gold coated silicon nanowire of diameter 100 nm (figure 4.6b) was calculated via the finite difference time domain (FDTD) methodology. Calculations for bare silicon nanowire (figure 4.6b,

solid black curve) indicated that the cavity mode was resonant with the excitation wavelength of 532 nm with a peak absorption value of ~ 8% in TM polarization. Silicon is an indirect bandgap (E_g) material (E_g ~ 1.12 eV, 1.11μm)[19] and since the pump wavelength used in the current work (532 nm and 660 nm) is above the bandgap of silicon but below the direct bandgap, the absorption is high but during relaxation of charge carriers, the rate of nonradiative recombination is ~ 10^6 times faster than that of radiative recombination[20]. As a result, most of the photons absorbed decay nonradiatively generating a large number of phonons thereby generating heat. Calculations also indicated that after deposition of a 10 nm gold layer around the silicon nanowire (figure 4.6b, solid golden curve) the cavity absorption increased to 14% in the TM polarization, leading to increased heat generation in the cavity. Almost the entire amount of increased absorption in gold generates heat since only a small fraction (~10^{-10}) of the absorbed light in gold is emitted radiatively via d-band transitions[21].

Polarization (incident electric field) dependent measurements of cavity heating were also conducted. It was observed that the bare silicon nanowire and the gold coated silicon nanowire were heated to higher temperature in the TM polarization compared to TE polarization (figure 4.6a, solid vs. dashed curves): 500 K vs. 360 K in bare silicon nanowire and 1000 K vs. 860 K in gold coated silicon nanowire. Absorption values from FDTD calculations supported the experimentally observed polarization dependence at 532 nm (figure 4.6b, vertical green dashed line), with higher absorption in the TM polarization in both, bare (7.5% vs. 5%) and gold (14% vs. 9%) coated silicon nanowire.

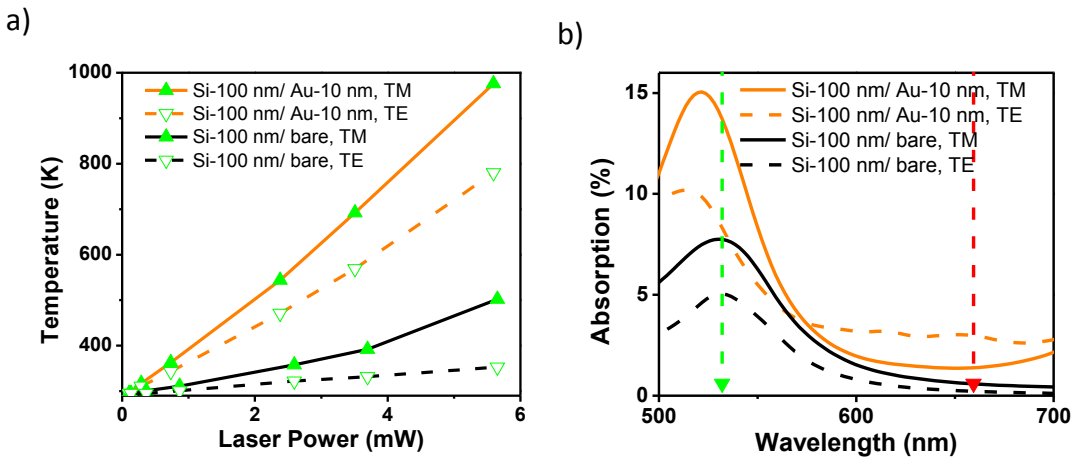

Figure 4.6: Extra ordinary heating of gold coated silicon nanowires: a) Temperature vs. laser power for the gold coated nanowire calculated from the Raman spectra shown in figure 4.5) and also for the same nanowire after coating 10 nm gold; b) Computational simulations of absorption spectra of the nanowire cavity for gold coated and bare nanowire of diameter 100 nm in TM and TE polarization. Vertical green and red arrows indicate the wavelength of the pump (532 nm and 660 nm)

In order to better understand the mechanism of cavity absorption and heating, spatial distribution of the electric field intensity was calculated from the FDTD calculations in bare and gold coated silicon nanowire of diameter 100 nm. Calculations revealed that at 532 nm excitation, at cavity mode resonance in TM polarization, the electric field mode is confined inside the bare silicon nanowire (figure 4.7) with low mode volume and with a fourfold enhancement in field intensity compared to incident intensity; a consequence of high refractive index of silicon. This highly intense electric field leads to high cavity absorption (8%) and consequently high heating. The intense evanescent field also extends into the gold film (in the gold coated cavity, figure 4.7) leading to a significant increase in cavity absorption (14%) and heating, since gold[22] is

much more lossy than silicon[23] (imaginary part of permittivity of gold ε''_{Au} = 2.2 vs. ε''_{Si} = 0.39 for silicon at 532 nm).

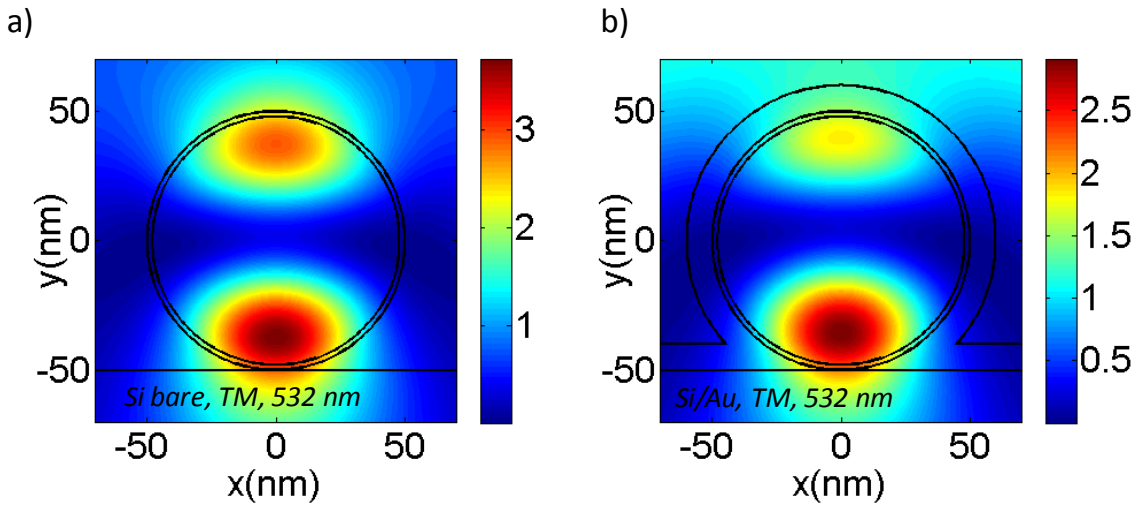

Figure 4.7: Mechanism of heating: a-b) Electric field distribution inside the cavity in TM polarization for bare and 10 nm gold coated nanowire of diameter 100 nm respectively at 532 nm

To further investigate the effect of mode confinement, the intense evanescent field and cavity absorption on heating, measurements were performed on this cavity with a 660 nm excitation wavelength. This excitation wavelength was chosen because according to FDTD calculations, the electric field is poorly confined by the silicon nanowire at 660 nm resulting in weaker electric field in silicon and in gold. The peak electric field intensity inside the cavity is ~ three times lower at 660 nm (figure 4.8b) than at 532 nm (figure 4.7b) in the gold coated nanowire in TM polarization. Moreover both silicon[23] and gold[22] are less lossy at 660 nm compared to at 532 nm (ε''_{Si} = 0.39 at 532 nm vs. ε''_{Si} = 0.12 at 660 nm, ε''_{Au} = 2.2 at 532 nm vs. ε''_{Au} = 1.0 at 660 nm). These factors lead to

lower cavity absorption in bare (0.6%) and in gold coated silicon nanowire (1.4%) as can be seen in figure 4.6b. Experiments performed on bare silicon nanowire revealed that the temperature of bare nanowire was ~ 320 K (figure 4.8a) at a pump power of ~ 6E5 W/cm^2, in agreement with the low absorption value obtained from calculations. Since there is only a marginal increase in absorption value after coating gold on the silicon nanowire (1.4% vs. 0.6%), only a small increase in temperature of the gold coated silicon nanowire (from 320K in bare silicon nanowire) is expected at comparable laser excitation powers. But there was a substantial increase in cavity heating and a temperature close to 550 K was attained in the cavity. This sudden increase in cavity heating is because of excitation of LSPs in the gold film. It can be seen in the SEM micrograph (figure 4.1) that the gold layer breaks into small particles of size 20-30 nm and a thickness of ~ 10 nm (10 nm gold layer was deposited). These particles support LSP modes[24] in the visible range because of the evanescent field extending from the silicon nanowire. Moreover since the particles in the film are separated by a distance of only ~ 5 nm, the gold particles interact with each other leading to further strengthening of the LSP excitations[25]. Thus excitation of these LSPs from the evanescent field leads to a drastic increase in cavity heating after coating gold.

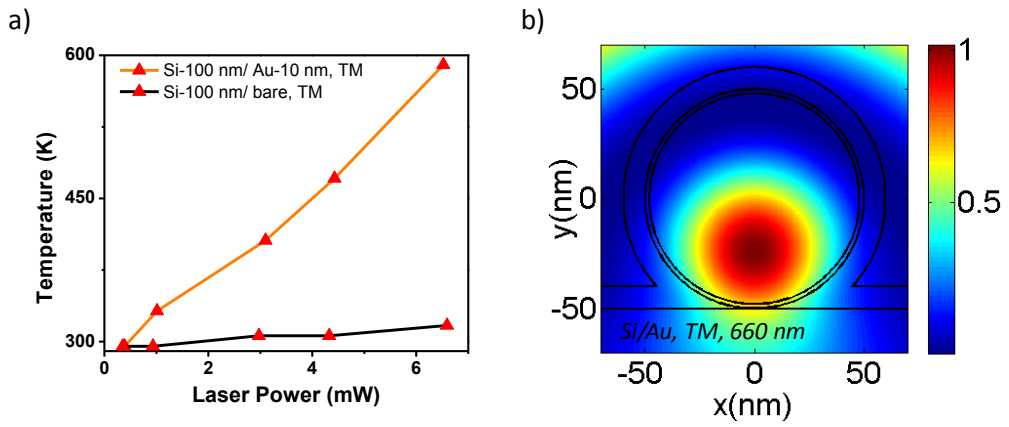

Figure 4.8: Heating in a cavity with off resonance excitation: a) Temperature vs. laser power for gold coated and bare nanowire of diameter 100 nm in TM polarization at 660 nm excitation; d) Electric field distribution inside the silicon nanowire of diameter 100 nm coated with 10 nm gold in TM polarization at 660 nm

The strength of LSP excitation can be controlled by altering the strength of evanescent field extending into the gold film. When a cavity mode exists at the excitation wavelength, the evanescent field intensity in the gold film is more intense than otherwise, leading to stronger LSP excitation (and more absorption) and consequently higher heating as was seen at 532 nm excitation (figure 4.6a) where temperature of the cavity increased from 500K to 1000K after coating gold. The broadband and polarization independent nature of these LSP excitations because of the random shape, size and orientation of the gold particles in the film makes the cavity heating less anisotropic. Thus decreasing the strength of the evanescent field in the gold film by detuning the cavity mode of the silicon nanowire at 660 nm, drastically reduces the cavity heat generation and the strength of LSPs excitation (and cavity absorption), highlighting the importance of presence of a cavity mode of silicon nanowire at the excitation wavelength.

In order to ascertain the contribution of LSPs towards heating, two control experiments were performed. In the first experiment, to prevent LSP excitation at the silicon-gold interface, a cavity was fabricated by coating a 150 nm thick gold film on a silicon nanowire of diameter 100 nm. Since the field penetration depth in gold at 532 nm is ~ 50 nm, laser irradiation was done through the glass substrate (schematic in inset of figure 4.9a). As a result of this, the electric field would be too weak to excite any LSPs at the air-gold interface thereby decreasing the heat generation in this cavity with a 150 nm gold film compared to a cavity with only 10 nm gold film. Raman measurements done with pump power up to ~6E5 W/cm^2 revealed (figure 4.9a) that while the bare silicon nanowire was heated to a temperature of 500 K, the temperature of the cavity after coating 150 nm gold was only 380 K, lower than that of even the bare silicon nanowire even though the cavity absorption increased fourfold after coating gold (27% vs. 7%, figure 4.9b). This decrease in temperature is because of two reasons: prevention of LSP excitation in the cavity with 150 nm gold layer; and availability of a larger heat sink (thicker gold film) to dissipate heat.

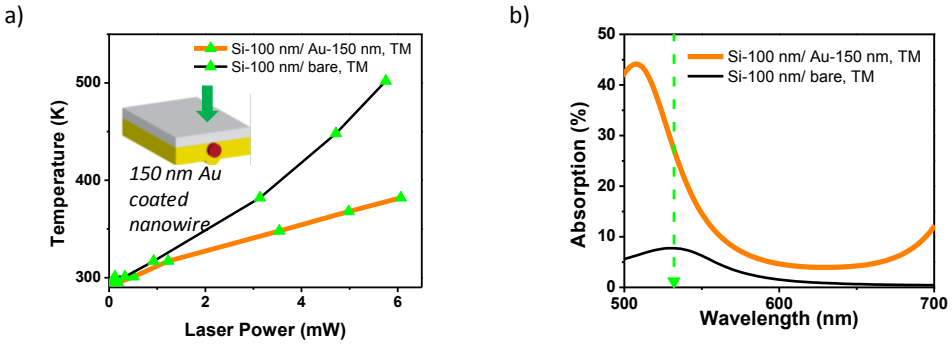

Figure 4.9: Role of localized surface plasmons in heating: a) Temperature vs. laser power of a silicon nanowire of diameter 100 nm coated with 150 nm gold in TM polarization (532 nm excitation), inset shows the schematic of the experiment; b) Computational simulations of absorption spectra of the metal-nanowire cavity in a)

In the second experiment, to prevent the formation of LSPs in the thin metallic film while maintaining the same cavity structure and thickness of metal, a 10 nm thick titanium (Ti) layer (instead of gold) was coated on a silicon nanowire of diameter 100 nm. While Ti does not support any plasmon modes at this wavelength[23], it is more lossy than gold[22] at 532 nm (ε''_{Ti} = 9.3 vs. ε''_{Au} = 2.2). This should lead to higher absorption in this cavity compared to a similar cavity with gold, a hypothesis supported by FDTD calculations (figure 4.10a), which should cause higher heat generation if LSPs were not contributing to cavity heat generation in the gold coated cavity. Since the thermal conductivity of Ti (21.9 W/m/K)[26] is more than an order of magnitude lower than that of gold (317 W/m/K)[26] and both have similar specific heat capacities (Ti = 2.35 J/cm^3/K, gold = 2.49 J/cm^3/K)[26], temperature in Ti cavity should be higher than in gold cavity even for the same amount of cavity heat generation. In other words, if LSPs do not contribute to heating in the gold cavity, then under otherwise similar experimental conditions in a Ti cavity, temperature of 1000K should be achieved at powers much lower than 6E5 W/cm^2 at 532 nm excitation. But experiments revealed that temperature in the Ti coated cavity was only 650K (figure 4.10b), much lower than in the gold coated cavity (1000K at pump powers ~ 5.7E5 W/cm^2). This is only possible if LSPs contribute significantly to heat generation in the gold cavity. In essence, without any LSP activity in gold particles, temperature of the gold coated cavity should be lower than 650K. But contributions from LSPs excited from a strong evanescent field (at silicon nanowire cavity mode resonance) increase the temperature of the silicon-gold cavity to 1000K (figure 4.6a).

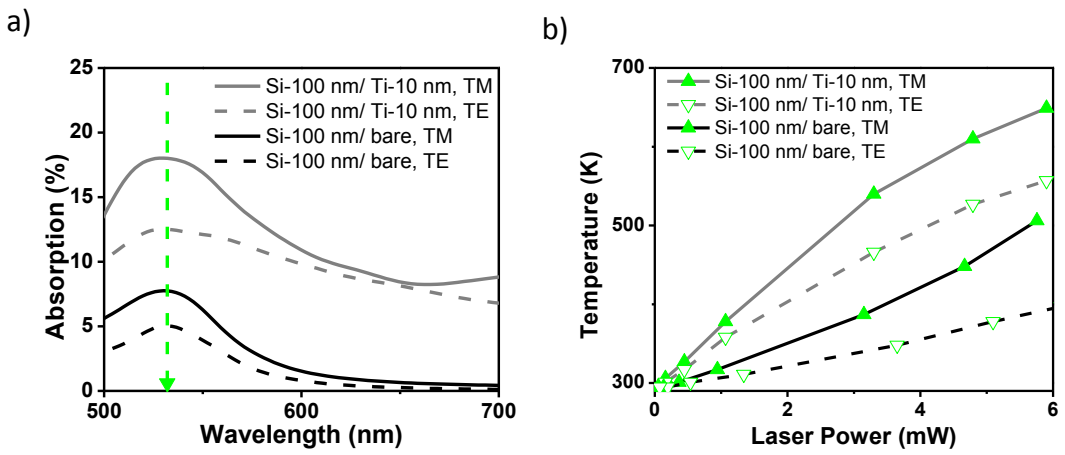

Figure 4.10: Heating in Ti coated cavities: a) Computational simulation of the absorption spectra of silicon nanowire of diameter 100 nm coated with 10 nm Ti; b) Experimentally observed temperature vs. laser power of the cavity in (a) at 532 nm.

Moreover, when the cavity mode is not resonant with the excitation wavelength, the evanescent field extending into the gold film is weaker which would excite relatively weaker LSPs in the gold particles of the film and cause a relatively lower increase in cavity temperature. This was evident in silicon nanowire of diameter 100 nm coated with 10 nm gold, at 660 nm excitation (figure 4.8a) when the cavity temperature increased to only 550 K from 320 K after coating gold. This once again highlights the importance of a nanowire cavity mode at excitation wavelength in excitation of LSPs and total cavity heat generation. It is important to note that the absorption in the silicon-gold cavity is greater than the sum of absorption values inside the individual components of the cavity of corresponding sizes if excited separately: a bare silicon nanowire and a hollow gold shell (figure 4.11) highlighting the advantage of this highly engineered cavity structure.

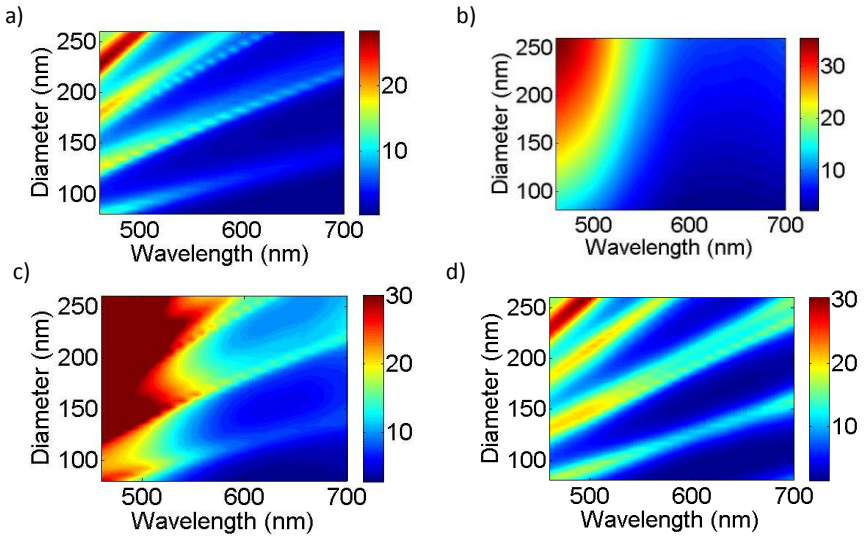

Figure 4.11: Higher absorption in cavity modes: a-d) Computational simulations showing diameter and wavelength dependence of absorption modes in TM polarization for a bare silicon nanowire, hollow gold shell, bare silicon nanowire + hollow gold shell, and for cavity respectively, color bar represents % of absorbed incident power

To show the tunability of silicon nanowire cavity mode to different wavelengths, experiments were conducted on a silicon nanowire of 240 nm diameter with and without a 10 nm gold film. This particular nanowire size and wavelength combination was chosen because while both gold and silicon are less lossy at 660 nm than at 532 nm, a cavity mode exists at this nanowire size for 660 nm excitation (figure 4.12a). This should cause high absorption in silicon and gold film and strong LSP excitation in the gold particles of the film leading to high temperatures in these cavities (bare and 10 nm gold coated silicon nanowire). Experiments in TM polarization indicated that the bare silicon nanowire was heated to a temperature of ~400 K and after coating gold the cavity attained a temperature of 900 K (figure 4.12b, solid black and golden curves). The temperatures attained in the TE polarization in bare (380 K) and gold coated (770 K)

silicon nanowire are lower than in the corresponding cavity in TM polarization (400 K and 900 K respectively) and are in accordance with lower absorption values in TE polarization (2% and 10% in bare and gold coated nanowire respectively) than TM polarization (3% and 13% in bare and gold coated nanowire respectively) predicted from FDTD calculations. These temperatures in gold coated cavity (silicon nanowire diameter 240 nm) at 660 nm are similar to the temperatures attained in the gold coated cavity (silicon nanowire diameter 100 nm) resonant at 532 nm (figure 4.6a), in spite of lower lossy nature of silicon and gold at 660 nm, and are attained because of a combined effect of three separate but related mechanisms. Silicon nanowire confines the light to highly intense electric field modes which causes high absorption and heat generation in silicon. Because of the gold layer outside the silicon nanowire, the field enhancement and cavity absorption in the silicon-gold cavity is enhanced and is greater than the sum of absorption in individual components of the cavity. The evanescent field from these intense modes that extends into the particles of the gold film excites strong LSPs leading to further heat generation. The silicon-gold engineered cavities thus simultaneously take advantage of a high refractive index dielectric silicon, enhanced cavity mode because of the gold shell outside the nanowire and LSPs in the gold particle in the shell. Moreover the cavity mode resonance can be tuned easily by changing the silicon nanowire diameter and is unaffected by changes in shape and size of gold particles in the film.

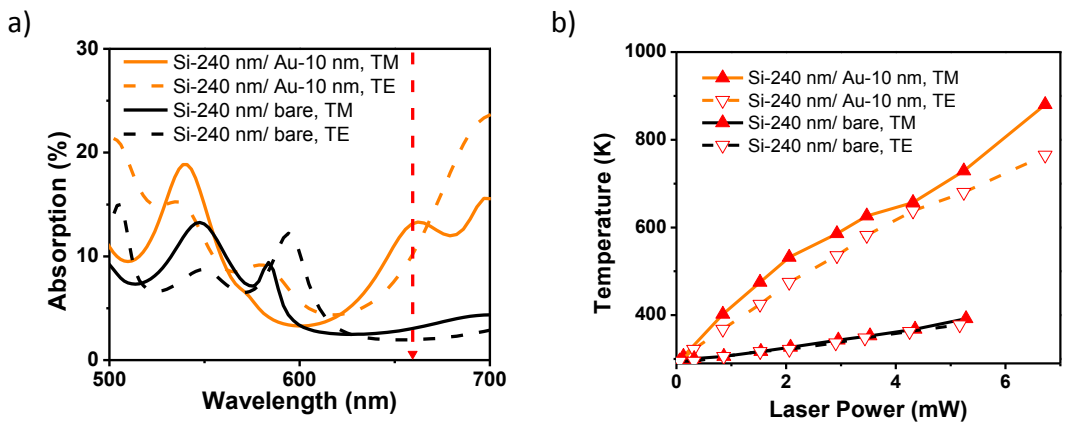

Figure 4.12: Cavity size tuning of resonant mode: a) Computational simulations of absorption spectra of gold coated and bare nanowire of diameter 240 nm in TM and TE polarizations (660 nm excitation); b) Temperature vs. laser power of cavity in a)

To capture this wavelength-nanowire cavity size dependence of modes, cavity absorption spectra for silicon nanowire with diameter ranging from 80 nm to 250 nm coated with 10 nm gold film in the wavelength range 450 nm - 700 nm have been presented in figure 4.13a and 4.13b (TM and TE polarization respectively). A silicon nanowire size resonant with the excitation wavelength creates intense electric field in the cavity, which would lead to high absorption in silicon and gold and also excite strong LSPs, maximizing cavity heating and temperature. This has been tested at two different wavelengths; at 532 nm excitation in a 100 nm diameter silicon nanowire (figure 4.6a), and at 660 nm excitation in a 240 nm diameter silicon nanowire (figure 4.12a). The nanowire can also be used as a thermometer for measuring temperature of the system up to temperatures as high as 1000 K. These graphs provide a roadmap for silicon nanowire size selection for maximizing the LSP activity and temperature in the cavity depending on the excitation wavelength for applications such as photocatalysis.

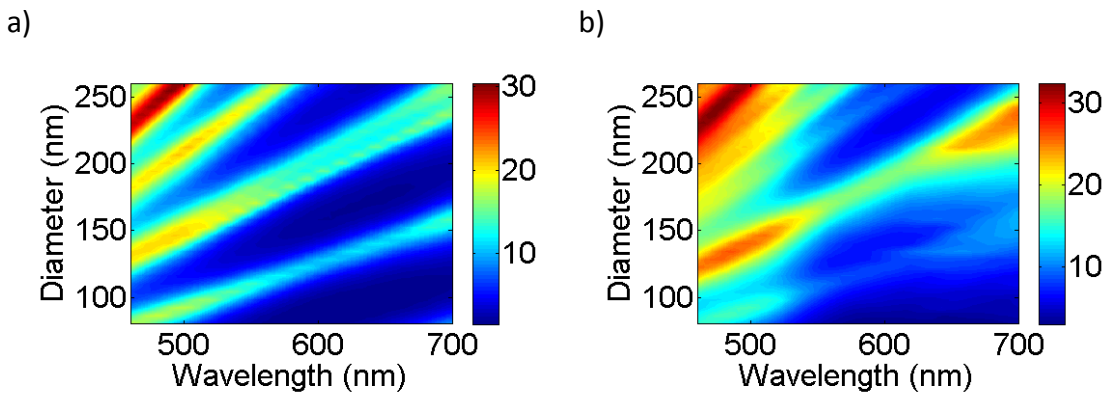

Figure 4.13: Wavelength and size dependence of resonant modes: a,b) Computational simulations showing diameter and wavelength dependence of absorption modes in TM and TE polarization respectively, color bar represents % of absorbed incident power

The high temperatures that develop in the proximity of the gold layer are potentially attractive for enhancing the rate of several chemical reactions[9]. In this work we take advantage of these high temperatures to drive photothermochemical transformations for the conversion of ethanol to generate hydrogen using the combined effect of light and heat. Photocatalytic production of hydrogen from renewable sources such as alcohols is important to sustainably provide a crucial industrial building block and a promising clean fuel[27]. This is attained by reducing protons to hydrogen and oxidizing carbon-containing compounds to CO_2 via photogenerated electrons and holes in a semiconductor catalyst, a process generally called photoreforming. The use of plasmonic materials has been shown to improve the rate of photocatalytic reactions thanks to higher temperatures developed around the plasmonic structures, typically by the use of a laser[28] [29]. But there is a lot of scope for improvement, since cavity enhanced plasmonic structures have not been explored for photocatalysis till now. To show

enhanced photoreforming rates by cavity enhanced plasmonic structures, a layer of colloidal titania nanorods (~40 nm in length and 5 nm in diameter), was deposited on top of the silicon-gold cavity structures. This was done by drop-casting a solution of titania nanorods in hexanes/octane (schematic in figure 4.14b). By tuning the concentration and volume of the drop-casting solution, a 5nm layer of titania nanorods was deposited onto the substrate on top of the gold-silicon cavity. This creates a thin, porous titania film that increases reactant transport to the active sites that are located at the gold-titania interface[30]. The films were tested for photoreforming of ethanol as a model compound for sustainable hydrogen production[27] ($C_2H_5OH + 3H_2O \rightarrow 2CO_2 + 6H_2$) with. Films that contained either the complete cavity (silicon nanowires/gold/titania) or only the photocatalytically active components (gold/titania, thus simulating conditions in which plasmonic but not cavity-enhanced photocatalysis exists) were compared under UV/Vis illumination, and otherwise identical conditions. Blank experiments with only gold/silicon cavity and no titania were tested but did not show any hydrogen production activity even after several hours under illumination (figure 4.14a) confirming the role of titania as a catalyst in the photoreforming reaction. Films that contained the complete cavity showed superior H_2 production rate compared to films which only had gold/titania catalyst (figure 4.14a), showing the importance of cavity-enhanced plasmonics in driving the reaction rate. A regression analysis yielded an intrinsic rate of H_2 production of 90 $\mu mol\ g^{-1}\ min^{-1}$ vs. 66 $\mu mol\ g^{-1}\ min^{-1}$ for silicon nanowire/gold/titania and gold/titania samples, respectively, demonstrating that an activity boost of ~40 % was obtained by simply introducing the cavity design. Furthermore, while the gold/titania catalyst

progressively deactivated under reaction conditions as evidenced by a change in the slope of H_2 production, the silicon nanowire/gold/titania sample produced hydrogen at a constant rate for as long as three consecutive days, after taking the evaporation of the solution into account. Because of the reduced amount of photocatalyst in the experiment, limiting incident light to >400 nm did not produce detectable amounts of hydrogen, and further tests need to be conducted in order to fully understand the activity of the samples under visible light. Nevertheless, cavity enhanced plasmonics provide a new, easy and stable way to enhance the activity of photocatalyst for hydrogen production from ethanol compared to other hydrogen-evolving systems[31].

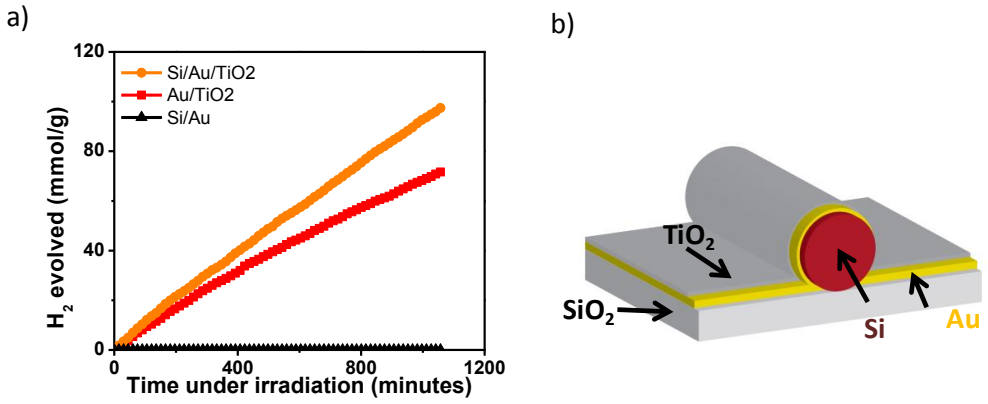

Figure 4.14: a) Hydrogen evolution from the silicon-gold-titania nanocavities gold-titania catalyst and from silicon-gold; b) Schematic of silicon/gold/titania cavity catalyst

4.5 Thermal stability measurements on the cavity

Temperature calculations done using Raman shift have shown that cavities (with 10 nm gold) have achieved temperatures up to 1000 K. Since silicon and gold form a eutectic system with a eutectic temperature of ~ 640 K[32], it was important to check

whether a eutectic reaction was taking place in between silicon and gold or not and how would it change the experimental results. With this objective, measurements were performed on 3 different silicon nanowires coated with a 10 nm gold layer using a 532 nm laser. Power dependent Raman measurements were performed and data was recorded at multiple powers by slowly increasing the power, until the temperature of the cavity reached ~630K. The nanowire was continuously irradiated with laser at each power for a few minutes to allow for any potential damage to take place. Once the nanowire was kept at 630 K for a few minutes, the laser was turned off to allow for the cavity cool down and reach steady state. Even though the cooling is instantaneous, as was evidenced by Raman spectrum recorded at lower power immediately after the nanowire was heated, the nanowire was allowed to cool for 3 minutes to ensure that the cavity is completely cooled to room temperature and is at equilibrium. Following this, same power dependent measurements were repeated at the exact same powers, for the exact time in the exactly same order of increasing power. This entire cycle was repeated three times. Following 3 successive cycles, the entire set of measurements (of three cycles) was repeated with a slightly higher maximum power than earlier so that the nanowire is now heated to a maximum temperature of ~ 750 K, i.e. slightly above the eutectic temperature. The same was then repeated with the nanowire temperature set to ~ 950 K and then for temperature > 1000 K.

This entire set of measurements, gives three sets of data for the cavity for each of the following etmperatires: 630 K, 750 K, 950 K and 1000 K. Integrated Stokes Raman intensity and temperature was calculated from each of this spectrum and was plotted with

pump power. Following these the same laser power cycle was carried on the gold film where no nanowire was present to compare the physical damage of the gold film that was on top of the nanowire with the gold film elsewhere. SEM measurements were then performed on the nanowires and on the gold film where the laser was irradiated to corroborate findings of Raman measurements with visual proof. If there is no physical damage to the cavity then the nanowire should be heated to similar temperatures and have similar Stokes scattering intensity at similar powers upon repeated measurements. But if there is some physical damage to the cavity, the cavity shape or size or both would change. This would change the field distribution inside the cavity, since that is dependent on the cavity shape and size. The changed field confinement should change the heating of the nanowire and also Stokes scattering intensity. Thus any physical damage would cause the repeated measurements to differ from the previous ones.

Figure 4.15 a, b, c and d show the 3 sets of Raman measurements collected with the peak temperature of 630 K and SEM image of the nanowire and of the gold film subjected to the same laser irradiation cycle. Clearly, the temperature (figure 4.15a) and the Raman scattering intensity (figure 4.15b) of the wire is consistent at all the powers in all the 3 cycles indicating that there is no physical damage to the cavity up to a temperature of 630 K. This is expected since the temperature of the cavity is below the eutectic temperature of silicon-gold system. The SEM images of the wire (figure 4.15c) and the gold film (figure 4.15d) show that the gold film has annealed and started to form distinct particles. This process had happened to a greater degree in the case of gold film on top the nanowire confirming that the cavity is heated to a higher temperature than just

the gold film. In spite of the change in arrangement of the gold particles/film, the Raman results are still extremely self consistent which proves that the gold film acts as an effective medium and Raman spectrum shows this average response of the effective medium even though the particles in the film are distinct and disconnected.

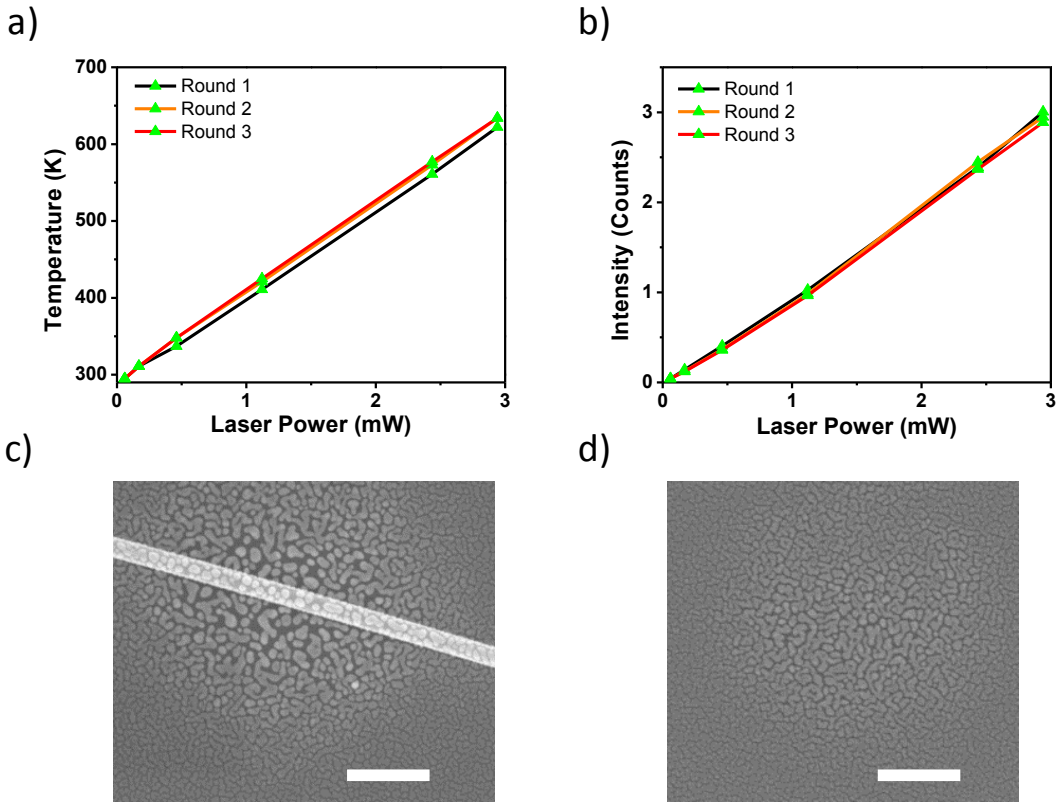

Figure 4.15: Cavity stability tests: Temperature – a) and Raman intensity – b) vs. laser power for three repeated cycle at the same spot on the nanowire with a maximum temperature of 630 K. c, d) SEM images of the nanowire on which the test was carried out and of the film on which same cycle of laser irradiation was repeated. Scale bar is 500 nm in each image.

Figure 4.16 a, b, c and d show similar data for temperature (a, c) and Stokes intensity (b, d) with maximum temperature set to 750 K (a, b) and 950 K (c, d). The

Raman data for repeated cycles at each power during multiple cycles is very consistent barring small fluctuations. It must be noted that the cavity must have been for a total period of more than 10 minutes each at 750 K and at 950 K with no evidence of any physical damage to the cavity, even though the temperature of the cavity was above the eutectic temperature.

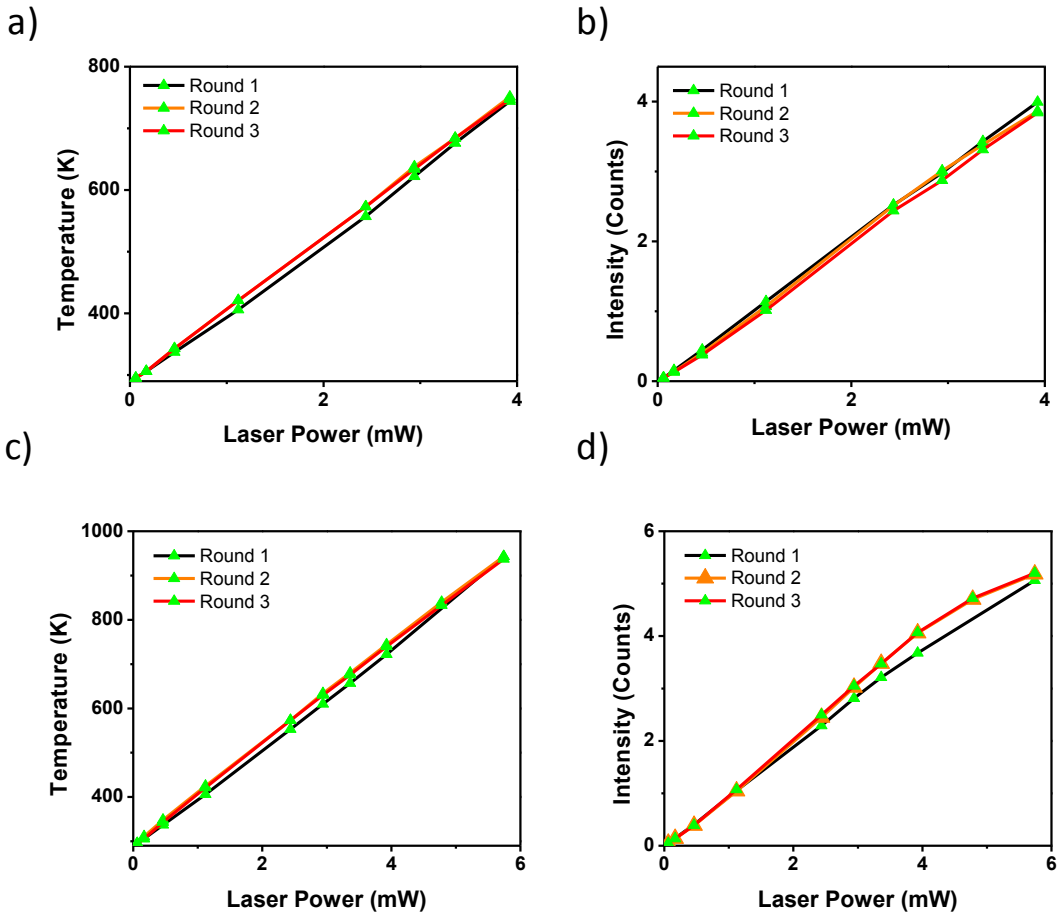

Figure 4.16: Cavity stability tests: Temperature – a) and Raman intensity – b) vs. laser power for three repeated cycle at the same spot on the nanowire with a maximum temperature of 750 K; c, d) Similar data except with a maximum temperature of 950 K

Figure 4.17 shows the SEM image of the nanowire which was kept at 950 K for over ten minutes without any evident signs of damage.

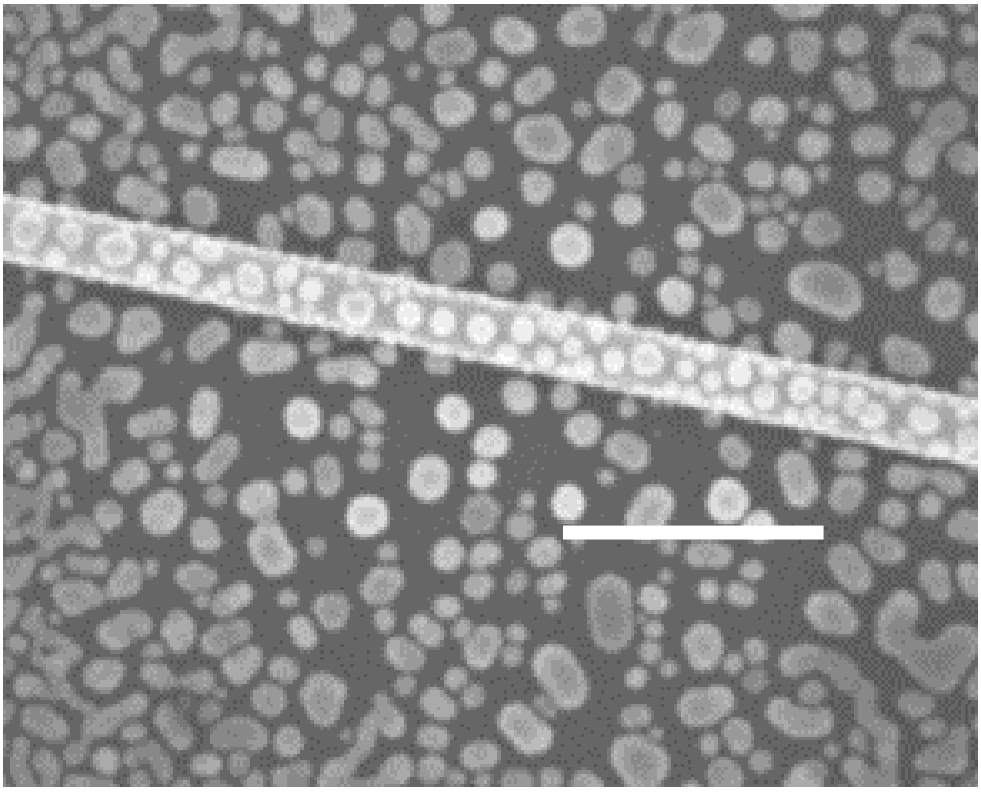

Figure 4.17: SEM image of the nanowire region kept at 950 K. Scale bar is 500 nm

This confirms that with a 10 nm gold shell, the cavity is stable even at temperatures up to 950 K. The SEM image in figure 4.17 reveals that the gold film is slightly more granular at 950 than it was at 630 K because of stronger annealing effects at higher temperature. The slight difference in temperature and scattering intensity could have been caused by thermal fluctuations in the laser power or in the spectrometer grating itself. It is also possible that the change in the morphology of gold film has a minor effect. But that happens in the first few minutes of exposure since the second and third set

of reading of readings are exactly consistent. Overall as corroborated by the SEM image, there is no physical change in the cavity besides for some annealing effects in the gold film up to a temperature of 950 K.

Once the temperature of the nanowire crosses 1000 K, there is definite damage to the nanowire as is evidenced by the change in nanowire temperature and in integrated intensity upon performing repeated measurements (figure 4.18 a and b). SEM image (figure 4.19) of this section of the wire shows that the wire cross section has been damaged and is no longer circular. This change in nanowire cross section leads to a different field confinement in the cavity which leads to different temperature and scattering intensity. It is quite possible that the wire was still undergoing physical damage even until the third cycle of measurements since the Raman intensity of the second round of tests is different from the third round of tests.

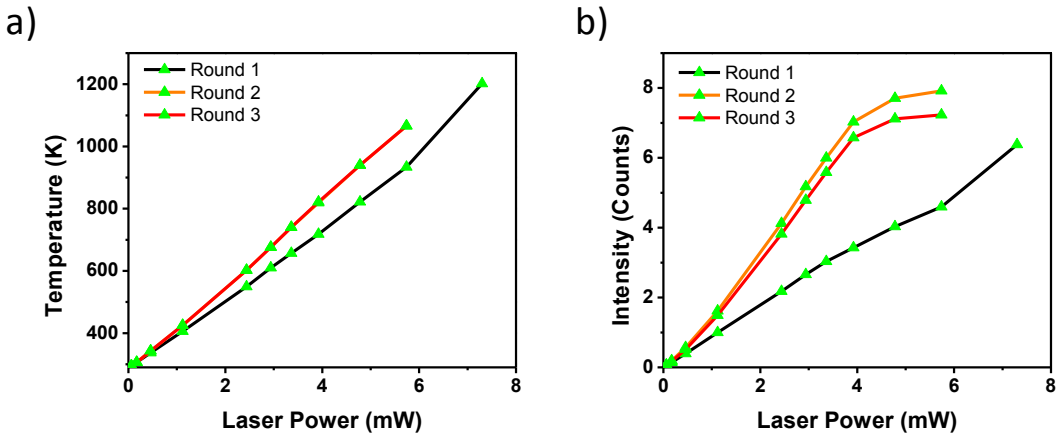

Figure 4.18: Cavity stability tests: Temperature – a) and Raman intensity – b) vs. laser power for three repeated cycle at the same spot on the nanowire with a maximum temperature > 1000 K

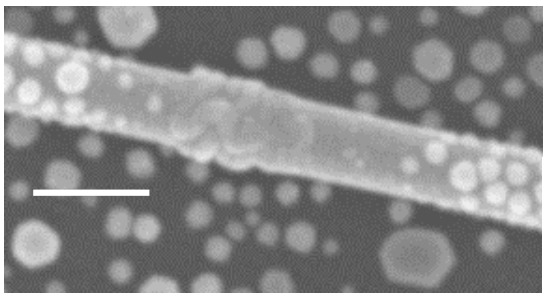

Figure 4.19: SEM image of the nanowire region heated to a temperature > 1000 K. Scale bar is 200 nm

Similar results have been obtained on multiple wires confirming that the cavity consisting of silicon nanowire coated with a 10 nm gold film is stable up to temperatures ~ 1000K beyond which the nanowire starts to melt and the cavity is destroyed.

4.6 Conclusions and future work

It would be interesting to understand the mechanism that leads to enhancement of the photocatalysis rate. There have been various reports published in literature attributing the enhancement either to hot electrons or to heat or to s synergic effect of both. Various experiments were tried to estimate the temperature change of the nanowire while simultaneously irradiating with the UV-Vis lamp used for photocatalysis. But due to the strong emission from the lamp and the relatively weak Raman signal, it was very difficult to attain a signal. Nevertheless, after blocking by the visible part of the spectrum from the UV/vis lamp (which constitutes a major part of the emission) there was some evidence for temperature rise of at least 10 K, though higher temperatures could easily have been attained. Attempts were also made to measure the temperature increase in the photocatalysis set up using an infrared thermometer but they were unsuccessful too. It is possible that the localized heat which may be good enough to enhance the rate of

photocatalysis reaction may not be strong enough to increase the temperature of entire solution.

The silicon-gold cavities show incredibly strong heat generation and incredibly high temperatures when irradiated with a laser. Various studies have been done to enhance the rate of chemical reactions using plasmonic heating with laser irradiation as was mentioned previously. But they have all used simple plasmonic structures such as spheres or cuboids without any cavity enhanced plasmonics. It would be very interesting to perform some of those chemical reactions using the silicon-gold cavities and compare the enhancement brought by the use of these cavities with the enhancement from just plasmonic structures.

In conclusion, we have demonstrated significant enhancement and easy tunability of plasmonic properties of gold, using highly engineered silicon-gold nanocavities. Because of the high refractive index of silicon core, highly intense electric field is generated inside the cavity. This intense electric field not only leads to high absorption in silicon and gold but also excites strong LSPs in the gold particles of the thin gold film (further enhanced by the close proximity of the gold particles to each other), leading to high heat generation in the cavity. By calculating temperature from change in Raman shift of silicon nanowires, we have shown that temperatures close to 1000K at a pump power ~ 5.7E5 W/cm^2 can be achieved in the cavity because of enhanced plasmonic activity and that the resonant wavelength can be tuned by varying the nanowire diameter. The cavities show enhanced hydrogen generation rate from photoreforming reactions by up to 40% over extended periods of time. The temperature insensitive resonant behavior

of these cavities makes them ideal for applications in catalysis and as model systems to study the high temperature properties of semiconductors. The silicon nanowire cavities also provide a robust method for temperature calculation of the system.

---

[1]Carlson M.T., Green A.J., Richardson H.H.; Superheating Water by CW Excitation of Gold Nanodots; Nanoletters 12(3), 1534-1537 (**2012**)

[2]Fang Z., Zhen Y., Halas N.J. et.al; Evolution of Light-Induced Vapor Generation at a Liquid-Immersed Metallic Nanoparticle; Nanoletters 13(4), 1736-1742 (**2013**)

[3]Baral S., Green A.J., Richardson H.H. et.al; Comparison of Vapor Formation of Water at the Solid/Water Interface to Colloidal Solutions Using Optically Excited Gold Nanostructures; ACS Nano 8(2), 1439-1448 (**2014**)

[4] Cao L., Barsic D.N., Guichard A.R., Mark L. Brongersma M.L.; Plasmon-Assisted Local Temperature Control to Pattern Individual Semiconductor Nanowires and Carbon Nanotubes; Nano Letters 7 (11), 3523–3527 (**2007**)

[5] Boyd D.A., Greengard L.,Brongersma M., El-Naggar M.Y., Goodwin D.G.; Plasmon-Assisted Chemical Vapor Deposition; Nanoletters 6(11), 2592-2597 (**2006**)

[6] Fasciani C., BuenoAlejo C.J., Scaiano J.C. et.al; High-Temperature Organic Reactions at Room Temperature Using Plasmon Excitation: Decomposition of Dicumyl Peroxide; Organic Letters 13(2), 204-207 (**2011**)

[7]Haas K.M., Lear B.J. ; Degradation of polypropylene carbonate through plasmonic heating; Nanoscale 5, 5247-5251 (**2013**)

[8] Karakouz, T., Maoz, B.M., Lando, G., Vaskevich, A. & Rubinstein I. Stabilization of Gold Nanoparticle Films on Glass by Thermal Embedding. Applied Materials and Interfaces **3**(4), 978-987, (2001).

[9]Aspetti, C.O., Cho, C., Agarwal, R. & Agarwal R. Studies of Hot Photoluminescence in Plasmonically Coupled Silicon via Variable Energy Excitation and Temperature-Dependent Spectroscopy. Nanoletters **14**(9), 5413-5422 (2014).

[10] Balkanski, M., Wallis, R. & Haro, E. Anharmonic effects in light scattering due to optical phonons in silicon. *Phys. Rev. B* **28,** 1928–1934 (1983).

[11] Gupta, R., Xiong, Q., Adu, C.K., Kim, U.J. & Eklund P.C. Laser-Induced Fano Resonance Scattering in Silicon Nanowires. Nanoletters **3**(5), 627-631 (2003).

[12] Buonsanti, R., Grillo, V., Carlino, E., Giannini, C., Kipp, T., Cingolani, R. & Cozzoli, P.D. Nonhydrolytic Synthesis of High-Quality Anisotropically Shaped Brookite TiO2 Nanocrystals.Journal of the American Chemical Society **130**, 11223-11233 (2008).

[13]Gordon, T.R., Cargnello, M., Paik, T., Mangolini, F., Weber, R.T., Fornasiero, P. & Murray C.B. Nonaqueous Synthesis of TiO2 Nanocrystals Using TiF4 to Engineer Morphology, Oxygen Vacancy Concentration, and Photocatalytic Activity. Journal of the American Chemical Society **134**, 6751-6761 (2012).

[14]Haro, E., Balkanski, M. Wallis, R.F. & Wanser K.H. Theory of the anharmonic damping and shift of the Raman mode in silicon. Physical Review B **34**(8), 5358-5367 (1986).

[15] Adleman, J.R., Boyd, D.A., Goodwin, D.G. & Psaltis D. Heterogeneous catalysis mediated by plasmon heating. Nano Letters **9** (12), 4417–4423 (2009).

[16]Fasciani, C., BuenoAlejo, C.J., Scaiano, J.C. et.al. High-Temperature Organic Reactions at Room Temperature Using Plasmon Excitation: Decomposition of Dicumyl Peroxide. Organic Letters **13**(2), 204-207 (2011).

[17] Haas, K.M. & Lear, B.J. Degradation of polypropylene carbonate through plasmonic heating. Nanoscale **5**, 5247-5251 (2013).

[18]Fang, Z., Zhen, Y. & Halas N.J. et.al. Evolution of Light-Induced Vapor Generation at a Liquid-Immersed Metallic Nanoparticle. Nanoletters **13**(4), 1736-1742 (2013).

[19] Sze, S.M. & Kwok K.N. Physics of semi conductor devices, third edition. 2006.

[20] Liang, D. & Bowers J.E. Recent progress in lasers on silicon. Nature Photonics **4**, 511-517 (2010).

[21] Lin, A., Son, D.H., Ahn, H., Song, G.H. &Han, W. Visible to infrared photoluminescence from gold nanoparticles embedded in germano-silicate glass fiber. Optics Express **15**(10), 6374-6379 (2007).

[22] Johnson, P.B. & Christy, R.W. Optical constants of noble metals. Phys. Rev. B **6**, 4370–4379 (1972).

[23] Palik, E. D. Handbook of Optical Constants of Solids. (Academic, 1998).

[24] Cao, L., Barsic, D.N., Guichard, A.R. & Brongersma M.L. Plasmon-Assisted Local Temperature Control to Pattern Individual Semiconductor Nanowires and Carbon Nanotubes. Nano Letters **7**(11), 3523–3527 (2007).

[25]Wang, H., Levin, C.S. & Halas N.J. Nanosphere Arrays with Controlled Sub-10-nm Gaps as Surface-Enhanced Raman Spectroscopy Substrates. Journal of the American Chemical Society **127**(43), 14992-14993 (2005).

[26] Lide, D.R. CRC Handbook of Chemistry and Physics. 84th Edition (2003).

[27]Barreca, D., Carraro, G., Gombac, V., Gasparotto, A., Maccato, C., Fornasiero, P. & Tondello, E. Supported Metal Oxide Nanosystems for Hydrogen Photogeneration: Quo Vadis?. Advanced Functional Materials **21**, 2611-2623 (2011).

[28]Zhang, Z., Wang, W., Gao, E., Sun, S. & Zhang, L. Photocatalysis Coupled with Thermal Effect Induced by SPR on Ag-Loaded Bi_2WO_6 with Enhanced Photocatalytic Activity. The Journal of Physical Chemistry C **116**, 25898-25903 (2012).

[29]Christopher, P., Xin, H., Marimuthu, A. & Linic S. Singular characteristics and unique chemical bond activation mechanisms of photocatalytic reactions on plasmonic nanostructures. Nature Materials **11**, 1044-1050 (2012).

[30]Duonghong, D., Borgarello, E. & Graetzel, M. Dynamic of light induced water cleavage in colloidal systems. Journal of the American Chemical Society **103**, 4685-4690(1981).

[31]Ma, Y., Wang, X., Jia, Y., Chen, X., Han, H. & Li C. Titanium Dioxide-Based Nanomaterials for Photocatalytic Fuel Generations. Chemical Reviews **114**, 9987-10043(2014).

[32] Abouie, M., Liu, Q. & Ivey, D. G. Eutectic and solid-state wafer bonding of silicon with gold. *Mater. Sci. Eng. B* **177,** 1748–1758 (2012).

CHAPTER 5: Conclusions and future work

5.1: Conclusions

Cavity effects of silicon, silicon-gold (a thick as well as a 10 nm layer), silicon-silver and silicon-titanium cavities have been investigated by varying the nanowire diameter, cavity structure and excitation wavelength. These cavities support wavelength dependent resonant modes which can be exploited to tailor the interactions in between photons, phonons, plasmons and electrons. At cavity mode resonance, the electric field is tightly confined in the cavity which leads to high field intensities in the cavity, much stronger than in bulk silicon.

Using these highly confined modes, stimulated Stokes Raman scattering and stimulated anti Stokes Raman scattering was obtained for the first time in homogeneous silicon nanostructures. Raman lasers built out of this cavity design would enable the development of on-chip, low powered, easily monolithically integratable optical interconnects. The ease of fabrication and integration and the low powered nature of these cavities could lead to next generation of ultrafast and cheap devices.

Cavity modes could also be tuned to enhance the relative proportion of the anti Stokes Raman scattering. In a few cases, the state of "population" inversion was reached in which the intensity of anti Stokes scattering was greater than the intensity of Stokes scattering. At the other extreme, almost complete Stokes emissions (~96%) was also achieved. These cavities along with the use of Stimulated anti Stokes Raman scattering

could be designed to make an anti Stokes laser and devices for mitigating heat in Raman lasers by enhancing the anti Stokes interactions. An anti Stokes laser would be advantageous because the lasing emission would involve a destruction of phonon which would lead to cooling of the cavity. Therefore anti Stokes lasers would function more efficiently than Stokes lasers.

Lastly, the interactions in highly confined electric fields inside the silicon nanowire were used to excite extremely strong localized surface plasmons in gold which led to cavity heating and temperatures close to 1000 K at a pump power of 5E5 W/cm^2. These cavities were shown to enhance the hydrogen (a crucial industrial building block and a promising clean fuel) evolution rate from ethanol. These cavities should also have applications in high temperature catalysis.

5.2: Future work

Because of high losses in silicon in the visible spectrum lasing was not achieved in the cavities, although gain in SRS was observed which looks extremely promising. Because losses at 1.55 μm, where majority of the silicon Raman lasers have been built, are ~ eight orders of magnitude lowers than in the visible spectrum, it should be much easier to attain Raman lasing using this pump wavelength. Therefore experiments need to be conducted at this wavelength or anywhere below the bandgap of silicon with the direction of wave propagation along the nanowire long axis in order to increase the interaction length in between silicon and pump. It should be possible to achieve lasing at both Stokes and anti Stokes wavelength.

Cavities could be designed to enhance anti Stokes scattering to such a degree that it becomes greater than Stokes scattering. This has already been shown although at high temperatures. Higher anti Stokes scattering would have applications in optical cooling as well as building an anti Stokes laser.

The silicon-gold (10 nm layer) cavities have the potential to attain extremely high temperatures at much lower pump powers. Future applications of these cavities in catalysis and energy conversions can be explored.